이학박사 학위논문

일산화탄소에 의한 면역 관련 이상 반응 억제 기전 및 필버톤의 아밀로이드 생성 완화 작용

Inhibitory Mechanisms of Carbon Monoxide on Immune-related Adverse Events and Reductive Effects of Filbertone on Amyloidogenesis

울 산 대 학 교 대 학 원

생 명 과 학 과

공 정 헌

일산화탄소에 의한 면역 관련 이상 반응 억제 기전 및 필버톤의 아밀로이드 생성 완화 작용

지도교수 정헌택 · 박정우

이 논문을 이학박사 학위논문으로 제출함

2023년 6월

울 산 대 학 교 대 학 원
생 명 과 학 과
공 정 헌

공정헌의 이학박사 학위논문을 인준함

심사위원장 백승훈 인

심사위원 정헌택 인

심사위원 양재하 인

심사위원 유리나 인

심사위원 박정우 인

울 산 대 학 교 대 학 원

2023년 6월

Inhibitory Mechanisms of Carbon Monoxide on Immune-related Adverse Events and Reductive Effects of Filbertone on Amyloidogenesis

Supervisor: Prof. Dr. Hun Taeg Chung and Jeong Woo Park

A Dissertation

Submitted to
The Graduate School of the University of Ulsan
In the partial Fulfillment of the Requirements
for the degree of

DOCTOR OF PHILOSOPHY

BY

JEONGHEON GONG

Department of Biological Science
Ulsan, Korea
June 2023

PART I

CO-induced TTP attenuates combined CTLA-4 and PD-1 blockade immunotherapy toxicity and promotes anti-tumor immunity

CONTENTS

PART II

Activation of ROS-PERK-TFEB by filbertone ameliorates neurodegenerative disease via enhancing the autophagy-lysosomal pathway

PART III

Filbertone attenuates MPP^+/MPTP-induced ferroptosis in neurological diseases via Nrf2-GPX4 activation

PART I

CO-induced TTP attenuates combined CTLA-4 and PD-1 blockade immunotherapy toxicity and promotes anti-tumor immunity

I-I. ABSTRACT

Combined immune checkpoint blockade (ICB) targeting CTLA-4 and PD-1 has improved the prognosis of malignancies but has also led to a high rate of immune-related adverse events (irAEs). The manifestation of these toxicities is an important limiting factor for the successful implementation of ICB, restraining its antitumor efficacy. Carbon monoxide (CO) is a pivotal endogenous signaling molecule that can maintain cell and tissue homeostasis and may have therapeutic uses. In our previous reports, CO regulates inflammatory diseases by increasing tristetraprolin (TTP) levels, which binds to the AU-rich elements in a target mRNA. In this study, we observed that CO-induced TTP activation ameliorated colitis and hepatitis and improved antitumor efficacy in ICB treatment. We found that the colitis and hepatitis in TTP deficient mice were further exacerbated by ICB treatment. CO enhances ICB efficacy by disrupting tumor associated macrophages (TAM) metabolic adaptation in the tumor microenvironment (TME). TTP destabilizes CD36 mRNA, causing metabolic maladaptation in TAMs within the TME. Thus, we suggest that CO may efficiently decouple antitumor effectiveness and toxicity of ICB by enhancing TTP.

Keywords

Immune checkpoint blockade; immune-related adverse events; Carbon monoxide; Tristetraprolin; tumor associated macrophage, CD36

I-II. INTRODUCTION

Treatment with combined immune checkpoint blockade (ICB), such as anti-CTLA-4 and anti-PD-1 monoclonal antibodies shows more frequent, strong, and sustained clinical responses over time than monotherapy[1-6]. However, more than 50% of patients suffered serious immune-related adverse events (irAEs), which sometimes require discontinuation of therapy[6-9]. Several studies have demonstrated that, prophylactic or concomitant treatment with tumor necrosis factor (TNF) blockade is an attractive strategy to alleviate combined ICB-induced irAEs[6,9,10]. TNF-α is considered the major inflammatory cytokine involved in patients with numerous autoimmune diseases, such as rheumatoid arthritis, spondyloarthropathies, psoriasis, and inflammatory bowel disease[11-13].

The inflammatory response can be modulated by post-transcriptional control[14,15]. The post-transcriptional control of inflammatory transcripts strongly depends on AU-rich element (ARE)-mediated mechanisms[15,16]. Tristetraprolin (TTP) is an ARE-binding protein that has a destabilizing function to regulate the target transcripts[15,17]. Most organs can be affected by irAEs that result from ICB. Colitis is among the most frequent and problematic irAEs associated with combined ICB[9,18]. Our previous study demonstrated the importance of TTP in limiting the inflammatory response in the DSS-induced colitis model[15,19]. Furthermore, it was reported that CO can protect against DSS-induced colitis via enhanced TTP expression[15,20].

Many tumors respond poorly or even not to ICB, partly caused by the absence of tumor-infiltrating lymphocytes (TILs). This significantly limits the application of ICB due to immunosuppressive cell in TME[21-23]. TAMs are a key component of TME[22,24] and are often

correlated with poor prognosis and therapy resistance[25]. Emerging evidence suggests that macrophages undergo metabolic changes to adapt to TME, with alterations of glucose, lipid, and glutamine metabolism[26,27]. These metabolic changes enhance functional reprogramming of macrophage that promote tumors with immunosuppressive and anti-inflammatory activities[21,23,25,26,28-30]. Recent studies explored that the possible role of lipid homeostasis in controlling the functional state of macrophages to enhance ICB response in cancer patients[28,30-33].

Cluster of differentiation 36 (CD36) is a widely expressed transmembrane glycoprotein and plays a crucial role in lipid metabolism and signaling[26,28,29,34-37]. The CD36 receptor has been detected in immune cells, such as macrophages and neutrophils, as well as in cancer cells[29,35,37]. Intratumoral macrophages exhibit enhanced lipid accumulation through increased CD36 expression, which contributes to tumor metastasis and stemness[26,28,29]. Depletion of CD36 in immune cells in the TME can boost antitumor immune response[26,29,34,38,39]. TTP binds to the ARE region in the 3´ untranslated regions (3'UTRs) of CD36 mRNA and promotes its degradation[36]. Based on this evidence, we hypothesize that CO treatment can ameliorate irAEs and enhance the antitumor efficacy of ICB by inducing TTP. In addition, we focus on the mechanism by which TTP enhances antitumor effects. Consequently, we provide evidence that CO inhalation combined with ICB therapy prevents autoimmune adverse events in mouse models by increasing TTP expression. Furthermore, the enhanced efficacy of ICB can be attributed to the elevated levels of TTP within the TME. Increased TTP levels convert M2-TAM to M1-TAM in TME contributes more effective antitumor response.

I-III MATERIALS AND METHODS

1. Reagents and Chemicals

Carbon monoxide-releasing molecule- (CORM-) 2, resveratrol (Res), metformin (Met) and oleic acid (OA) were purchased from Sigma-Aldrich (St. Louis, MO, USA).

2. Cell culture

Mouse macrophage RAW 264.7 cells (KCLB, Seoul, Korea) were cultured in DMEM containing 10% FBS and 1% penicillin-streptomycin solution, at 37°C in humidified incubators containing an atmosphere of 5% CO_2. RAW 264.7 cells were pretreated with CORM2 (20 μM) or Res (1 μM) or Met (2 mM) for 1h and then stimulated with IL-4 and IL-13 (10 ng/ml) or OA (100 μM) or cocultured with MC38 mouse colorectal cancer cell for 24h. Bone marrow-derived macrophages (BMDM) from C57BL/6 mice were isolated from the tibia and femur of 6-8-week-old mice and differentiated in the presence of M-CSF (10 ng/mL) in DMEM medium.

3. Mice

Male C57BL/6 mice were purchased from Koatech (Pyeongtaek, South Korea). TTP knockout (KO) mice were kindly provided by Dr. Perry J. Blackshear. Mice were bred and maintained at specific pathogen-free conditions at 18–24°C and 40–70% humidity, with a 12 h light-dark cycle. All mice were handled in accordance with guideline of the Institutional Animal Care and Use Committee (IACUC) of the University of Ulsan.

4. DSS-induced colitis models and tumor models

Mice were orally administered 3% DSS (36–50 kDa; MP Biomedicals) in their drinking water for three days to induce acute colitis. The experiments were performed in these conditions because a protocol reported previously, which included 3% DSS in water over seven days, proved to be very toxic and produced high mortality in our model. To generate the tumor model, on day 0, 8-week-old male C57BL/6 mice were inoculated subcutaneously with 5×10^5 MC38 cells. On day 9 after tumor cell inoculation, mice were administered 3% DSS for three days. The size of tumors was measured every two days using a caliper.

5. Treatments

Mice received 100 μg of anti-CTLA-4 antibody (InVivoMAb BioXCell; anti-mouse CTLA-4) and 100 μg of anti-PD-1 antibody (InVivoMAb BioXCell; anti-mouse PD-1) per injection intraperitoneally. Colitis treatment consisted of the intraperitoneal administration of anti-mouse TNF antibody (125 μg per injection per mice; InVivoMAb BioXCell).

6. Magnetic activated cell sorting (MACS)

To isolate the TAMs, freshly isolated tumor tissues were cut into pieces. The pieces were then subjected to enzymatic digestion using a solution of Hanks' buffer containing collagenase I, IV and DNAse I (Sigma) for 30 min at 37°C. The cells that had been dissociated were passed through a 70 μm nylon mesh and subsequently centrifuged at 450 g for 6 min at 4°C. Remove the red blood cells by using RBC lysis buffer. Neutralization with PBS the cells were passed through a 70 μm nylon mesh. The samples were centrifuged at 450 g for 6 min at 4°C and

discarded the supernatants. Three-phase gradients can be obtained by slowly covering a cell suspension with a percoll gradient solution consisting of 35% and 60%. The suspension underwent centrifugation at 2000 g for 10 min without any acceleration or break. The low interphase layer was collected and subsequently washed with MACS buffer. The resulting mixture was centrifuged at 800 g for 5 min at 4°C. The cells should be resuspended with MACS buffer at a concentration of 10^8 cells/mL. The cells were subjected to incubation with CD11b microbeads 10μl volume per 10^7 total cells. The procedure for isolating the TAMs followed the manufacture procedure.

7. Flow cytometry analysis

The following antibodies were used: FITC anti-mouse CD206 antibody, PE anti-mouse F4/80 antibody, PE anti-mouse CD86 antibody, FITC anti-mouse F4/80 antibody. Fluorescence data were collected using a FACSAria II flow cytometer (BD Biosciences, USA) and analyzed employing a FlowJo software.

8. RNA Isolation and Reverse Transcription-Polymerase Chain Reaction

Total RNA was isolated from RAW 264.7 cells, BMDM, liver, colon and tumor tissues using TRIzol reagent (Invitrogen). 2 μg of total RNA was used to synthesize cDNA by using M-MLV reverse transcriptase (Promega). The synthesized cDNA was subject to PCR-based amplification. The following primers were mouse GAPDH (f-aggccggtgctgagtatgtc, r-tgcctgcttcaccttct), mouse TNF-α (f-agcccacgtcgtagcaaaccaccaa, r-acacccattcccttcacagagcaat), mouse TTP (f-ctctgccatctacgagagcc, r-gatggagtccgagtttatgttcc), mouse CD36 (f-

gatgacgtggcaaagaacag, r-cagtgaaggctcaaagatgg), mouse PD-L1 (f-gctccaaaggacttgtacgtg, r-tgatctgaagggcagcatttc), mouse NOS2 (f-tttgcttccatgctaatgcgaaag, r-gctctgttgaggtctaaaggctccg), mouse Arg1 (f-cagaagaatggaagagtcag, r-cagatatgcagggagtcacc) and mouse 18S (f-cagtgaaactgcgaatggct, r-tgccttccttggatgtggta). To perform real-time quantitative PCR (RT-qPCR), the synthesized cDNA was amplified with SYBR Green qPCR Master Mix (2x, USB Production; Affymetrix) on an ABI 7500 Fast Real-Time PCR System (Applied Biosystems, Carlsbad, CA). The following RT-qPCR primers were mouse GAPDH (f-cggcctcaccccatttg, r-gggaagcccatcaccatct), mouse TTP (f-ccaggctggctttgaactca, r-acctgtaacccagaacttgga), mouse IL-12b (f-tggtttgccatcgttttgctg, r-acagggtgaggttcactgtttct), mouse CD86 (f-ctggactcctacgacttcacaatg, r-agttggcgatcactgacagtt), mouse CD206 (f-ctctgttcagctattggacgc, r-cggaatttctgggattcagcttc), mouse IRF4 (f-tccgacagtggttgatcgac, r-cctcacgattgtagtcctgctt), mouse PD-L1 (f-agtatggcagcaacgtcacg, r-tccttttcccagtacaccacta).

9. Western blot

Total proteins extracted from harvested tissues and cells were prepared in mammalian lysis buffer containing phosphatase and protease inhibitors, and the protein concentration was determined using the BCA protein assay kit (Pierce Biotechnology, Rockford, IL, USA). The protein was fractionated on polyacrylamide-SDS gels and transferred to polyvinylidene difluoride membranes. The membrane was blocked with 5% nonfat milk in phosphate-buffered saline Tween 20 (PBS-T) and then incubated with a primary antibody against TNF-α (1 : 2000 v/v in PBS-T, Cell signaling, MA), TTP (1 : 2000 v/v in PBS-T, sigma) or α-tubulin (1 : 2500 v/v in PBS-T, Cell Signaling) followed by incubation with a secondary antibody. Antibody binding was visualized with an ECL chemiluminescence system (GE Healthcare

BioSciences, Little Chalfont, UK).

10. Statistical Analysis

For statistical comparisons, all values were expressed as mean ± SD. Statistical differences between samples were assessed by ANOVA with post hoc Tukey's honestly significant difference (HSD) test. Moreover, for statistical differences between groups in $Ttp^{+/+}$ and $Ttp^{-/-}$ genotypes, data were assessed by two-way ANOVA with Bonferroni post-tests. Data were analyzed and presented with GraphPad Prism software version 7.00 (San Diego, CA). Probability values of $p \leq 0.05$ were considered to represent a statistically significant change.

I-IV RESULTS

1. irAEs, exacerbated by ICB, is attenuated by CO

To investigate the protective effect of CO on ICB-induced irAEs, mice with 3% DSS-induced colitis were treated intraperitoneally (i.p.) with anti-PD-1 and anti-CTLA-4 antibodies (ICB), either anti-TNF antibodies or CO inhalation (Fig. 1a). The ICB treatment resulted in weight loss and a reduction in colon length compared to DSS receiving group (Fig. 1b-d). The data suggest that ICB may exacerbate inflammation in colon tissue. In previous study, we demonstrated that inhalation of CO in a DSS-induced colitis model resulted in lowered inflammatory features[15]. As anticipated, the inhalation of CO or treatment with anti-TNF group effectively improved the exacerbation of colitis (Fig. 1 b-d). Similarly, inhalation of CO and treatment with anti-TNF reduce the severity of colon deterioration and liver damage induced by ICB in MC38 tumor bearing irAEs model (Fig. 1 f-i). The presented data indicate that ICB-induced irAEs were more severe than those induced by DSS alone, manifested in the colon and liver. However, the inhalation of CO was found to mitigate these adverse events.

2. TTP is required for the protective effects of CO on ICB-induced irAEs

Our previous studies have indicated that both CO and 4-PG exhibit protective effects against DSS-induced colitis and are necessary for the expression of TTP[15,40]. Previous studies have demonstrated that the deficiency of TTP results in the blockade of the inhibitory effects of CO or 4-PG. The experimental model employed in this study demonstrates that inhalation of CO leads to an increase in TTP protein and mRNA levels in both colon and liver tissue (Fig. 2 a-

d). The protein and mRNA expression levels of TNF-α, a crucial mediator of inflammatory response, were observed to be downregulated by CO (Fig. 2 a-d). Anti-TNF treatment shows decrease of TNF-α levels in colon and liver tissue, but it does not increase TTP expression levels. Therefore, the therapeutic effects of irAEs mediated by anti-TNF are not associated with the expression of TTP. To evaluate the necessity of TTP in the protective effects of CO, we utilized a TTP knockout mouse model. The inhalation of CO resulted in a decrease of TNF-α mRNA and protein levels, which was attributed by induction of TTP (Fig.2 e, f). Additionally, the inhalation of CO was found to rescue AST and ALT levels in comparison to ICB treatment (Fig.2 g, h). However, in comparison to the TTP wild type, the absence of TTP did not show any protective effects induced by CO inhalation (Fig. 2 e-h). These findings suggest that CO can protect against irAEs by activating TTP, provide an avenue for therapeutic intervention of irAEs.

3. CO-induced TTP augments ICB efficacy

We next studied whether CO would affect antitumor activity of ICB in mice with MC38 tumors. ICB, combination with CO inhalation or anti-TNF treatment significantly decreases tumor growth (Fig. 3a, b). Furthermore, it has been observed that inhalation of CO leads to a significantly increases of IFN-γ and GrB levels in tumor tissue (Fig. 3c, d). The increased levels of IFN-γ and GrB indicate that inhalation of CO enhances the immune response more than ICB alone. Interestingly, the deficiency of TTP exhibits a significantly greater tumor volume in comparison to the TTP wild-type model (Fig. 3e, f). Furthermore, the deficiency of TTP did

not result in an increase of IFN-γ cytokine mRNA in the tumor tissue (Fig. 3g). The data indicate that the enhancement of ICB efficacy by CO inhalation was depends on TTP.

4. CO dampens the immunosuppressive M2-TAM population in TME

TAM play a crucial role in the TME and are frequently associated with unfavorable prognosis and resistance to therapy[22,24,25]. TAM undergoes metabolic changes in response to their local TME. The regulation of lipid homeostasis is considered in modulating the functional phenotype of macrophages[28,30-33]. CD36, a pivotal regulator of lipid metabolism, facilitated metabolic adaptation of M2-TAM, leading to the development of a highly immunosuppressive TME[26,28,29,34-37]. A recent study has shown that the deletion of CD36 in myeloid cells led to an augmentation of the CD8+ T cell activity and a conversion of M2-TAM into M1-like macrophages within the tumor region[26,29,38]. Furthermore, the CD36 mRNA has been identified as a target of TTP[36]. TTP found that potentially regulate tumor immunity targets by degrading CD36 mRNA. Herein, inhalation of CO leads to an elevated TTP mRNA levels in tumor tissue, whereas CD36 mRNA levels were decreased (Fig. 4 a). Furthermore, the expression of NOS2, as a marker for M1 macrophages, was significantly elevated upon exposure to CO (Fig. 4a). Based on this evidence, we performed flow cytometry analysis to validate the functional phenotype of tumor-infiltrating macrophages. Inhalation of CO resulted in an increase in CD86+ M1 type macrophages, while CD206+ M2 type macrophages were decreased (Fig. 4b, c) Additionally, the protein levels of NOS2 and TNF-α were increased by CO inhalation (Fig. 4d). These data suggest that the synergistic immunotherapeutic effects of CO inhalation may be associated with the reprogramming of macrophage phenotype, which is mediated by TTP.

5. TTP reprogrammed M2 macrophages to an M1-like population

To investigate the impact of TTP on macrophage polarization, we treated Raw264.7 mouse macrophage cells with TTP inducers before treated with M2 polarization cytokines. As expected, RT-PCR data indicate that both Raw264.7 cells were treated with M2 polarization cytokines or stimulated with cancer cells exhibited a significant increase of CD36 mRNA levels (Fig. 5 a, b). Furthermore, M2 phenotype markers, including PD-L1, Arg1, and IL-10 were increased (Fig. 5 a, b). This data indicates that the polarization of macrophages towards M2 is influenced by cancer cells in TME (Fig. 5 b). The administration of TTP inducers resulted in a significant reduction of M2 markers, indicating TTP has an ability of M2 polarization inhibition. The immunosuppressive phenotype of TAM has been found to be associated with the nutrient state of the TME. Specifically, it has been reported that high levels of fatty acids and cholesterol are present in the TME, which may contribute to this phenotype[26,28,29,34,35,38]. To assess impact of TME metabolic state to macrophages, Raw264.7 cells were treated with oleic acid (OA). Similarly, the treatment with OA resulted in the increase of CD36 and M2 markers which is reduced by administration of TTP inducers (Fig. 5 c). To verify CD36 functional defects induced by TTP, we tested lipid uptake levels. In OA-treated macrophages, lipid uptake was higher than M0 macrophages and to attenuated by TTP inducers. (Fig. 5 d). The presented data implies that the modulation of TTP levels could potentially play a role in promoting antitumor immunity. Next, IL-4 and IL-13 stimulated BMDM, both expression of CD36 and PD-L1 mRNA levels were higher than M0 macrophages, whereas lowered by administration of TTP inducers (Fig. 6a). However, the decrease of M1 phenotype markers, including NOS2, IL-12b, and CD86, were markedly increased after treated with TTP inducers

(Fig. 6b). The data presented that TTP may exert antitumor effects by inhibiting the adaptation of M2 macrophages in TME and inducing their reprogramming to M1-like macrophages.

I-V FIGURES

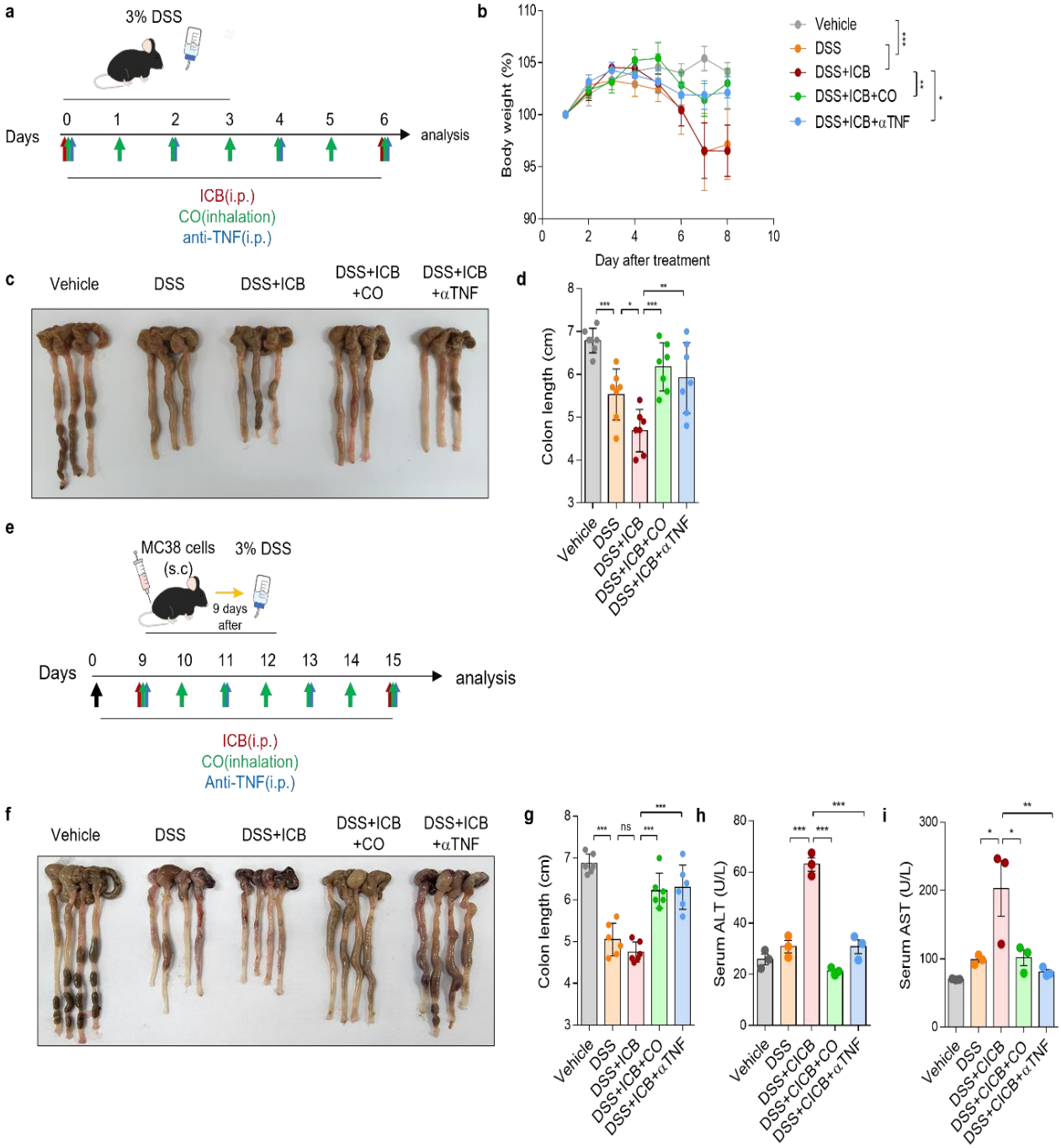

Figure 1. Protective effects of CO inhalation on irAEs. (a) Diagram of experimental procedure. (b) Normalization of body weight as a surrogate measure for assessing colitis severity in murine models. (c, d) Representative image of colons (c) and bar graph depicting the colon length (d). (e) To demonstrate the protection effects of CO in ICB-induced irAEs,

colitis and hepatitis, a tumor xenograft model was employed. The MC38 colon cancer cells were subcutaneously injected into mice, and after 9 days, those with 3% DSS-induced colitis were administered intraperitoneal (i.p.) treatment. The treatment options include the administration of in combination with anti-PD-1 and anti-CTLA-4 antibodies, either TNF blockade or CO inhalation. (f) Representative image of mouse colons. (g) Bar graph depicting the colon length. (h, i) Bar graph represents the levels of serum ALT (h) and AST (i), which are commonly used as indicators of hepatic damage. Data represent mean ± SD; *p<0.05, **p<0.01, and ***p<0.001, ns : not significant.

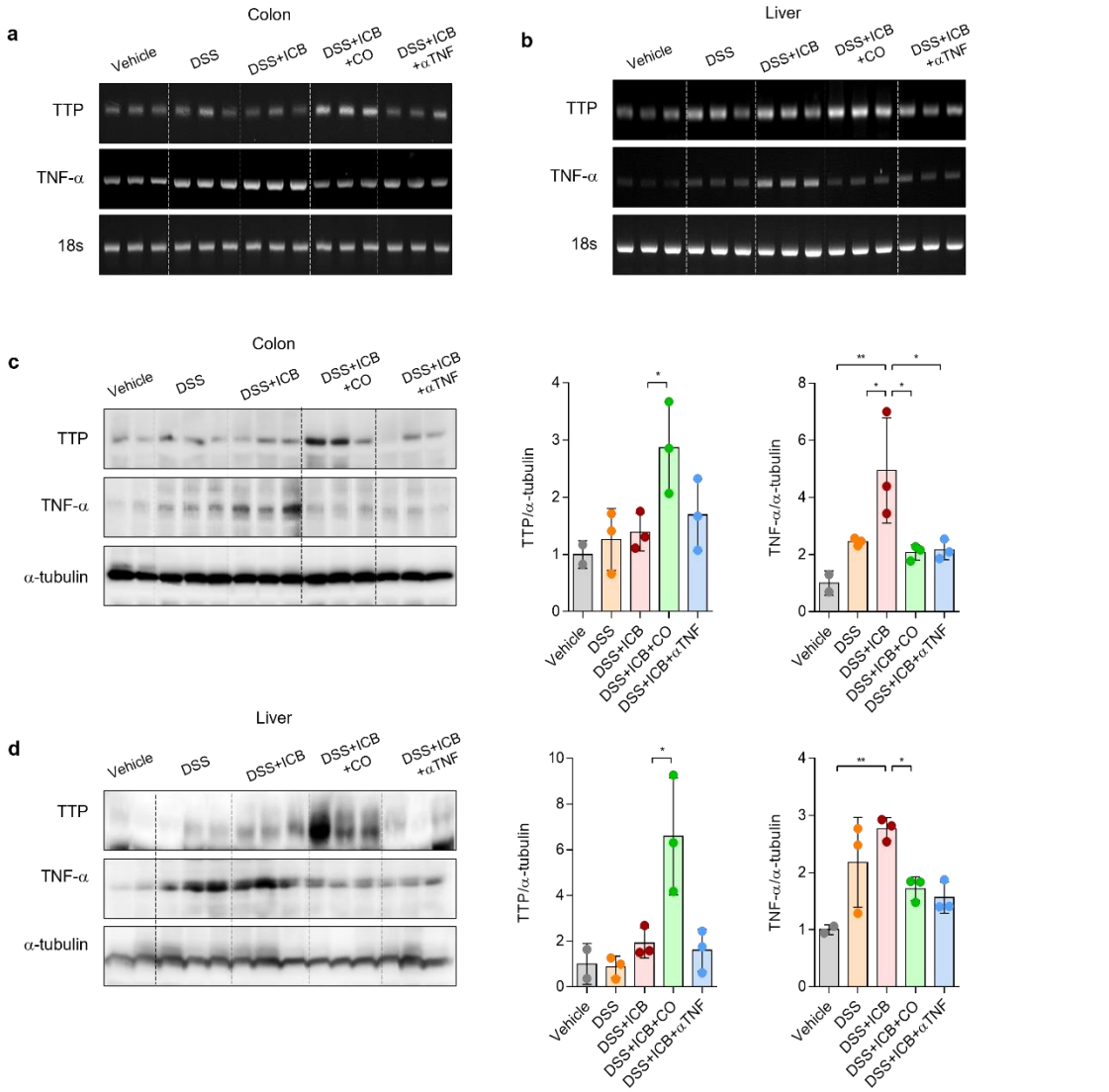
a
Colon
Vehicle
DSS
DSS+ICB
DSS+ICB +CO
DSS+ICB +αTNF
TTP
TNF-α
18s
b
Liver
c
α-tubulin
TTP/α-tubulin
TNF-α/α-tubulin
d
e
Ttp+/+
Ttp-/-
CTRL
ICB
ICB+CO
ICB+αTNF
f
g
Serum ALT (U/L)
h
Serum AST (U/L)
ns
Vehicle
ICB
ICB+CO

Figure 2. Effects of TTP on CO-induced protection of irAEs. (a-d) Mice bearing MC38 tumors were administrated 3% DSS and injected with ICB. (a) The levels of mRNA expression of TTP and TNF-α in colon tissues. (b) The levels of mRNA expression of TTP and TNF-α in liver tissues. (c) The levels of protein expression of TTP and TNF-α in colon tissues. The quantification of proteins is presented in right panel. (d) The levels of protein expression of TTP and TNF-α in liver tissues. The quantification of proteins is presented in right panel (e-h) To explore the mechanism by which CO protects against ICB-induced irAEs, we administered ICB, anti-TNF antibodies, or CO inhalation to both $Ttp^{+/+}$ and $Ttp^{-/-}$ mice. Following a 7-day treatment period, the mice were sacrificed, and serum samples were collected for molecular assays. (e) The levels of mRNA expression of TTP and TNF-α in colon tissues. (f) The levels of protein expression of TTP and TNF-α in colon tissues. The quantification of proteins is presented in right panel (g, h) Bar graph represents the levels of serum ALT (g) and AST (h). Data represent mean ± SD; *p<0.05, **p<0.005, ns: not significant.

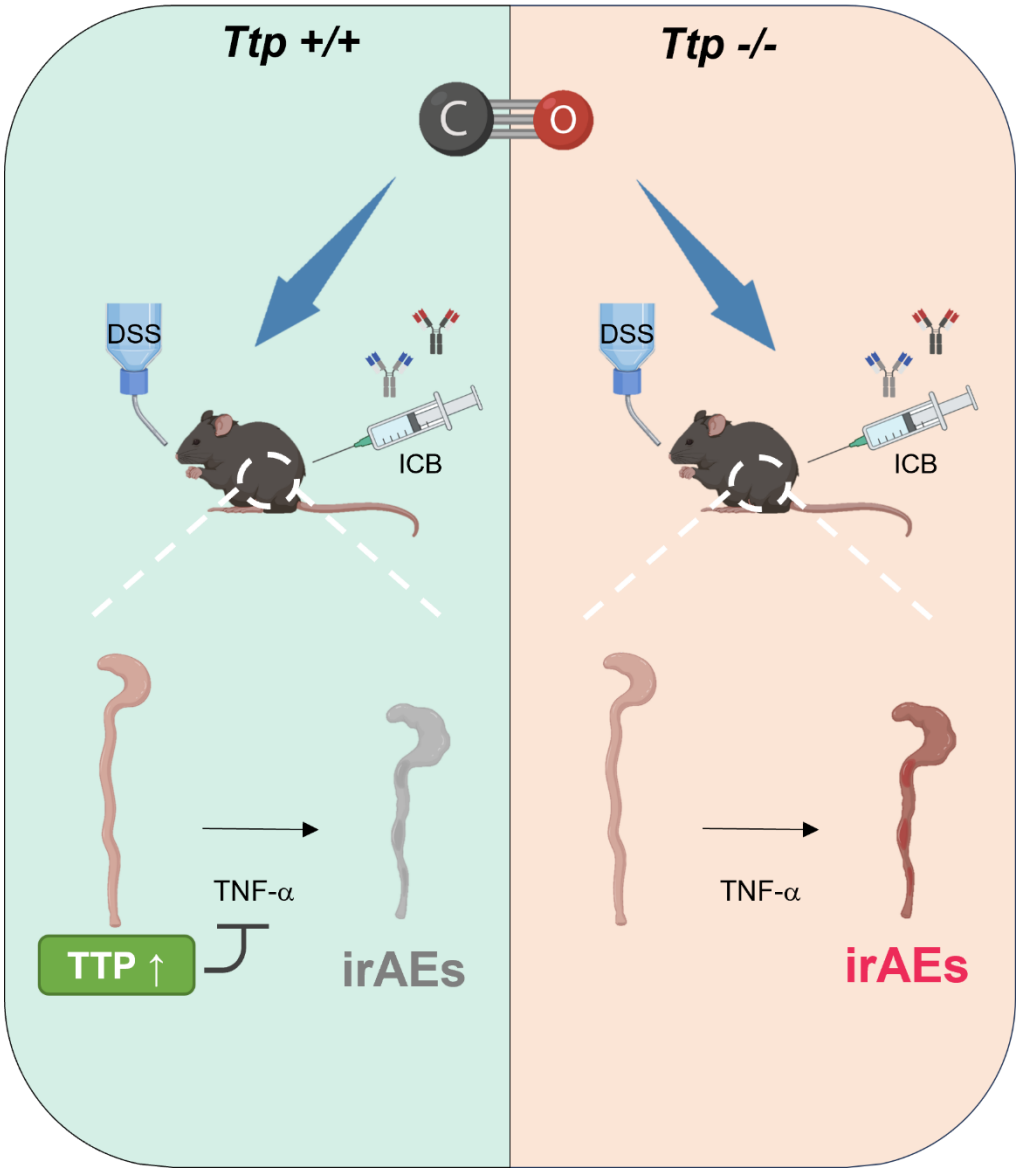

Schematic figure 1. CO-induced TTP protects against ICB-induced irAEs. TTP, increased by inhalation of CO, ameliorates ICB-induced irAEs by reducing levels of TNF-α in colon and liver. The absence of TTP increased the severity of irAEs and eliminated the protective effects of CO on irAEs. Thus, the protective effects of CO on irAEs depend on TTP expression.

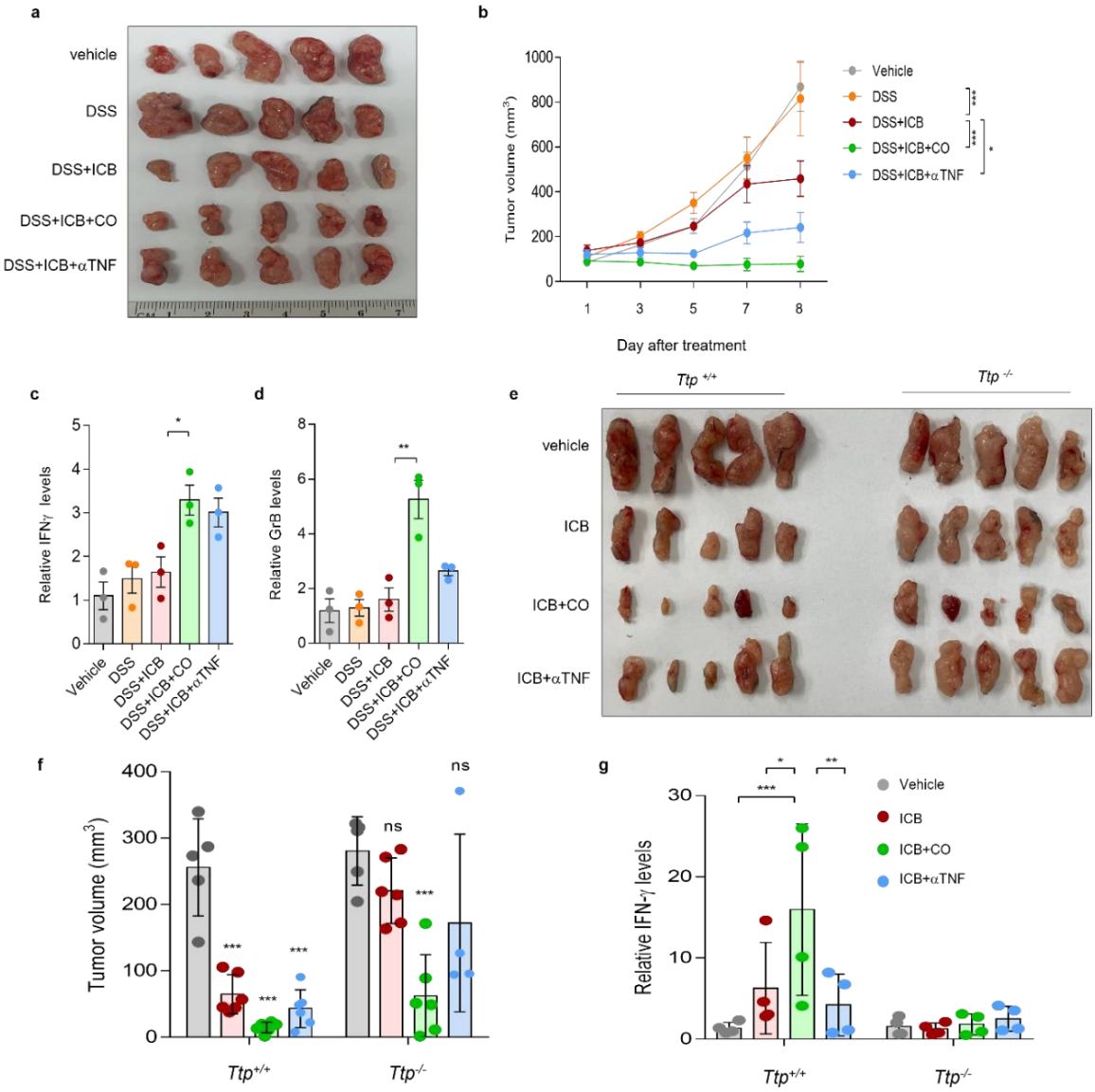

Figure 3. TTP is required for CO-induced antitumor effects. (a) Representative image of tumor tissues. (b) Mean tumor size during experimental period. (c-d) The mRNA levels of IFN-γ (c) and GrB (d) mRNA in tumor tissues. To investigate whether the antitumor properties of CO were facilitated by TTP, $Ttp^{+/+}$ and $Ttp^{-/-}$ mice were treated with ICB, either TNF blockade or CO inhalation. (e) Representative image of the tumor tissues. (f) Mean tumor volume. (g) The levels of mRNA expression of IFN-γ in tumor tissue. Data represent mean ± SD; *p<0.05, **p<0.005, ***p<0.001, ns: not significant.

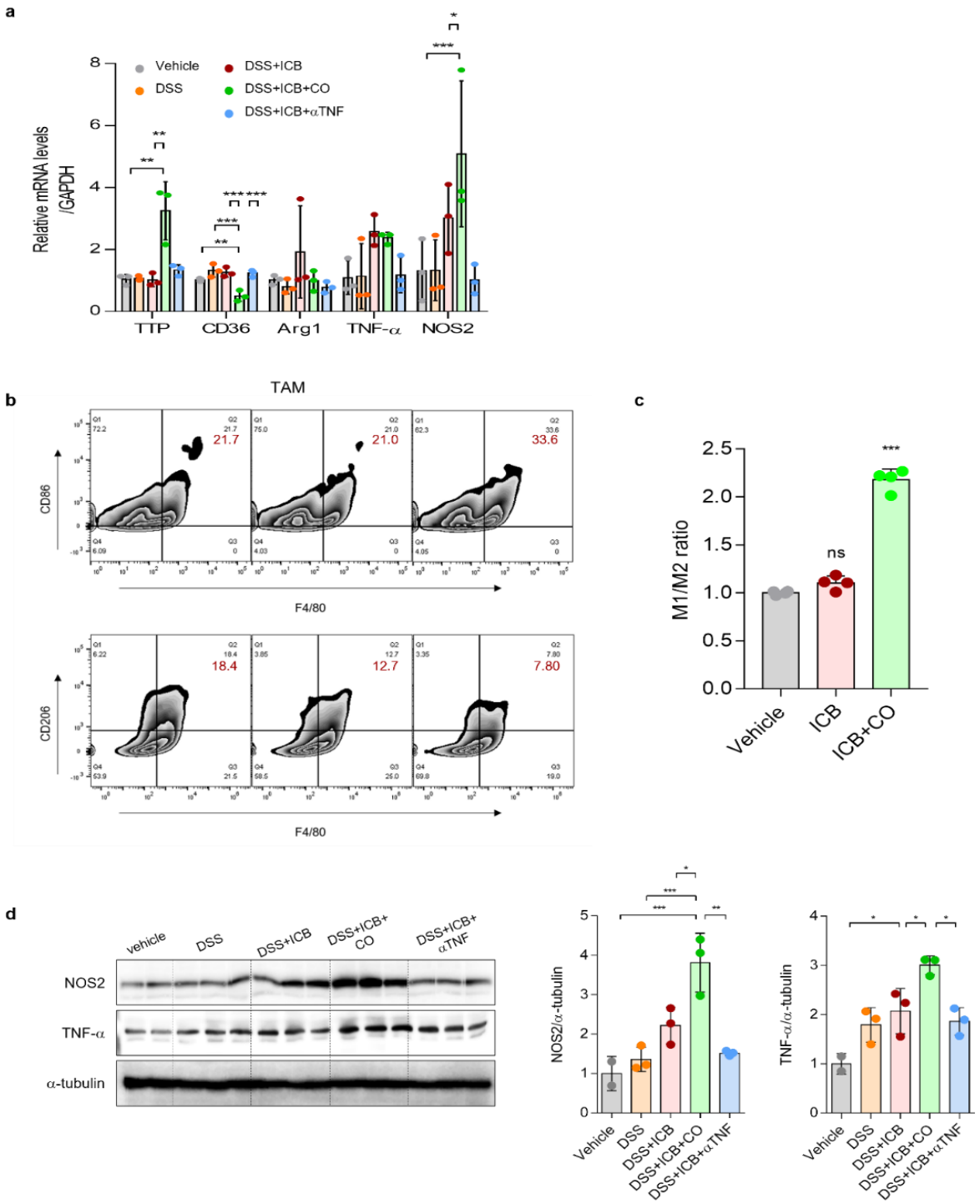

Figure 4. CO decreases M2-TAM in tumor tissues. (a) The mRNA levels of TTP, CD36, Arg1, TNF-α, and NOS2 were quantified by using real-time Q-PCR. (b) The CD86+F4/80+ or CD206+F4/80+ cell population of TAM was isolated by magnetic-activated cell sorting

(MACS) in the tumor tissue. (c) M1/M2 ratio. (d) The protein expression levels of NOS2 and TNF-α in tumor tissue. Data represent mean ± SD; *p<0.05, **p<0.005, ***p<0.001, ns: not significant.

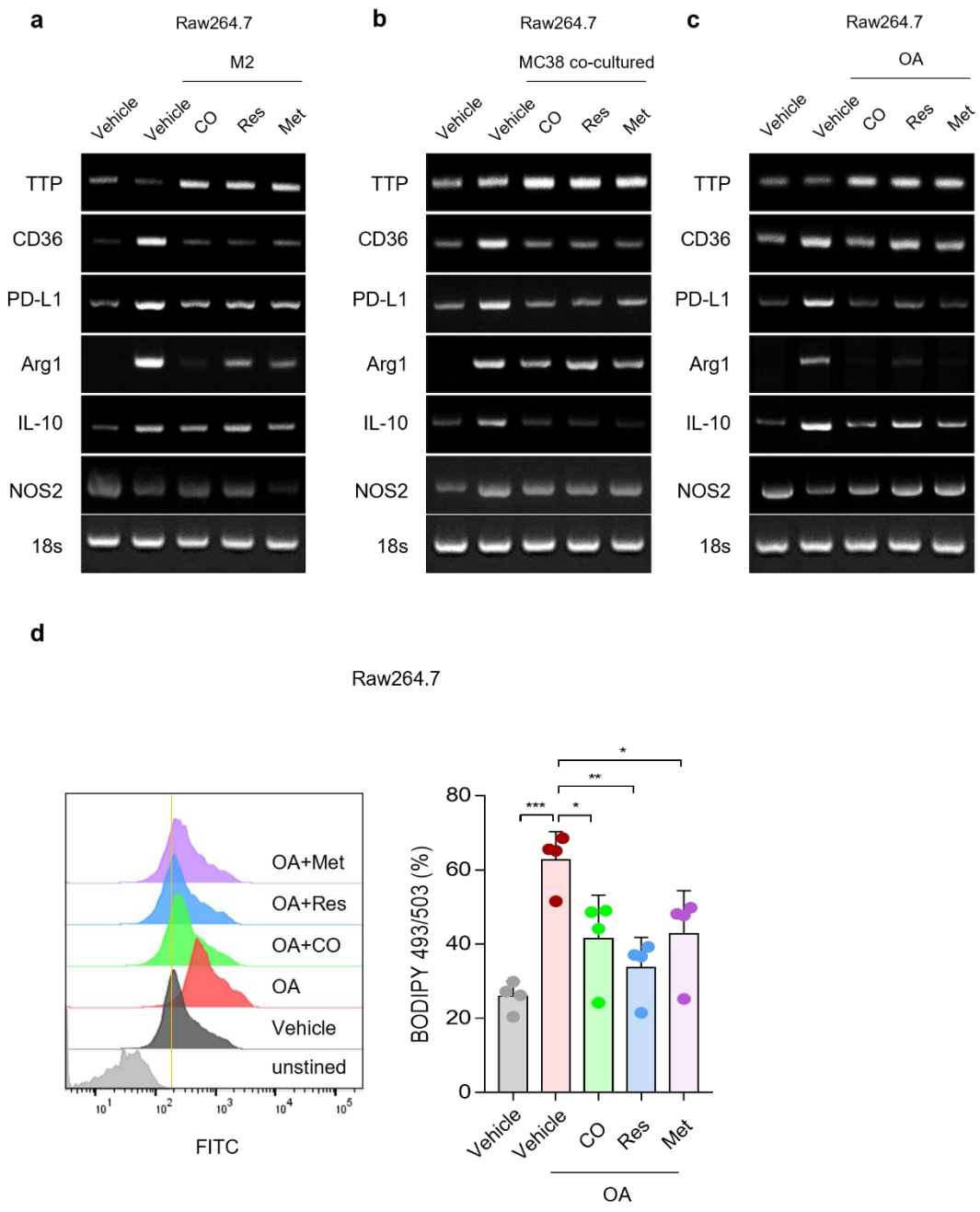

Figure 5. TTP reduces macrophage M2 polarization. To investigate the effect of TTP on M2 polarization, Raw264.7 cells were incubated with mIL-4 (10 ng/mL) and mIL-13 (10 ng/mL). Prior to treatment of mIL-4 and mIL-13, TTP inducers including CORM2 (20 μM), Res (1 μM) or Met (2 mM) were incubated for a duration of 1 h. (a) mRNA levels of TTP, CD36, PD-L1, Arg1, IL-10, and NOS2 were measured in M2-polarized Raw264.7 cells using RT-PCR. (b) To

investigate the roles of TTP on macrophages within TME, Raw264.7 cells were co-cultured with MC38 mouse colorectal cancer cells or treated with OA (100 mM). Prior to treatment of OA, TTP enhancers including CORM2 (20 μM), Res (1 μM) or Met (2 mM) were administered for a duration of 1 h. (b) The mRNA levels of TTP, CD36, PD-L1, Arg1, IL-10, and NOS2 were measured in Raw264.7 cells cocultured with cancer cells using RT-PCR. (c) The mRNA levels of TTP, CD36, PD-L1, Arg1, IL-10, and NOS2 levels in Raw264.7 cells treated with OA, measured by RT-PCR. (d) Lipid uptake levels in Raw264.7 cells treated with OA. Data represent mean ± SD; *p<0.05, **p<0.005, ***p<0.001.

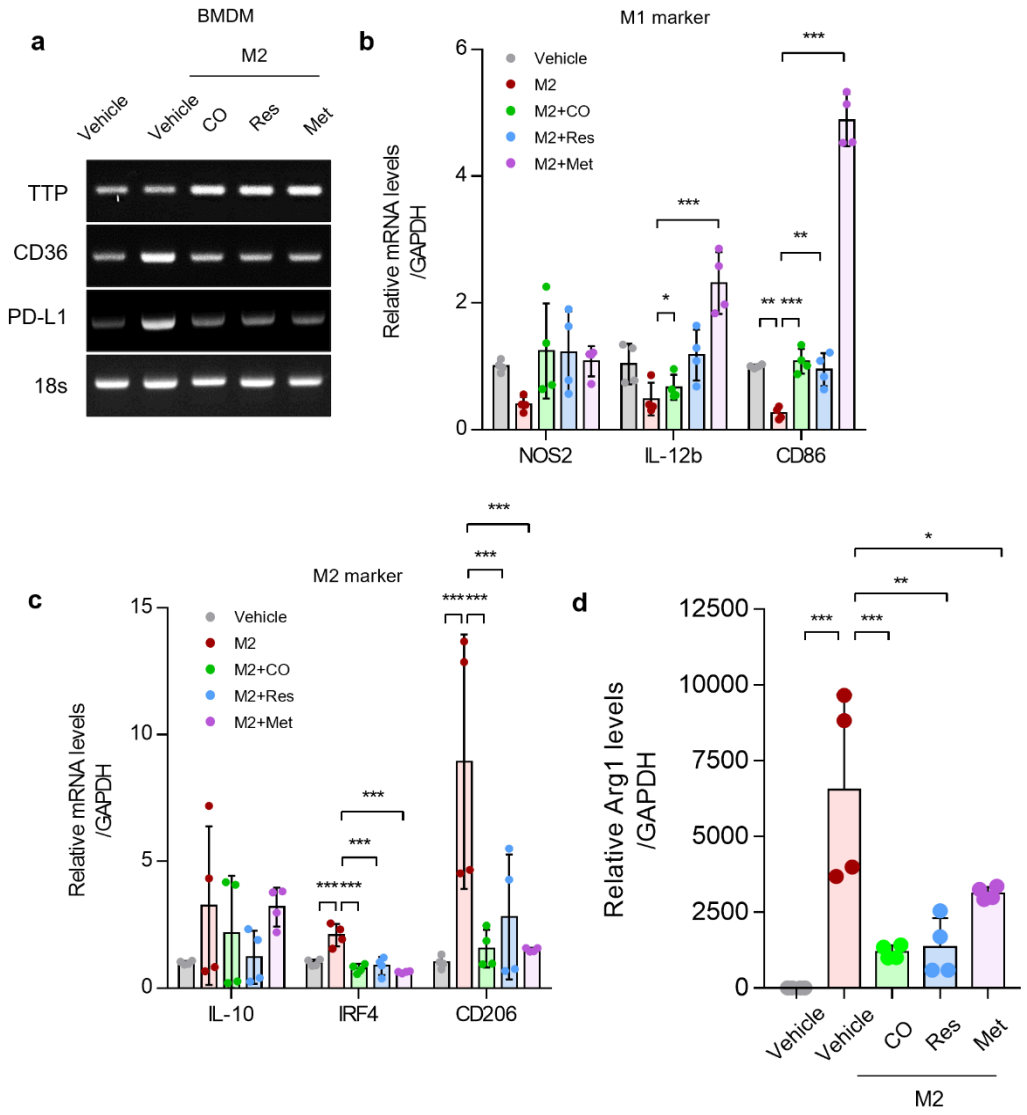

Figure 6. TTP induces macrophage M1 polarization. To investigate the effect of TTP on the polarization of macrophages, BMDM cells were treated with TTP inducers for 1 h prior to M2 polarization. (a) mRNA levels of TTP, CD36, and PD-L1 were measured in M2-polarized BMDM using RT-PCR. (b) The mRNA levels of M1 polarization markers, including NOS2, IL-1b, and CD86, were evaluated in M2-polarized BMDM. (c, d) The mRNA levels of IL-10, IRF4, and CD206 (c) and Arg1 (d) were evaluated in M2-polarized BMDM. Data represent mean ± SD; *p<0.05, **p<0.005, ***p<0.001, ns: not significant.

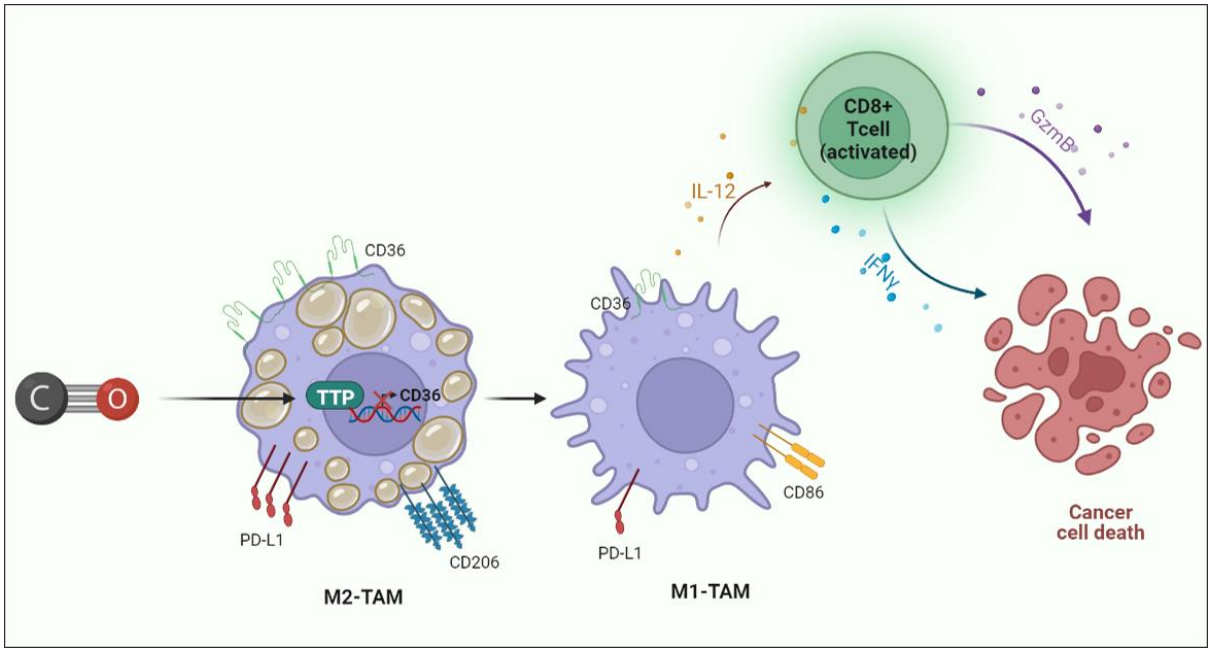

Schematic figure 2. CO-induced TTP enhances immune response by reprogramming macrophages. TTP induced by CO leads to the degradation of CD36 mRNA in M2-TAM. Decrease in CD36 levels reprograms M2-TAM to M1-TAM. As a result, the anti-tumor response was increased by activating CD8+ T cells. Therefore, TTP could be a promising target for cancer therapy.

I-VI DISCUSSION

Immune checkpoint blockade has emerged as a promising approach for enhancing the host immune system to target cancer cells in patients with cancer[1]. Combined anti-CTLA-4 and anti-PD-1 blockade therapy has been shown to improve the response rate in patients compared with monotherapy[6]. However, it is noteworthy that more than 50% of patients experienced serious immune-related adverse events (irAEs)[2-9,41,42] The dose-limiting toxicity of ICB has hindered its use in clinical settings, highlighting the necessity to gain a better understanding whether its toxicities can be dissociated from its efficacy[9].

ICB can lead to irAEs that affect various organs. In cases of irAEs which are severe or resistant to steroids, second-line agents such as TNF blockade with infliximab are recommended[6,9-13,42-44]. Vedolizumab[45], mycophenolate mofetil (MMF)[46,47], calcineurin inhibitors (tacrolimus and cuclosporine)[48-50], and tocilizumab[48] have also been reported to treatment irAEs[18]. TNF inhibitors frequently employed in the management of inflammatory autoimmune disorders, including rheumatoid arthritis, spondyloarthropathies, and inflammatory bowel disease (IBD)[10]. Colitis is one of the most common and challenging irAEs linked to ICB therapy[6,43].

In our previous study, we demonstrated the effect of TTP on inflammatory autoimmune diseases. The TTP knockout mouse model exhibited heightened vulnerability to colitis, reduced colon length, and an upregulation of pro-inflammatory cytokines and chemokines, including TNF-α, IL-6, CXCL1, and CXCL2, in the mucosa of the large intestine[51]. Therefore, it can be inferred that the absence of TTP in mice may lead to the impairment of their capacity to suppress the production of inflammatory cytokines upon experiencing colon tissue injury, ultimately exacerbating colitis. Given that inflammatory cytokines have been observed in both

animal models of colitis[52] and human IBD[53], it is plausible to hypothesize that a reduction of level and/or activity of TTP in patients with ulcerative colitis could result in impaired resolution of intestinal inflammation and worsened symptoms of IBD. Previous studies have reported that CORM exhibits the protective effects against colitis induced by DSS[15,20]. The aggravated colitis observed in TTP KO mice prompted us to investigate the potential of CORM in mitigating DSS-induced colitis in TTP wild-type mice. Consistent with previous findings[15,20], our observations indicate that CO mitigates DSS-induced colitis by inhibiting the production of inflammatory cytokines in mice with wild-type TTP gene expression[15].

Previous research has indicated that CO may have therapeutic benefits for autoimmune diseases by increasing the levels of TTP. Our study aimed to investigate the potential therapeutic effects of CO in ICB-induced irAEs (Fig. 1). Furthermore, CO enhances the anti-tumor effect of ICB by augmenting the activity of CD8+ T cells and reducing the infiltration of M2-TAM in the tumor microenvironment (Fig. 3 and 4). The findings of this study indicate that combining CO and ICB therapy may have synergistic therapeutic effects. It is noteworthy that the observed synergistic therapeutic effects are weakened in the absence of TTP (Fig. 3). Numerous studies have demonstrated a positive correlation between elevated CD36 expression and the infiltration of protumoral M2-type macrophages, resulting in the formation of a highly immunosuppressive TME[26]. According to Xiao-Yan Dai et al[36]., TTP can bind to the 3'UTR of CD36 mRNA, thereby causing destabilization of the CD36 mRNA[36]. Based on the gathered evidence, it was observed that CO-induced TTP leads to a reduction in CD36 mRNA expression in both tumor tissue and macrophages (Fig. 4, Fig. 5 and 6). Furthermore, it has been observed that TTP downregulates the M2 phenotype of macrophages, leading to a shift towards the M1-like phenotype of macrophages (Fig. 5 and 6). Intratumoral macrophages

exhibit increased lipid accumulation and promote the utilization of fatty acids to fuel mitochondrial oxidative phosphorylation by upregulating CD36[26,28,29]. We observed that treatment with OA resulted in an increase of CD36 expression and lipid uptake, which were attenuated by an increase of TTP (Fig. 5 and 6). Additionally, the levels of CD36 expression and immunosuppressive molecules were elevated in macrophages that were co-cultured with cancer cells. The data presented in this study suggest that the metabolic shift observed in cancer, as well as its metabolites, plays an important role as a crucial mediator of macrophage functional changes within the TME[26,29]. As a result, TTP destabilizes CD36 mRNA in M2 macrophages. Thus, targeting TTP could potentially serve as a therapeutic strategy for cancer treatment by dissociating the toxicity and efficacy of ICB therapy.

I-VII CONCLUSION

In summary, the findings of our study suggest that TTP plays an inhibitory role in the development of immune checkpoint blockade (ICB)-induced immune-related adverse events (irAEs), specifically colitis and hepatitis, while also enhancing the efficacy of ICB. The levels of TTP were found to be increased by CO in the colon and liver tissues of mice treated with ICB. CO-induced TTP plays a significant role as a mediator in irAEs. Additionally, inhalation of CO increased TTP levels in the tumor tissue, while reducing the levels of CD36. The decrease of CD36 levels leads to functional phenotypic changes of M2-TAM. As a result, the activity of M1-TAM and CD8+ T cells were increased. Our findings suggest that TTP could be a promising therapeutic target, as it effectively decouples the anti-tumor efficacy and toxicity of ICB.

I-VIII REFERENCES

1 Hansen, E. D., Wang, X., Case, A. A., Puzanov, I. & Smith, T. Immune Checkpoint Inhibitor Toxicity Review for the Palliative Care Clinician. *J Pain Symptom Manage* **56**, 460-472, doi:10.1016/j.jpainsymman.2018.05.015 (2018).

2 Wolchok, J. D., Rollin, L. & Larkin, J. Nivolumab and Ipilimumab in Advanced Melanoma. *N Engl J Med* **377**, 2503-2504, doi:10.1056/NEJMc1714339 (2017).

3 Motzer, R. J. *et al.* Nivolumab plus Ipilimumab versus Sunitinib in Advanced Renal-Cell Carcinoma. *N Engl J Med* **378**, 1277-1290, doi:10.1056/NEJMoa1712126 (2018).

4 Hellmann, M. D. *et al.* Nivolumab plus Ipilimumab in Lung Cancer with a High Tumor Mutational Burden. *N Engl J Med* **378**, 2093-2104, doi:10.1056/NEJMoa1801946 (2018).

5 Wolchok, J. D. *et al.* Nivolumab plus ipilimumab in advanced melanoma. *N Engl J Med* **369**, 122-133, doi:10.1056/NEJMoa1302369 (2013).

6 Perez-Ruiz, E. *et al.* Prophylactic TNF blockade uncouples efficacy and toxicity in dual CTLA-4 and PD-1 immunotherapy. *Nature* **569**, 428-432, doi:10.1038/s41586-019-1162-y (2019).

7 Larkin, J., Hodi, F. S. & Wolchok, J. D. Combined Nivolumab and Ipilimumab or Monotherapy in Untreated Melanoma. *N Engl J Med* **373**, 1270-1271, doi:10.1056/NEJMc1509660 (2015).

8 Conroy, M. & Naidoo, J. Immune-related adverse events and the balancing act of immunotherapy. *Nat Commun* **13**, 392, doi:10.1038/s41467-022-27960-2 (2022).

9 Jacoberger-Foissac, C. *et al.* Concomitant or delayed anti-TNF differentially impact on immune-related adverse events and antitumor efficacy after anti-CD40 therapy. *J*

Immunother Cancer **8**, doi:10.1136/jitc-2020-001687 (2020).

10 Chen, A. Y., Wolchok, J. D. & Bass, A. R. TNF in the era of immune checkpoint inhibitors: friend or foe? *Nat Rev Rheumatol* **17**, 213-223, doi:10.1038/s41584-021-00584-4 (2021).

11 Braaten, T. J. *et al.* Immune checkpoint inhibitor-induced inflammatory arthritis persists after immunotherapy cessation. *Ann Rheum Dis* **79**, 332-338, doi:10.1136/annrheumdis-2019-216109 (2020).

12 Hosseini, A., Gharibi, T., Marofi, F., Babaloo, Z. & Baradaran, B. CTLA-4: From mechanism to autoimmune therapy. *Int Immunopharmacol* **80**, 106221, doi:10.1016/j.intimp.2020.106221 (2020).

13 Roberts, J. *et al.* Hydroxychloroquine is a safe and effective steroid-sparing agent for immune checkpoint inhibitor-induced inflammatory arthritis. *Clin Rheumatol* **38**, 1513-1519, doi:10.1007/s10067-019-04451-2 (2019).

14 Ohwada, S., Ishigami, K., Akutsu, N. & Nakase, H. Pharmacological Treatments Available for Immune-Checkpoint-Inhibitor-Induced Colitis. *Biomedicines* **10**, doi:10.3390/biomedicines10061334 (2022).

15 Stoecklin, G. & Anderson, P. Posttranscriptional mechanisms regulating the inflammatory response. *Adv Immunol* **89**, 1-37, doi:10.1016/S0065-2776(05)89001-7 (2006).

16 Joe, Y. *et al.* Tristetraprolin mediates anti-inflammatory effect of carbon monoxide against DSS-induced colitis. *PLoS One* **9**, e88776, doi:10.1371/journal.pone.0088776 (2014).

17 Khabar, K. S. The AU-rich transcriptome: more than interferons and cytokines, and its

role in disease. *J Interferon Cytokine Res* **25**, 1-10, doi:10.1089/jir.2005.25.1 (2005).

18 Shyu, A. B. & Wilkinson, M. F. The double lives of shuttling mRNA binding proteins. *Cell* **102**, 135-138, doi:10.1016/s0092-8674(00)00018-0 (2000).

19 Taylor, G. A. *et al.* A pathogenetic role for TNF alpha in the syndrome of cachexia, arthritis, and autoimmunity resulting from tristetraprolin (TTP) deficiency. *Immunity* **4**, 445-454, doi:10.1016/s1074-7613(00)80411-2 (1996).

20 Takagi, T. *et al.* Carbon monoxide liberated from carbon monoxide-releasing molecule exerts an anti-inflammatory effect on dextran sulfate sodium-induced colitis in mice. *Dig Dis Sci* **56**, 1663-1671, doi:10.1007/s10620-010-1484-y (2011).

21 Lu, W. *et al.* Reprogramming immunosuppressive myeloid cells facilitates immunotherapy for colorectal cancer. *EMBO Mol Med* **13**, e12798, doi:10.15252/emmm.202012798 (2021).

22 Lesokhin, A. M. *et al.* Monocytic CCR2(+) Myeloid-Derived Suppressor Cells Promote Immune Escape by Limiting Activated CD8 T-cell Infiltration into the Tumor Microenvironment. *Cancer Research* **72**, 876-886, doi:10.1158/0008-5472.Can-11-1792 (2012).

23 Yang, M. *et al.* Identification of a cytokine-dominated immunosuppressive class in squamous cell lung carcinoma with implications for immunotherapy resistance. *Genome Med* **14**, 72, doi:10.1186/s13073-022-01079-x (2022).

24 Ghosh, A. *et al.* Increased p53 expression induced by APR-246 reprograms tumor-associated macrophages to augment immune checkpoint blockade. *J Clin Invest* **132**, doi:10.1172/JCI148141 (2022).

25 Xiang, X., Wang, J., Lu, D. & Xu, X. Targeting tumor-associated macrophages to

synergize tumor immunotherapy. *Signal Transduct Target Ther* **6**, 75, doi:10.1038/s41392-021-00484-9 (2021).

26 Yang, P. *et al.* CD36-mediated metabolic crosstalk between tumor cells and macrophages affects liver metastasis. *Nat Commun* **13**, 5782, doi:10.1038/s41467-022-33349-y (2022).

27 Netea-Maier, R. T., Smit, J. W. A. & Netea, M. G. Metabolic changes in tumor cells and tumor-associated macrophages: A mutual relationship. *Cancer Lett* **413**, 102-109, doi:10.1016/j.canlet.2017.10.037 (2018).

28 Su, P. *et al.* Enhanced Lipid Accumulation and Metabolism Are Required for the Differentiation and Activation of Tumor-Associated Macrophages. *Cancer Res* **80**, 1438-1450, doi:10.1158/0008-5472.CAN-19-2994 (2020).

29 Zaidi, N. E. *et al.* CD36-Fatty Acid-Mediated Metastasis via the Bidirectional Interactions of Cancer Cells and Macrophages. *Cells* **11**, doi:10.3390/cells11223556 (2022).

30 Zhang, Y. *et al.* Fatty acid-binding protein E-FABP restricts tumor growth by promoting IFN-beta responses in tumor-associated macrophages. *Cancer Res* **74**, 2986-2998, doi:10.1158/0008-5472.CAN-13-2689 (2014).

31 Xiang, W. *et al.* Monoacylglycerol lipase regulates cannabinoid receptor 2-dependent macrophage activation and cancer progression. *Nat Commun* **9**, 2574, doi:10.1038/s41467-018-04999-8 (2018).

32 Liu, C. *et al.* Treg Cells Promote the SREBP1-Dependent Metabolic Fitness of Tumor-Promoting Macrophages via Repression of CD8(+) T Cell-Derived Interferon-gamma. *Immunity* **51**, 381-397 e386, doi:10.1016/j.immuni.2019.06.017 (2019).

33 Yin, X. *et al.* PPARalpha Inhibition Overcomes Tumor-Derived Exosomal Lipid-Induced Dendritic Cell Dysfunction. *Cell Rep* **33**, 108278, doi:10.1016/j.celrep.2020.108278 (2020).

34 Ao, Y. Q. *et al.* Tumor-infiltrating CD36(+)CD8(+)T cells determine exhausted tumor microenvironment and correlate with inferior response to chemotherapy in non-small cell lung cancer. *BMC Cancer* **23**, 367, doi:10.1186/s12885-023-10836-z (2023).

35 Chen, Y. J. *et al.* Prognostic and immunological role of CD36: A pan-cancer analysis. *J Cancer* **12**, 4762-4773, doi:10.7150/jca.50502 (2021).

36 Dai, X. Y. *et al.* Intermedin inhibits macrophage foam-cell formation via tristetraprolin-mediated decay of CD36 mRNA. *Cardiovasc Res* **101**, 297-305, doi:10.1093/cvr/cvt254 (2014).

37 Gharib-Naseri, K. *et al.* Necrotic enteritis challenge regulates peroxisome proliferator-1 activated receptors signaling and beta-oxidation pathways in broiler chickens. *Anim Nutr* **7**, 239-251, doi:10.1016/j.aninu.2020.08.003 (2021).

38 Wang, H. *et al.* CD36-mediated metabolic adaptation supports regulatory T cell survival and function in tumors. *Nat Immunol* **21**, 298-308, doi:10.1038/s41590-019-0589-5 (2020).

39 Ma, X. *et al.* CD36-mediated ferroptosis dampens intratumoral CD8(+) T cell effector function and impairs their antitumor ability. *Cell Metab* **33**, 1001-1012 e1005, doi:10.1016/j.cmet.2021.02.015 (2021).

40 Chen, Y. *et al.* Pterostilbene 4'-beta-Glucoside Protects against DSS-Induced Colitis via Induction of Tristetraprolin. *Oxid Med Cell Longev* **2017**, 9427583, doi:10.1155/2017/9427583 (2017).

41 Arnaud-Coffin, P. *et al.* A systematic review of adverse events in randomized trials assessing immune checkpoint inhibitors. *Int J Cancer* **145**, 639-648, doi:10.1002/ijc.32132 (2019).

42 Smith, M. H. & Bass, A. R. Arthritis After Cancer Immunotherapy: Symptom Duration and Treatment Response. *Arthritis Care Res (Hoboken)* **71**, 362-366, doi:10.1002/acr.23467 (2019).

43 Postow, M. A. & Hellmann, M. D. Adverse Events Associated with Immune Checkpoint Blockade. *N Engl J Med* **378**, 1165, doi:10.1056/NEJMc1801663 (2018).

44 Kim, S. T. *et al.* Successful treatment of arthritis induced by checkpoint inhibitors with tocilizumab: a case series. *Ann Rheum Dis* **76**, 2061-2064, doi:10.1136/annrheumdis-2017-211560 (2017).

45 Hsieh, A. H., Ferman, M., Brown, M. P. & Andrews, J. M. Vedolizumab: a novel treatment for ipilimumab-induced colitis. *BMJ Case Rep* **2016**, doi:10.1136/bcr-2016-216641 (2016).

46 Quandt, D., Jasinski-Bergner, S., Muller, U., Schulze, B. & Seliger, B. Synergistic effects of IL-4 and TNFalpha on the induction of B7-H1 in renal cell carcinoma cells inhibiting allogeneic T cell proliferation. *J Transl Med* **12**, 151, doi:10.1186/1479-5876-12-151 (2014).

47 Mir, R., Shaw, H. M. & Nathan, P. D. Mycophenolate mofetil alongside high-dose corticosteroids: optimizing the management of combination immune checkpoint inhibitor-induced colitis. *Melanoma Res* **29**, 102-106, doi:10.1097/CMR.0000000000000543 (2019).

48 Kunogi, Y. *et al.* Refractory Immune Checkpoint Inhibitor-Induced Colitis Improved

by Tacrolimus: A Case Report. *Healthcare (Basel)* **9**, doi:10.3390/healthcare9040418 (2021).

49 Zhang, E., Kiely, C., Sandanayake, N. & Tattersall, S. Calcineurin inhibitors in steroid and anti-TNF-alpha refractory immune checkpoint inhibitor colitis. *JGH Open* **5**, 558-562, doi:10.1002/jgh3.12531 (2021).

50 Iyoda, T., Kurita, N., Takada, A., Watanabe, H. & Ando, M. Resolution of Infliximab-Refractory Nivolumab-Induced Acute Severe Enterocolitis After Cyclosporine Treatment in a Patient with Non-Small Cell Lung Cancer. *Am J Case Rep* **19**, 360-364, doi:10.12659/ajcr.908570 (2018).

51 Yan, Y. *et al.* Temporal and spatial analysis of clinical and molecular parameters in dextran sodium sulfate induced colitis. *PLoS One* **4**, e6073, doi:10.1371/journal.pone.0006073 (2009).

52 Garside, P. Cytokines in experimental colitis. *Clin Exp Immunol* **118**, 337-339, doi:10.1046/j.1365-2249.1999.01088.x (1999).

53 Autschbach, F. *et al.* Cytokine/chemokine messenger-RNA expression profiles in ulcerative colitis and Crohn's disease. *Virchows Arch* **441**, 500-513, doi:10.1007/s00428-002-0684-z (2002).

I-IX 국문 요약

항암 효과를 증가시키기 위해 CTLA-4와 PD-1과 같은 두가지 이상의 면역항암제(ICB)를 투여하면, 항암 효과가 증가함과 동시에 면역 관련 부작용 (irAEs)의 발생 비율 또한 높아지는 것으로 보고되고 있다. irAEs의 발생은 ICB의 항암 효과를 저해하므로 irAEs의 발생이 ICB 효능과 함께 나타나지 않도록 분리할 필요가 있다. 우리는 이전에 일산화탄소(CO) 투여를 통해 표적 mRNA의 AU-rich element (ARE)에 결합하는 Tristetraprolin (TTP)의 수준을 증가시켜 염증성 질환을 조절할 수 있음을 보고하였다. 본 연구에서 ICB 사용에 의해 유도된 대장염과 간염이 CO 투여에 의해 개선되는 것을 관찰할 수 있었다. TTP knock-out (TTP KO) 마우스를 사용하였을 때, ICB 사용으로 인해 유도되는 대장염과 간염이 CO를 투여하여도 대장염과 간염의 개선이 나타나지 않는 것을 확인함으로써 irAEs에 대한 CO의 효과는 TTP 의존적인 것을 확인할 수 있었다. 또한, CO의 투여가 ICB 효능을 향상시키는 것을 관찰할 수 있었다. CO에 의한 ICB의 항암 효과 증가는, 종양 미세 환경 (TME)에 존재하는 면역 억제성 종양 관련 대식세포 (M2-TAM)의 대사 적응을 저해하여 나타난다. M2-TAM의 대사 적응과 관련 있는 분자인 CD36의 발현은 TTP 증가에 의해 조절된다. 따라서, CO에 의해 증가된 TTP는 ICB의 항암 효과와 독성을 효율적으로 분리할 수 있음을 제시한다.

PART II

Activation of ROS-PERK-TFEB by filbertone ameliorates neurodegenerative disease via enhancing the autophagy-lysosomal pathway

J Nutritional Biochem. Volum 118, Agust 2023, 109325

II-I. ABSTRACT

The molecular mechanisms underlying the pathogenesis of neurodegenerative diseases such as Alzheimer's disease, Parkinson's disease [54], and Huntington's disease remain enigmatic, resulting in an unmet need for therapeutics development. Here, we suggest that filbertone, a key flavor compound found in the fruits of hazel trees of the genus *Corylus*, can ameliorate PD *via* lowering the abundance of aggregated α-synuclein. We previously reported that inhibition of hypothalamic inflammation by filbertone is mediated by suppression of nuclear factor kappa-B (NF-κB). Here, we report that filbertone activates PERK through mitochondrial ROS (mtROS) production, resulting in the increased nuclear translocation of transcription factor-EB (TFEB) in SH-SY5Y human neuroblastoma cells. TFEB activation by filbertone promotes the autophagy-lysosomal pathway (ALP), which in turn alleviates the accumulation of α-synuclein. We also demonstrate that filbertone prevented the loss of dopaminergic neurons in the substantia nigra and striatum of mice on high-fat diet (HFD). Filbertone treatment also reduced HFD-induced α-synuclein accumulation through upregulation of the ALP pathway. In addition, filbertone improved behavioral abnormalities (*i.e.*, latency time to fall and decrease of running distance) in the MPTP-induced PD murine model. In conclusion, filbertone may show promise as a potential therapeutic for neurodegenerative disease.

Keywords

α-Synuclein; Filbertone; Parkinson's disease; Reactive oxygen species; TFEB

Abbreviations

α-syn, α-synuclein; AD, Alzheimer's disease; ALP, autophagy-lysosomal pathway; ATF6, activating transcription factor 6; HD, Huntington's disease; HFD, high-fat diet; IRE1α, inositol-requiring enzyme 1α; MAMs, mitochondria-associated ER membrane; MPTP, 1-methyl-4-phenyl-1,2,3,6-tetrahydropyridine; mtROS, mitochondrial ROS; NCD, normal chow diet; PD, Parkinson's disease; PERK, PKR-like ER kinase; ROS, reactive oxygen species; SNpc, substantia nigra pars compacta; TFEB, transcription factor EB; Tg, thapsigargin; scRNA, scramble siRNA; TH, tyrosine hydroxylase; UPR, unfolded protein response.

II-II. INTRODUCTION

Neurodegenerative diseases, including Alzheimer's disease (AD), Parkinson's disease [54], and Huntington's disease [55] are caused by aging, genetic factors, brain injuries, vascular diseases, infections, and environmental factors [56,57]. PD, one of the most common neurodegenerative motor disorders, is characterized by the selective loss of dopaminergic neurons in the substantia nigra pars compacta (SNpc) [58]. In PD progression, accumulation of α-synuclein (α-syn) oligomer, representative of α-synucleinopathies, exerts neurotoxic effects through enhanced mitochondrial dysfunction and endoplasmic reticulum (ER) stress [59,60].

The ER and mitochondria engage in physical interactions, thus establishing a tight interplay between these compartments. Recently, reactive oxygen species [54] have emerged as crucial regulators of ER function and activation of the unfolded protein response (UPR). The accumulation of misfolded proteins in the ER lumen, leading to ER stress, activates the UPR to maintain ER homeostasis. The UPR signaling pathway is governed by three major ER stress sensors; PKR-like ER kinase (PERK), inositol-requiring enzyme 1α (IRE1α), and activating transcription factor 6 (ATF6) [61]. Among ER stress sensors, only PERK can regulate cerebral amyloid β (Aβ) accumulation by reducing β-secretase-1 levels and cognition deficits in AD [62,63]. PERK, a structural tether of the mitochondria-associated ER membranes (MAMs), can be activated by mitochondrial ROS (mtROS). The mtROS-PERK-ATF4 pathway promotes activation of the autophagy-lysosomal pathway (ALP), a cellular homeostatic program for the degradation of toxic aggregated proteins, which can ameliorate neurodegenerative diseases [59,64]. Deficits in the ALP promote neuronal accumulation of aggregated proteins and neurodegeneration such as found in PD, HD, and AD [65]. Transcription factor EB (TFEB), a

master regulator of the ALP, has emerged as a therapeutic target in neurodegenerative diseases [66,67].

Several natural bioactive compounds such as cinnamic aldehyde [68,69], caffeine [55], curcumin [70,71] have been shown to improve neuroinflammation and neurodegenerative impairment. The mechanisms of neuroprotective effects by these compounds involve reductions in lipid peroxidation, ER stress, inflammation, mitochondrial dysfunction, and autophagy dysfunction [72,73]. Filbertone, a key flavor compound in the fruits of hazel trees, ameliorates hypothalamic micro-mediated inflammatory responses via inhibiting the MAPK and NF-κB signaling pathways [74,75].

Based on the known neuroprotective effects of various natural compounds, we hypothesized that filbertone may improves neurodegenerative diseases by activation of the ALP. Here, we demonstrate that filbertone activates the ALP through PERK-dependent TFEB activation as the result of increasing mtROS production. Activation of ALP by filbertone reduced accumulation of α-syn in SH-SY5Y cells. In addition, in a murine model of PD, filbertone reduced α-syn accumulation and increased the expression of the autophagy and lysosome regulators LC3B and LAMP1 in the murine midbrain. Also, filbertone attenuated loss of tyrosine hydroxylase-positive, TH^+ neurons in SNpc and striatum. Finally, we suggest that filbertone may serve as a potential therapeutic to ameliorate neurodegenerative diseases. We propose a pathway by which this compound exerts neuroprotection through enhanced clearance of aggregated protein via mtROS-PERK-TFEB-dependent induction of the ALP.

II-III. MATERIALS AND METHODS

1. Reagents and Chemicals

Filbertone, PERK inhibitor GSK2606414, thapsigargin (Tg), and 1-methyl-4-phenyl-1,2,3,6-tetrahydropyridine (MPTP) were purchased from Sigma-Aldrich (St Louis, MO, USA). The mTORC1 inhibitor Torin 1 was from Tocris-Biotechne (Minneapolis, MN, USA).

2. Cell culture

The SH-SY5Y neuroblastoma cells were grown in Dulbecco's Modified Eagle medium, DMEM (Gibco, Grand Island, USA), supplemented with 10% fetal bovine serum (Gibco, Melbourne, Australia) and 1% penicillin-streptomycin solution (Gibco, Grand Island, USA). *Perk*$^{+/+}$ and *Perk*$^{-/-}$ mouse embryonic fibroblasts (MEFs) were cultured in DMEM supplemented with 1% MEM non-essential amino acid (Gibco). *Ire1α*$^{+/+}$, *Ire1α*$^{-/-}$, *Atf6α*$^{+/+}$, and *Atf6α*$^{-/-}$ mouse hepatocytes, which were kindly provided by Dr. S. H. Back (University of Ulsan, Ulsan, Korea), were maintained in medium 199, with 1% MEM non-essential amino acid solution. Cells were grown in humidified incubators, at 37℃ with 5% CO_2.

3. Mice

Seven-week-old male C57BL/6 wild-type mice were purchased from Koatech (Pyeongtaek, South Korea). Animals were grown in a specific pathogen-free facility with 12h light-dark cycle at 18–24°C and 40–70% humidity. Animal studies were approved by the University of Ulsan Animal Care and Use Committee. To establish high-fat diet (HFD)-induced PD murine

model, animals were randomly assigned into four dietary groups (ten per group) and fed for 16 weeks on (1) normal chow diet (NCD); [76] HFD (60% of calories from fat; Research Diets Inc., New Brunswick, NJ, USA); [77] the HFD supplemented with 0.2% filbertone (HFD + 0.2% Fil); and (4) NCD with 0.2% filbertone (NCD+0.2% Fil). After 16 weeks of feeding, the mice were sacrificed and brain tissues, as well as serum were collected. For the MPTP-induced PD model, mice were randomly assigned to four experimental groups. The normal control group and MPTP group received either vehicle or filbertone. The filbertone + MPTP group received 0.2% filbertone in vehicle once daily via oral gavage for 15 days. After oral gavage for 5 days, the MPTP and filbertone + MPTP groups received daily intraperitoneal (ip) injection of MPTP (25 mg/kg) for 5 days during the experimental period.

4. Behavioral tests

Motor coordination was analyzed by the rotarod test and the treadmill running test. For the rotarod test, we used the equipment divided into 4 equal sections, allowing 4 mice to walk on the rod at the same time. For training and testing, the equipment was set in accelerating mode from 5 rpm to 50 rpm for 3 min, and each trial was rested for 30 min. The test was performed after administration of MPTP and involved automatic records of when the mouse fell from the rotarod. The cutoff time was set at 3 min. In the treadmill test, before testing, the mice were adapted at 5 m/min for 3 min. After adaptation, speed was increased from 1 m/min to 10 m/min for 3 min, and each trial was rested for 30 min. When mice reached exhaustion, the time was noted.

5. Western blot

Cell pellets and brain tissues were lysed using prepared RIPA buffer (Thermo Scientific, Waltham, MA, USA) containing phosphatase and protease inhibitors (Sigma-Aldrich), and the total protein concentration was determined by BCA protein assay reagents (Pierce Biotechnology, Rockford, IL, USA) using bovine serum albumin (BSA) as the standard. Samples were boiled at 95℃ in 2X Laemmli buffer (Bio-Rad, Hercules, CA, USA) for 5 min. Protein were resolved by SDS-PAGE and transferred to polyvinylidene difluoride membrane (Millipore, Burlington, MA, USA). The membrane was blocked with 5% nonfat milk (BD bioscience, San Jose, CA, USA) in phosphate buffered saline-Tween 20 (PBS-T), and then the membrane was incubated with primary antibodies as follows: p-PERK (1:1000, Signalway antibody, Baltimore, MD, USA), PERK (1:1000, Cell Signaling, Danvers, MA, USA), p-eIF2α (1:1000, Cell Signaling), eIF2α (1:1000, Cell Signaling), ATF4 (1:1000, Cell Signaling), TFEB (1:1000, Bethyl Laboratories, Montgomery, TX, USA), PARP (1:2000, Cell Signaling), LC3B (1:2000, Novus Biologicals, Centennial, CO, USA), p62 (1:10000), LAMP1 (1:1000, Abcam, Cambridge, MA, USA), TH (1:1000, Cell signaling), α-synuclein (1:2000, Cell Signaling), α-tubulin (1:2000, Cell Signaling), and β-actin (1:2500, Thermo Scientific). These were incubated overnight at 4℃. Membranes were washed with 1X PBS-T 3 times 10 min and incubated with HRP-conjugated secondary antibodies. Chemiluminescence signals were read using an Azure Biosystems C300 analyzer (Azure Biosystems, Dublin, CA, USA) with an ECL substrate (Pierce Biotechnology).

6. Measurement of mitochondrial ROS

SH-SY5Y cells were treated with filbertone (20 μM) for 0.5 h in the presence or absence of 100 nM Mito-TEMPO (Sigma-Aldrich). After treatment, cells were stained with 5 μM MitoSOX Red (Invitrogen, Carlsbad, CA, USA) at 37℃ for 30 min. For flow cytometry analysis, cells were trypsinized and then washed three times with 1X PBS. mtROS were detected by using a FACSCanto flow cytometry system (BD Bioscience, CA, USA). Fluorescence intensities were analyzed with FlowJo software (Tree Star). For confocal microscopy, cells were fixed with formalin solution for 30 min and then washed three times with 1X PBS. The cells were stained with DAPI (Invitrogen). Samples were visualized by using an Olympus FV1200 confocal microscope (Olympus, Tokyo, Japan).

7. Real-time quantitative RT-PCR

Total RNA was isolated from cells and mid-brain using by QIAzol Lysis reagent (QIAGEN, CA, USA), according to the manufacturer's instructions. 2 μg of total RNA was used to synthesize cDNA using oligo (dT) primers (BIONICS, Daejeon, Korea) and M-MLV reverse transcriptase (Promega). To analyze real-time quantitative PCR (RT-qPCR), the synthesized cDNA was amplified with SYBR Green qPCR Master Mix on an ABI 7500 Fast Real-Time PCR System (Applied Biosystems, CA, USA). The following qRT-PCR primers were human GAPDH (f-caatgacccttcatcctc, r-agcatcgccccacttgatt), human CTSB (f-agtggagaatggcacacccta, r-aagagccattgtcacccca), human LAMP1 (f-cgtacctttccaacagcagc, r-cgctcacgttgtacttgtcc), human MCOLN1 (f-gagtgggtgcgacaagtttc, r-tgttctcttcccggaatgtc), human TPP1 (f-gatcccagctctcctcaatac, r- gccatttttgcaccgtgtg), mouse GAPDH (f-cggcctcaccccatttg, r-gggaagcccatcaccatct), mouse MCOLN1 (f-gcgcctatgacaccatcaa, r-

tatcctggactgctcgat), mouse TPP1 (f-aagccaggcctacatactcaga, r-ccaagtgcttcctgcagtttaga), mouse LAMP1 (f-taatggccagcttctctgcctcctt, r-aggctggggtcagaaacattttctt).

8. Transfection

pEGFP-N1-TFEB and α-Syn-A53T were purchased from Addgene (Watertown, MA, USA), and cells were transfected using the Lipofectamine™ 2000 in accordance with the manufacturer's protocol (Invitrogen). To knockdown the genes of *Tfeb*, SH-SY5Y cells were transfected with scramble siRNA (scRNA) (Ambion, Austin, TX, USA) and *Tfeb* siRNA (Santa Cruz Biotechnology, CA, USA) using the Lipofectamine™ 2000 (Invitrogen) method according to the manufacturer's protocol. After 36 h, cells were treated with indicated drugs.

9. Fluorescence cell imaging

SH-SY5Y cells grown on coverslips were transfected with pEGFP-N1-TFEB plasmids for 36 h and then were treated with indicated drugs. After treatment, cells were fixed with 10% formalin solution (Sigma-Aldrich) for 20 min, followed by three washes and DAPI staining. After an additional three washes, the slides were mounted with mounting medium (Sigma-Aldrich). Cells were visualized using the Olympus FV1200 confocal microscope (Olympus).

10. Immunofluorescence

To detect the α-synuclein using confocal microscopy, SH-SY5Ys were incubated on coverslips and transfected with α-syn-A53T. After treatment, the samples were fixed with 10% formalin solution (Sigma Aldrich) for 20 min. The cells were subsequently permeabilized with 0.1% Triton X-100 for 5 min and then blocked with 3% BSA for 30 min at RT. The cells were stained with anti-α-synuclein (1:500, Cell Signaling) antibodies overnight at 4℃. Alexa-Fluor 594

anti-rabbit (1:500, Invitrogen) secondary antibody was added for 2 h at RT, and then the cells were washed with 1X PBS-T followed by DAPI staining. To detect the TH in brain, brain was fixed in 10% neutral-buffered formalin solution and 10 % sucrose. Brain sections, including SNpc and Striatum, were stained with anti-TH (1:500, Cell signaling) antibodies for overnight at 4℃. Alexa-Fluor 488 anti-mouse (1:500, Invitrogen) secondary antibody was added for 2 h at RT. Images of the cells were obtained using an Olympus FV1200 confocal microscope (Olympus). The intensity of α-syn was analyzed by using ImageJ software.

11. Subcellular fractionation

After harvesting the cells, subcellular fractionation was performed according to the manufacturer's instructions using Nuclear/cytosol fractionation kit (Biovision, CA, USA). Briefly, cell pellets were resuspended with cytosolic extraction buffer A (CEB-A) and CEB-B. After 10 min, the lysates were centrifuged at 4℃ for 5 min at 16,000 X *g* in a microcentrifuge to obtain cytosolic protein containing supernatant. The remaining pellets were resuspended in nuclear extraction buffer [71] and vortexed for 15 s. This step was repeated every 10 min, for five times. Samples were centrifuged at 4° C for 10 min at 16,000 X *g* to acquire nuclear extracts. The purity of cytoplasmic and nuclear fractions was determined by western blotting using anti-α-tubulin and PARP antibodies.

12. Statistical analysis

Data were analyzed with Prism (GraphPad Software, San Diego, CA, USA). All values are expressed as means ± SD. Statistical analyses were performed using one-way ANOVA or two-way ANOVA with Tukey *post hoc* tests.

II-IV. RESULTS

1. Filbertone treatment activates the PERK-eIF2α-ATF4 pathway in SH-SY5Y human neuroblastoma cells.

Several studies have reported that the PERK branch of the UPR is a potent therapeutic target in neurodegenerative diseases [59,78,79]. In our previous study, filbertone was shown to reduce hypothalamic inflammation [75]. However, it is unclear whether filbertone can activate the PERK pathway, which is associated with amelioration of neuronal diseases. First, to investigate the effect of filbertone on the activation of the PERK pathway in SH-SY5Y human neuroblastoma cells, we treated SH-SY5Y cells with filbertone at different time points (0, 0.5, 1, 2, and 4 h) and at various concentrations (0, 5, 10, and 20 μM). As shown Fig. 1A and 1B, filbertone significantly increased PERK phosphorylation in a time- and dose- dependent manner in SH-SY5Y cells. Furthermore, downstream targets of the PERK pathway, eIF2α and ATF4, were activated by filbertone treatment (Fig. 1A and 1B). These results were similar to the effect exhibited by thapsigargin (Tg), an inhibitor of the ER Ca^{2+}-ATPase, used as a positive control (Fig. 1A and 1B). To examine whether filbertone can activate the other branches of the UPR (*i.e.,* IRE1α and ATF6), we determined the levels of ATF6 expression and IRE1α phosphorylation in filbertone-treated SH-SY5Y cells. IRE1α and ATF6 were not activated by filbertone treatment but were responsive to Tg (Fig. 1C). Together, these data suggest that filbertone can activate the PERK-eIF2α-ATF4 pathway, but not the IRE1α or ATF6 pathways.

2. PERK activation by filbertone requires mitochondrial ROS

Based on our previous studies indicating that mtROS can induce PERK activation [80-82], we sought to unravel the role of mtROS in filbertone-induced PERK activation. We first investigated whether filbertone can induce mtROS in SH-SY5Y cells. Production of mtROS was clearly induced after treatment with filbertone and by rotenone, used as a positive control for mtROS induction, as determined by increased MitoSOX staining (Fig. 2A and 2B). To determine the role of mtROS in filbertone-induced PERK activation, MitoTEMPO, a mitochondria-targeted antioxidant, was used to inhibit mtROS in SH-SY5Y cells. MitoSOX staining confirmed that filbertone-induced mtROS was attenuated in MitoTEMPO-treated cells (Fig. 2C and 2D). As anticipated, PERK phosphorylation in filbertone-treated SH-SY5Y cells was also reversed by MitoTEMPO (Fig. 2E). Together, these finding demonstrate that induction of mtROS by filbertone is required to mediate filbertone-induced PERK activation.

3. Filbertone promotes the autophagy-lysosomal pathway (ALP) in a PERK dependent manner

The PERK-eIF2α-ATF4 arm of the UPR has been implicated as a regulator of the autophagy-lysosomal pathway (ALP) [83,84]. The ALP can play an important role in the degradation of Lewy bodies [56]. To investigate whether filbertone treatment enhances the activation of autophagy in neuronal cells, SH-SY5Y cells were treated with filbertone followed by measurement of the expression levels of ALP-related proteins. As shown in the Fig. 3A, filbertone increased the conversion of LC3B-I to LC3B-II, increased LAMP1 expression, and decreased p62 expression in a dose-dependent manner. In addition, we found that the expression levels of

lysosomal genes including *LAMP1, MCOLN1, CTSB,* and *TPP1* were increased in filbertone-treated SH-SY5Y cells (Fig. 3B). To further investigate the effect of filbertone on autophagy flux, we analyzed autophagosome (yellow puncta) and autolysosome (red puncta) in SH-SY5Y cells transfected with the mCherry-EGFP-LC3 reporter. Autolysosome levels were increased by filbertone (Fig. 3C). To investigate the role of PERK in ALP induction by filbertone, we used MEF cells isolated from $Perk^{+/+}$ mice and $Perk^{-/-}$mice. The expression levels of lysosomal genes were increased by filbertone treatment in $Perk^{+/+}$ MEF cells, but not in $Perk^{-/-}$ MEF cells (Fig. 3D). However, the activation of ALP by filbertone was not affected by genetic deletion of either IRE1α or ATF6 (Fig. 3E and 3F). These results suggest that the PERK-eIF2α-ATF4 pathway is essential for induction of ALP by filbertone treatment, but not the IRE1α or ATF6 pathways.

4. PERK is required for TFEB nuclear translocation by filbertone

Previously, our studies have described that activation of the PERK-eIF2α-ATF4 pathway can prevent tissue injury through promoting the increase of TFEB nuclear translocation *in vivo* and *in vitro* [59,81]. We thus investigated whether the filbertone-induced PERK pathway can activate TFEB. Treatment with filbertone (10, 20 μM) increases TFEB nuclear translocation (Fig. 4A). Torin1, an mTORC1 inhibitor, was used as a positive control for TFEB activation (Fig. 4A). To confirm this result, we demonstrated that SH-SY5Y cells overexpressing enhanced green fluorescent protein (EGFP)-TFEB displayed an increase of TFEB nuclear translocation after treatment with filbertone (Fig. 4B). To investigate whether filbertone-induced TFEB nuclear translocation was dependent on PERK activity, we treated SH-SY5Y cells with filbertone in

the absence or presence of the PERK inhibitor, GSK2606414. Treatment with GSK2606414 prevented the nuclear translocation of TFEB that was increased by filbertone treatment (Fig. 4C). These results suggest that PERK activation is required for TFEB translocation by filbertone treatment.

5. Filbertone-induced PERK activation reduces α-syn accumulation by enhancing the TFEB-ALP axis

Activation of PERK and TFEB contributes to the amelioration of amyloid plaque in several neurodegenerative diseases, such as PD, AD, and HD [78,79,85,86]. To evaluate whether filbertone reduces α-syn accumulation, a hallmark of PD, through activation of PERK and TFEB, SH-SY5Y cells were transfected with A53T mutant α-syn plasmid and then treated with filbertone. As expected, filbertone treatment reduced α-syn levels in transfected cells (Fig. 5A). Calcineurin activation by PERK has been shown to contribute to TFEB activity [87]. We confirmed that the decrease of α-syn by filbertone was related to PERK and TFEB using a PERK inhibitor and calcineurin inhibitor. Consistent with Figure 5A, α-syn levels were decreased by filbertone. However, pretreatment with FK506 and CsA, calcineurin inhibitors, attenuated the decrease of α-syn levels in filbertone-treated cells (Fig. 5B). Furthermore, the PERK inhibitor, GSK2606414, suppressed filbertone-dependent decrease of α-syn levels, as determined by α-syn immunofluorescence staining (Fig. 5C).

Lysosomal function contributes to the degradation of α-syn [88]. To assess the effects of filbertone on lysosome function in α-syn degradation, we transfected SH-SY5Y cells with A53T mutant α-syn, followed by treatment with filbertone in the absence or presence of the

PERK inhibitor, GSK2606414. As expected, filbertone treatment led to significant increases in the expression of lysosomal genes, such as *LAMP1*, *MCOLN1*, *CTSB*, and *TPP1*, and the autophagy gene, *Beclin1* (Fig. 5D). In contrast, inhibition of PERK by GSK 2606414 resulted in decreased efficacy of filbertone with respect to induction of lysosomal and autophagy genes (Fig. 5D). Because induction of lysosomal and autophagy-related genes by filbertone is blocked by PERK inhibition, treatment with GSK2606414 prevented the reduction of α-syn by filbertone (Fig. 5E). To examine the functional significance of the PERK-TFEB-ALP axis in filbertone-induced α-syn reduction, we co-transfected SH-SY5Y cells with *siTfeb* and α-syn A53T mutant. Knock-down of *Tfeb* in SH-SY5Y cells antagonized the protective effect of filbertone on α-syn reduction (Fig. 5F and 5G). Together, these results suggest that filbertone represses the α-syn accumulation by activating the PERK-TFEB-ALP axis.

6. Filbertone exerts a neuroprotective effect in the HFD and MPTP murine models of Parkinson's disease

High-fat diet (HFD) contributes to neurological dysfunction, such as hypothalamic inflammation and Parkinson's disease risk [89-91]. In our previous study, we reported that filbertone protected against obesity-induced hypothalamic inflammation [75]. Based on these finding, we assessed whether filbertone could mitigate symptoms of PD in the HFD and MPTP-induced murine models. Consistent with previously reported results [89], the expression level of tyrosine hydroxylase (TH), a marker for dopaminergic neurons, in the midbrain of mice was decreased in HFD-fed mice substantia nigra pars compacta (SNpc) and striatum [92] (Fig. 6A). In contrast, HFD significantly increased α-syn levels in the midbrain (Fig. 6B). Filbertone

treatment restored the levels of TH and reduced α-syn expression caused by HFD (Fig. 6A and 6B). It has been previously reported that the ALP can ameliorate PD *via* the degradation of Lewy bodies [93]. Thus, to investigate whether the ALP is responsible for the enhanced degradation of α-syn by filbertone, we assessed the expression levels of autophagy- and lysosome- related proteins in the midbrain of mice. When treated with filbertone, the expression levels of autophagy and lysosomal proteins, LC3 and LAMP1, and lysosomal genes, *LAMP1*, *MCOLN1*, *CTSB*, and *TPP1*, were higher than in vehicle-treated HFD-fed mice (Fig. 6B and 6C). To validate the effects of filbertone on MPTP-induced PD model, mice were subjected to oral gavage of 0.2% filbertone for 15 days and then received MPTP for 5 days (25 mg/kg, beginning at 6 days) (Fig. 6D). The motor deficits observed in the MPTP murine model are due to significant reduction of dopaminergic nerves in the STR. In the rotarod test, the latency to fall from the rotating bar in the MPTP group was shorter than in the vehicle group, whereas filbertone treatment significantly recovered latency time to fall in mice (Fig. 6E). In the treadmill running test, filbertone treatment reversed the decrease of running distance by MPTP (Fig. 6F). These results indicated that filbertone treatment can ameliorate HFD- and MPTP- induced neuronal dysfunction, which is associated with activation of the ALP.

II-V. FIGURES

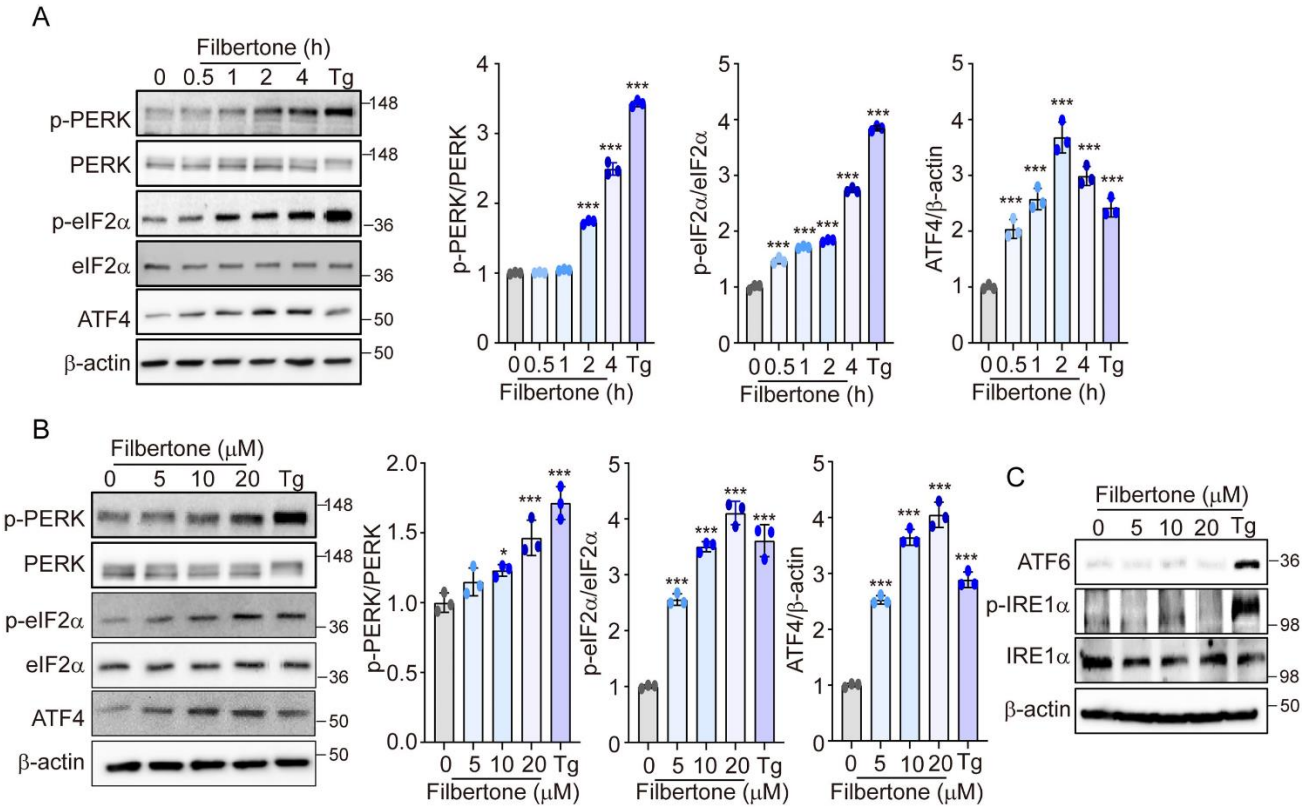

Fig. 1. Filbertone treatment activates the PERK-eIF2α-ATF4 pathway in SH-SY5Y human neuroblastoma cells. (A) SH-SY5Y cells were treated with 20 μM filbertone (0, 0.5 1, 2, and 4 h). 1 μM thapsigargin (Tg) was used as a positive control. (B, C) SH-SY5Y cells were incubated with filbertone at increasing concentrations (0, 5, 10, and 20 μM) for 4 h. (A, B) The protein expression of p-PERK, p-eIF2α, and ATF4 was detected by western blotting. (C) For analysis of the ATF6 and IRE1α pathway, the protein expression of ATF6, p-IRE1α, and IRE1α was determined by western blotting. Quantification of p-PERK, p-eIF2α, and ATF4 is shown in the right panel. Data represent mean ± SD; *p<0.05 and ***p<0.001

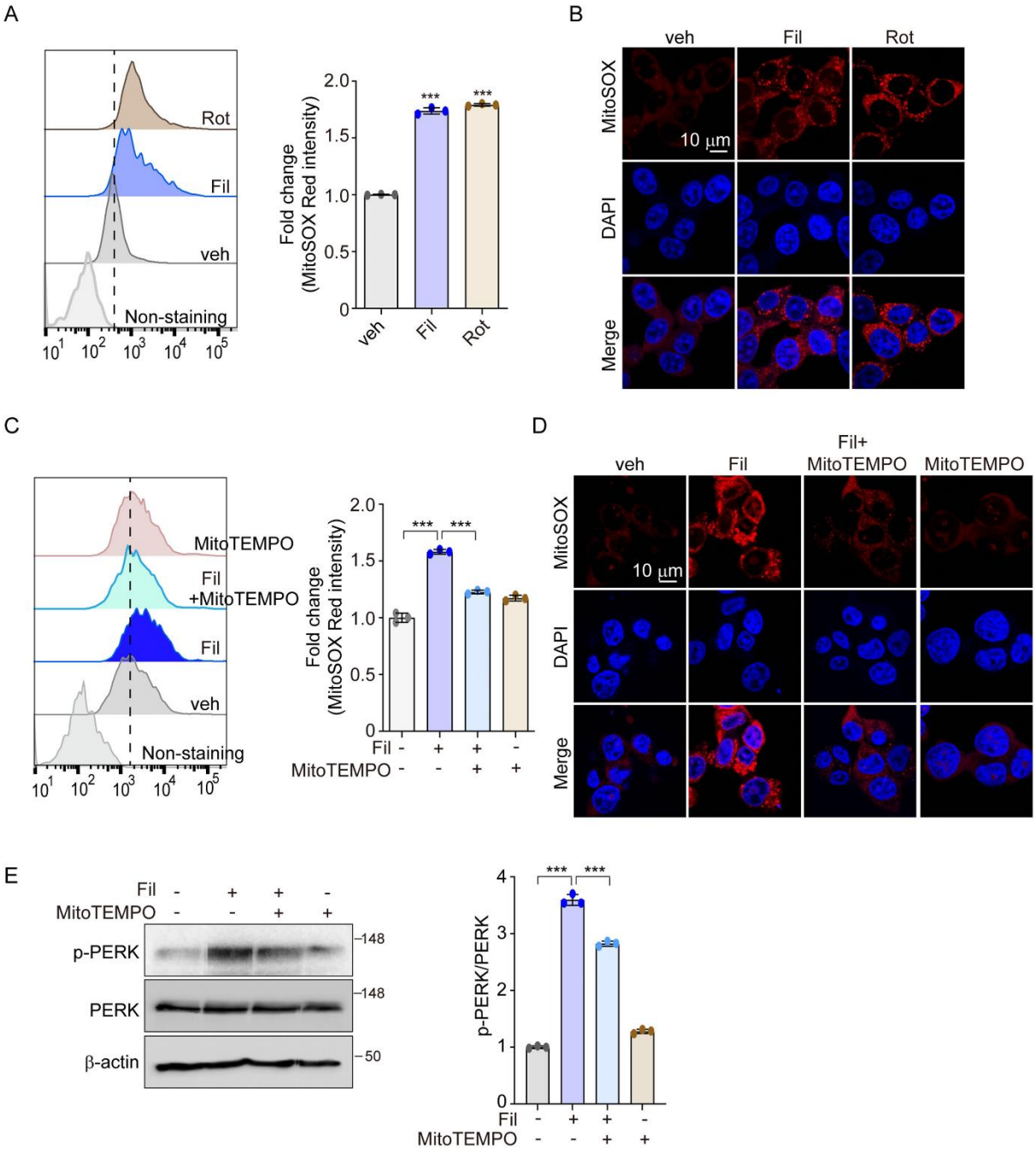

Fig. 2. PERK activation by filbertone requires mitochondrial ROS.

(A-B) To measure filbertone-induced mtROS, SH-SY5Y cells were incubated with 20 μM filbertone for 30 min. 1 μM rotenone was used as a positive control. (A) Cells were stained with MitoSOX, and then fluorescence was determined by flow cytometry. Fold changes in

MitoSOX intensity are indicated in the right panel. (B) mtROS was detected by confocal microscopy. DAPI was used for nuclear staining. Scale bar = 10 μm. (C-D) SH-SY5Y cells were pretreated with the mtROS scavenger MitoTEMPO (100 nM) for 30 min and then treated with 20 μM filbertone for 30 min. (C) MitoSOX fluorescence was analyzed by flow cytometry. Fluorescence intensity (fold change) was analyzed [94]. (D) Cells were stained with MitoSOX, followed by staining of the nuclei with DAPI. Images were obtained using a confocal microscope. Scale bar = 10 μm. (E) To investigate the association of mtROS with PERK activation, SH-SY5Y cells were exposed to 20 μM filbertone for 4 h after pretreatment with 100 nM MitoTEMPO for 30 min. The protein expression of p-PERK was detected by western blotting. Data represent mean ± SD; ***$p<0.001$.

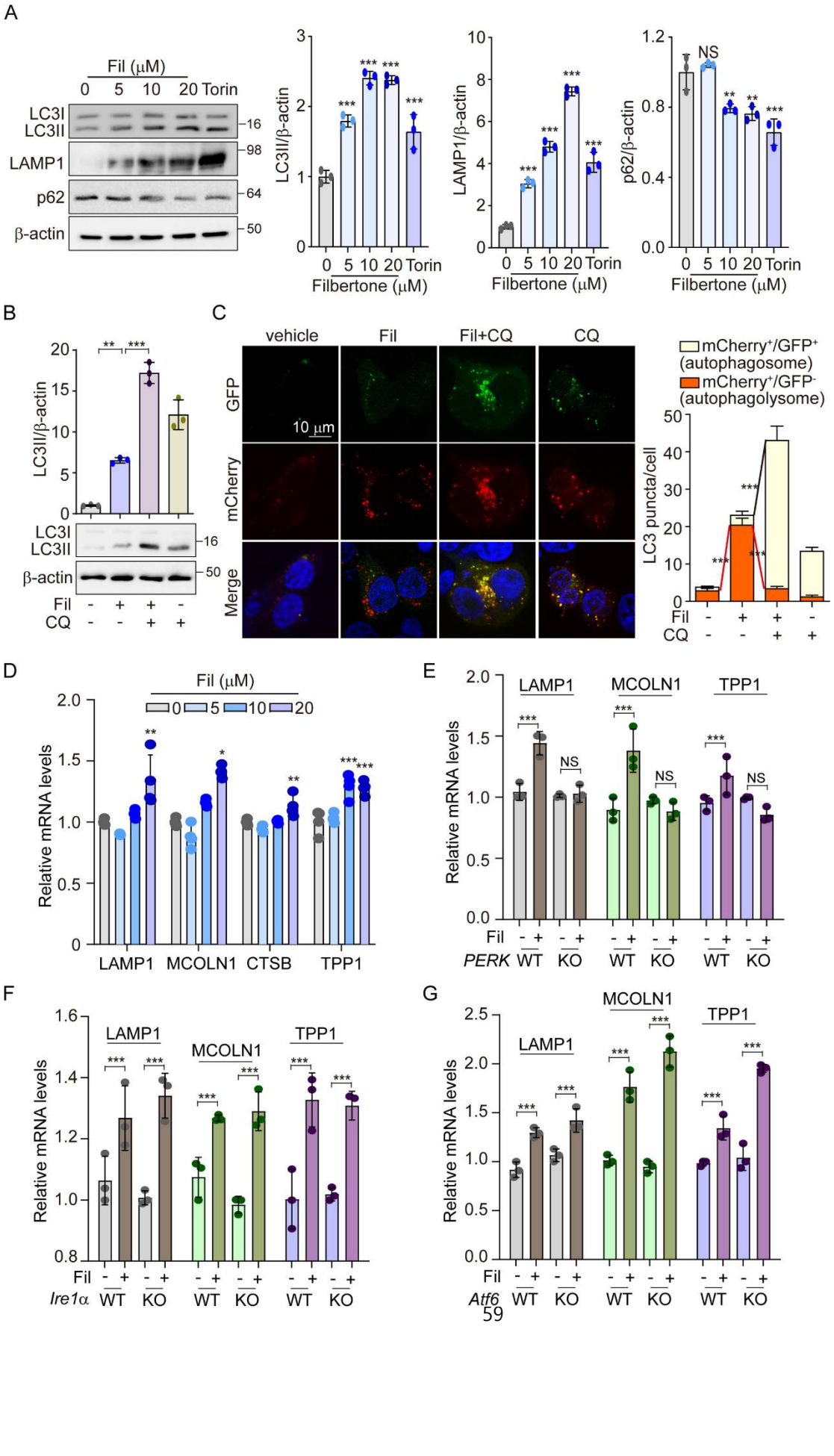
A
Fil (μM)
0 5 10 20 Torin
LC3I
LC3II
LAMP1
p62
β-actin
16
98
64
50
LC3II/β-actin
LAMP1/β-actin
p62/β-actin
NS
Filbertone (μM)
B
LC3II/β-actin
Fil
CQ
C
vehicle
Fil
Fil+CQ
CQ
GFP
mCherry
Merge
10 μm
mCherry+/GFP+ (autophagosome)
mCherry+/GFP- (autophagolysome)
LC3 puncta/cell
D
Fil (μM)
0 5 10 20
Relative mRNA levels
LAMP1 MCOLN1 CTSB TPP1
E
LAMP1 MCOLN1 TPP1
NS
PERK WT KO
F
Ire1α WT KO
G
Atf6 WT KO

Fig. 3. Filbertone promotes the autophagy-lysosomal pathway (ALP) in a PERK dependent manner. (A-B) SH-SY5Y cells were treated with filbertone (0, 5, 10, and 20 μM) for 12 h. (A) The protein expression of LC3, LAMP1, and p62 was measured by western blotting. (B) The mRNA expression of lysosomal genes, *LAMP1, MCOLN1, CTSB,* and *TPP1*, was detected by qRT-PCR. (C) SH-SY5Y cells were transiently transfected with mCherry-GFP-LC3 for 48 h and subsequently pretreated with chloroquine (CQ, 10 μM) for 1 h, and then treated with Fil (20 μM) for 4 h. Cells were observed for fluorescence of both GFP and mCherry using confocal microscopy. The number of autolysosomes ($GFP^{-}RFP^{+}$) and autophagosomes ($GFP^{+}RFP^{+}$) per cell in each condition were quantified. (D-E) $Perk^{+/+}$, $Perk^{-/-}$, $Ire1a^{+/+}$, $Ire1a^{-/-}$, $Atf6a^{+/+}$, and $Atf6a^{-/-}$ MEF cells were treated with 20 μM filbertone for 12 h. The mRNA expression of lysosomal genes, *LAMP1. MCOLN1,* and *TPP1*, were measured by qRT-PCR. Data represent mean ± SD; ***p<0.001 and NS, not significant.

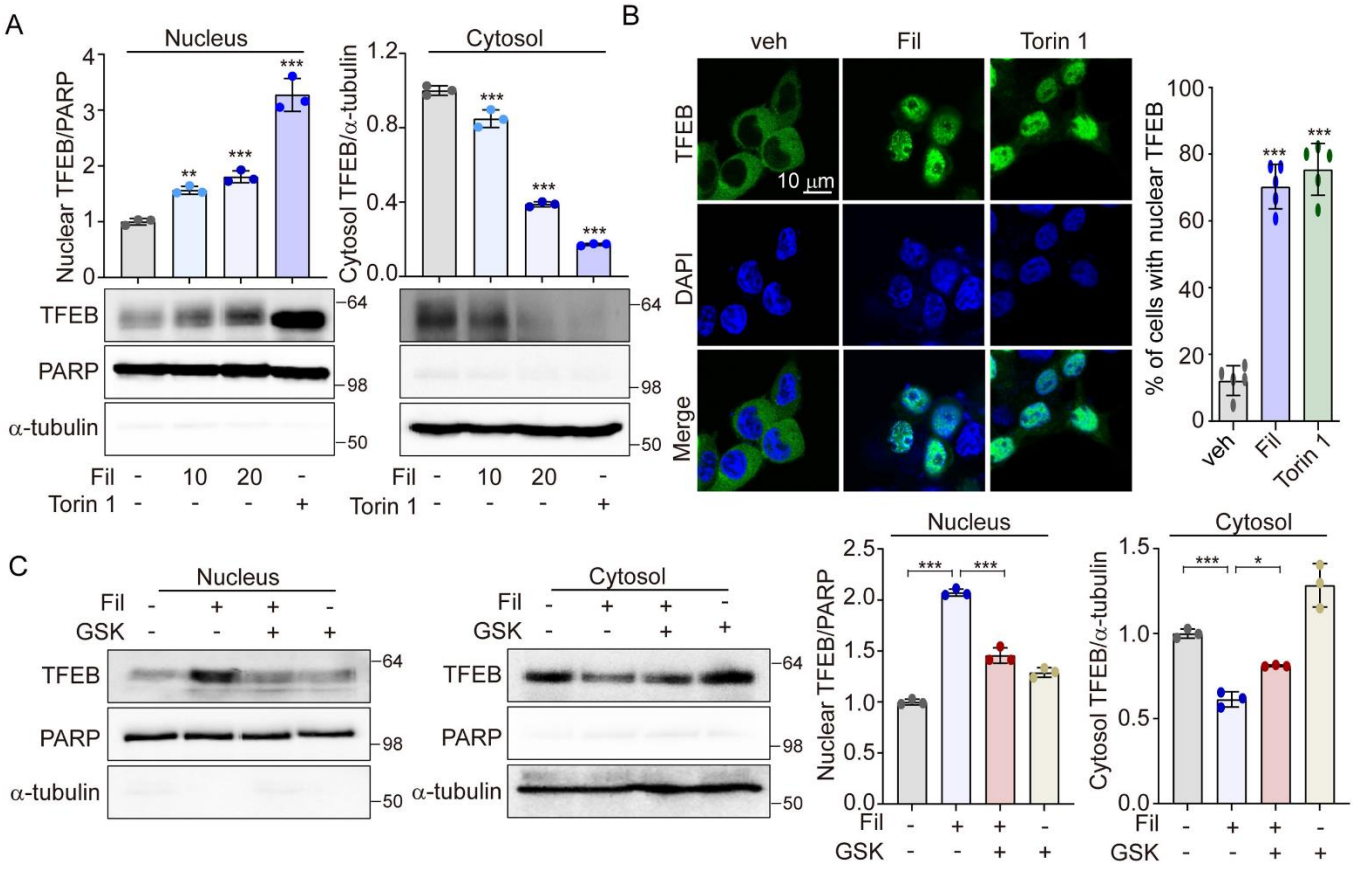

Fig. 4. PERK is required for TFEB translocation by filbertone

(A) SH-SY5Y cells were incubated with filbertone (0, 10, and 20 μM) for 3 h. Resulting fractions were then determined with antibody against TFEB. Torin (5 μM) was used as a positive control. (B) TFEB-EGFP transfected SH-SY5Y cells were treated with filbertone (20 μM). Torin (5 μM) was used as a positive control. The TFEB nuclear translocation was visualized by confocal microscopy. Scale bar = 10 μm. (C) SH-SY5Y cells were pretreated with GSK2606414, a PERK inhibitor, and then treated with 20 μM filbertone for 3 h. Measurement of TFEB nuclear translocation was performed by western blotting of nuclear and cytoplasmic extracts. Data represent mean ± SD; *p<0.05, **p<0.01, and ***p<0.001.

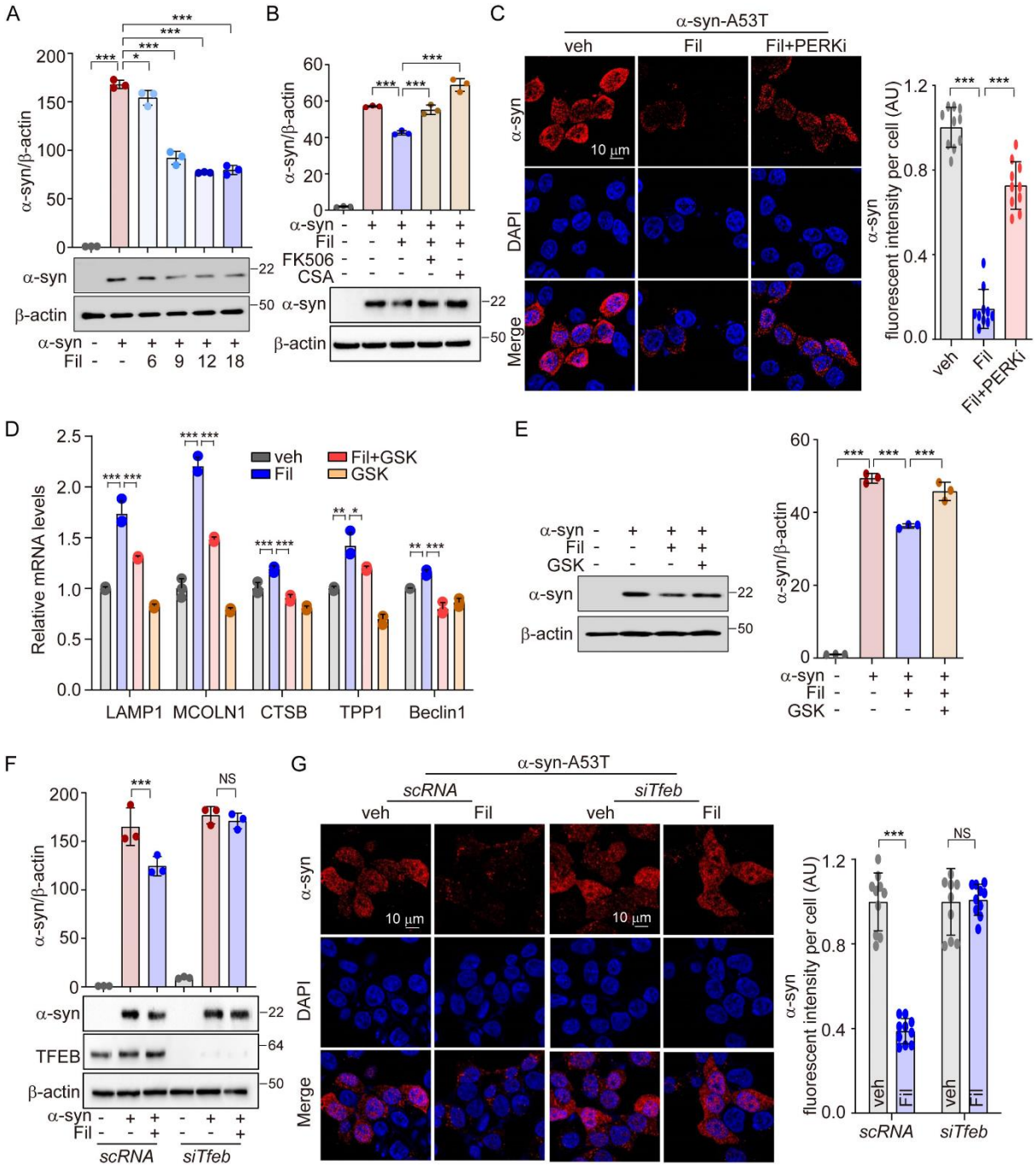

Fig. 5. Filbertone-induced PERK activation reduces α-syn accumulation by enhancing the TFEB-ALP axis.

(A) SH-SY5Y cells were transiently transfected with A53T mutant α-syn plasmid for 48 h, and the cells were treated with 20 μM filbertone (0, 6, 9, 12, and 18 h). (B) The A53T mutant α-

syn-transfected SH-SY5Y cells were treated with 20 μM filbertone for 18 h in the absence or presence of calcineurin inhibitor, FK506 and CsA. (A, B) The expression of α-syn was detected by western blotting. Quantification of α-syn expression was analyzed (*upper*). (C-E) α-syn-A53T plasmid-transfected cells were pretreated with 1 μM GSK2606414, a PERK inhibitor, for 1 h, and then treated with filbertone (20 μM) for 18 h. (C) Representative image of α-syn was detected by confocal microscopy (*left*) and quantification of α-syn intensity [94]. Scale bar = 10 μm. (D) The mRNA expression of lysosomal genes, *LAMP1. MCOLN1,* and *TPP1* and autophagy gene, *Beclin1*, were analyzed by qRT-PCR. (E) The expression levels of α-syn were determined by western blotting. Quantification of α-syn is shown in the right panel. (F, G) SH-SY5Y cells were co-transfected with α-syn -A53T and *siTfeb* for 48 h. Cells were treated with 20 μM filbertone for 18 h. (F) The protein expression of TFEB and α-syn was measured by western blotting and quantification of α-syn (*upper*). (G) Representative image of α-syn was detected by confocal microscopy (*left*) and quantification of α-syn intensity [94]. Scale bar, 10 μm. Data represent mean ± SD; ***$p<0.001$ and NS, not significant.

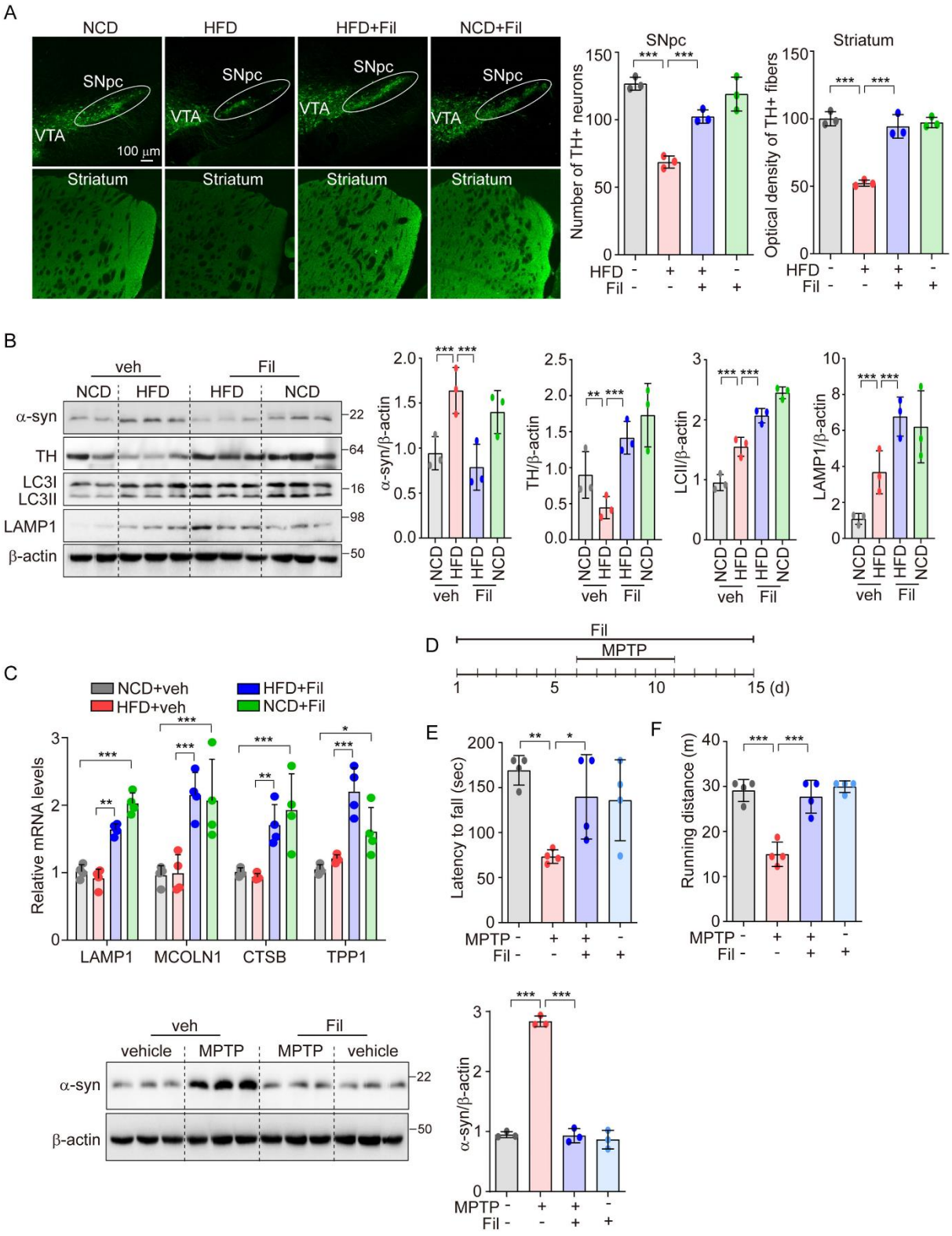

Fig. 6. Filbertone exerts a neuroprotective effect in the HFD and MPTP murine models

of Parkinson's disease

(A-C) Seven-week-old male C57BL/6 (10 mice/ group) were fed an NCD or HFD for 16 weeks with 0.2 % filbertone. (A) Immunofluorescence analysis of TH in SNpc and STR. Representative image was obtained by confocal microscopy. Scale bar = 100 μm. (B) α-syn, TH, LC3B-I/LC3B-II conversion, and LAMP1 from mouse midbrain were measured by western blotting. (C) In midbrain, the expression levels of lysosomal genes were detected by qRT-PCR. (D-F) (D) Seven-week-old male C57BL/6 (10 mice/ group) were treated with 25 mg/kg MPTP by intraperitoneal (ip) injection daily for 5 consecutive days. Mice were treated with 0.2 % filbertone for 15 days by oral administration. Behavioral response of mice in the rotarod test (E) and treadmill running test (F). Data represent mean ± SD; *p<0.05, **p<0.01 and ***p<0.001.

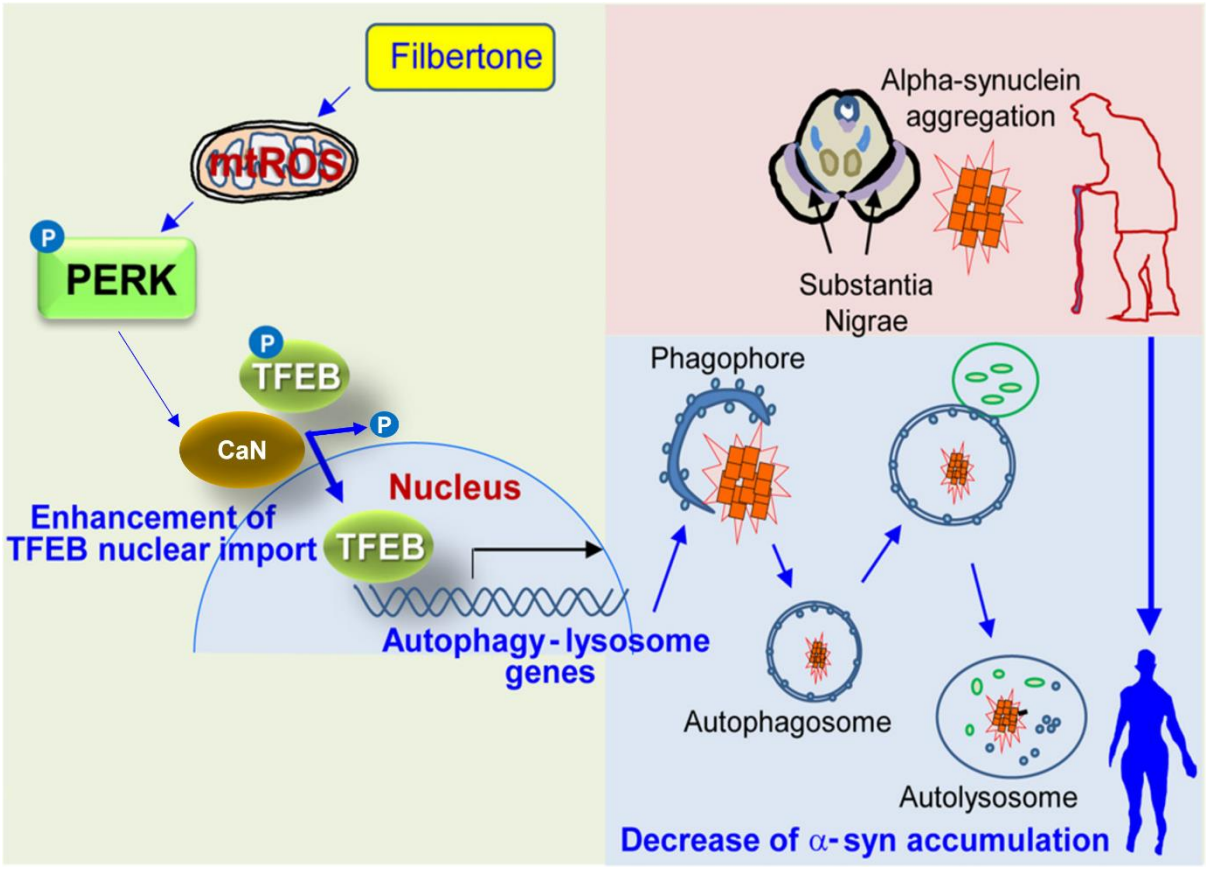

Schematic overview of the mechanisms by which filbertone ameliorates amyloidogenesis via PERK activation. PERK is activated by mitochondrial ROS (mtROS) in response to treatment with the filbertone. Activated PERK leads to increase in cytosolic Ca^{2+} levels and subsequently promotes the dephosphorylation of TEFB via calcineurin dependence. TFEB translocated into the nucleus, leading to increase transcription of autophagy-lysosome related genes. The activation of PERK increases the autophagy-lysosomal pathway (ALP), which enhances the degradation of α-synuclein in neurodegenerative disorders. Therefore, the PERK-TFEB-ALP pathway, activated by filbertone, suggests a novel target for ameliorating amyloidogenesis.

II-VI. DISCUSSION

Although the incidence and prevalence of neurodegenerative disease continues to increase, with significant contribution to the global burden of disease, the therapeutic targets and the underlying mechanisms remain unclear. Here, we revealed that ALP activation by filbertone decreases α-syn accumulation, to ameliorate the PD pathology in mice. Our previous study showed that filbertone protects against hypothalamic inflammation through activation of MAPK and NF-κB signaling pathways [75]. In addition, filbertone activates cAMP signaling, reducing lipid accumulation and body weight with reduced plasma levels of inflammatory cytokines in HFD-fed mice [75]. Given the known physiological effects of filbertone, we sought study its potential in ameliorating the progression of PD. Inhibiting the amyloidogensis via the increase of ALP is a promising strategy to protect neurodegenerative diseases such as PD [59]. Our previous study has shown that the decrease of amyloidogenesis by SB202190, a MAPK inhibitor, is promoted by mtROS-PERK activation, leading to enhanced degradation of accumulate α-syn [59]. mtROS function as redox messengers in intracellular signaling at physiologically low levels [74]. Low levels of mtROS can selectively activate PERK to preserve cellular homeostasis [80-82,95]. Among the three ER stress sensors, PERK, but not IRE-1α or ATF6, was activated by filbertone treatment. ALP-related genes, *LAMP1*, *MCOLN1*, and *TPP1* were also increased in a PERK dependent manner, but not dependent on either IRE-1α or ATF6 pathways. Beyond the canonical ER stress response, PERK can act as mitochondria-tethering molecule which is activated by mtROS [59]. PERK activation promotes the levels of autophagy and lysosomal-related genes through TFEB nuclear translocation [59]. In this study, we verified that filbertone can sensitize neuronal cells to activate the PERK-TFEB axis, alleviating α-syn

accumulation through increasing its degradation *via* ALP. Overexpression of the α-syn mutant, α-syn-A53T, caused α-syn accumulation, which was reduced by filbertone treatment. Filbertone-reduced α-syn accumulation was reversed by a PERK inhibitor and by inhibitors of calcineurin, which is known to regulate TFEB. Thus, we can conclude that filbertone activates the mtROS-PERK pathway, leading to reduction of α-syn accumulation through the increase of TFEB-ALP activation.

Metabolic syndrome [92] is coupled with a greater risk of developing PD because the increase of oxidative stress in MS caused neuroinflammation and mitochondrial dysfunction [54]. Thus, we showed that HFD-fed mice suffered PD progression and that filbertone supplementation could diminish HFD-induced TH^+ dopamine neuron loss in SNpc and decrease α-syn accumulation in mid brain. In addition, we demonstrated the protective effects of filbertone in the MPTP murine model of PD. MPTP (1-methyl-4-phenyl-1,2,3,6-tetrahydropyridin) is a mitochondrial complex I inhibitor that is known to damage the nigrostriatal dopaminergic pathway as seen in PD [96,97]. MPTP treatment caused impairment of motor function which was improved by filbertone. These findings suggest that filbertone ameliorates PD progression in HFD- or MPTP-treated mice by inhibiting α-syn accumulation via PERK-TFEB-ALP axis.

II-VII. CONCLUSION

In conclusion, our data revealed that the natural compound filbertone can confer neuroprotective effects in mice. We propose a pathway by which filbertone can induce PERK activation *via* increase of mtROS for signaling, to promote the nuclear translocation of TFEB, which in turn increases ALP. Activation of ALP by filbertone attenuated α-syn accumulation in SH-SY5Y human neuroblastoma cells. In addition, we found that HFD-induced the loss of dopamine neurons in the SNpc, which was ameliorated by filbertone treatment. Filbertone also increased autophagy-lysosomal related gene and protein expression in the mid-brain of mice on HFD. In the MPTP murine model of PD, motor dysfunction was improved by filbertone supplementation. Taken together, we suggest that filbertone may represent a novel therapeutic strategy for neurodegenerative disorders.

II-VIII. REFERENCES

1 Souza, A. *et al.* Effect of Metabolic Syndrome on Parkinson's Disease: A Systematic Review. *Clinics (Sao Paulo)* **76**, e3379, doi:10.6061/clinics/2021/e3379 (2021).

2 Kolahdouzan, M. & Hamadeh, M. J. The neuroprotective effects of caffeine in neurodegenerative diseases. *CNS Neurosci Ther* **23**, 272-290, doi:10.1111/cns.12684 (2017).

3 Beyer, K., Domingo-Sabat, M. & Ariza, A. Molecular pathology of Lewy body diseases. *Int J Mol Sci* **10**, 724-745, doi:10.3390/ijms10030724 (2009).

4 Breijyeh, Z. & Karaman, R. Comprehensive Review on Alzheimer's Disease: Causes and Treatment. *Molecules* **25**, doi:10.3390/molecules25245789 (2020).

5 Ren, H., Zhai, W., Lu, X. & Wang, G. The Cross-Links of Endoplasmic Reticulum Stress, Autophagy, and Neurodegeneration in Parkinson's Disease. *Front Aging Neurosci* **13**, 691881, doi:10.3389/fnagi.2021.691881 (2021).

6 Do, M. *et al.* PERK activation by SB202190 ameliorates amyloidogenesis via the TFEB-induced autophagy-lysosomal pathway. *Aging (Albany NY)* **14**, 1233-1252, doi:10.18632/aging.203899 (2022).

7 Shacham, T., Patel, C. & Lederkremer, G. Z. PERK Pathway and Neurodegenerative Disease: To Inhibit or to Activate? *Biomolecules* **11**, doi:10.3390/biom11030354 (2021).

8 Senft, D. & Ronai, Z. A. UPR, autophagy, and mitochondria crosstalk underlies the ER stress response. *Trends Biochem Sci* **40**, 141-148, doi:10.1016/j.tibs.2015.01.002 (2015).

9 Ma, T. *et al.* Suppression of eIF2alpha kinases alleviates Alzheimer's disease-related

plasticity and memory deficits. *Nat Neurosci* **16**, 1299-1305, doi:10.1038/nn.3486 (2013).

10 Colla, E. *et al.* Endoplasmic reticulum stress is important for the manifestations of alpha-synucleinopathy in vivo. *J Neurosci* **32**, 3306-3320, doi:10.1523/JNEUROSCI.5367-11.2012 (2012).

11 Yang, C. *et al.* A stress response p38 MAP kinase inhibitor SB202190 promoted TFEB/TFE3-dependent autophagy and lysosomal biogenesis independent of p38. *Redox Biol* **32**, 101445, doi:10.1016/j.redox.2020.101445 (2020).

12 Menzies, F. M., Fleming, A. & Rubinsztein, D. C. Compromised autophagy and neurodegenerative diseases. *Nat Rev Neurosci* **16**, 345-357, doi:10.1038/nrn3961 (2015).

13 Sardiello, M. *et al.* A gene network regulating lysosomal biogenesis and function. *Science* **325**, 473-477, doi:10.1126/science.1174447 (2009).

14 Settembre, C. *et al.* TFEB links autophagy to lysosomal biogenesis. *Science* **332**, 1429-1433, doi:10.1126/science.1204592 (2011).

15 Bae, W. Y., Choi, J. S. & Jeong, J. W. The Neuroprotective Effects of Cinnamic Aldehyde in an MPTP Mouse Model of Parkinson's Disease. *Int J Mol Sci* **19**, doi:10.3390/ijms19020551 (2018).

16 Hajinejad, M., Ghaddaripouri, M., Dabzadeh, M., Forouzanfar, F. & Sahab-Negah, S. Natural Cinnamaldehyde and Its Derivatives Ameliorate Neuroinflammatory Pathways in Neurodegenerative Diseases. *Biomed Res Int* **2020**, 1034325, doi:10.1155/2020/1034325 (2020).

17 Cole, G. M., Teter, B. & Frautschy, S. A. Neuroprotective effects of curcumin. *Adv Exp*

Med Biol **595**, 197-212, doi:10.1007/978-0-387-46401-5_8 (2007).

18 Nebrisi, E. E. Neuroprotective Activities of Curcumin in Parkinson's Disease: A Review of the Literature. *Int J Mol Sci* **22**, doi:10.3390/ijms222011248 (2021).

19 Larsson, S. C. Coffee, tea, and cocoa and risk of stroke. *Stroke* **45**, 309-314, doi:10.1161/STROKEAHA.113.003131 (2014).

20 Socala, K., Szopa, A., Serefko, A., Poleszak, E. & Wlaz, P. Neuroprotective Effects of Coffee Bioactive Compounds: A Review. *Int J Mol Sci* **22**, doi:10.3390/ijms22010107 (2020).

21 Puchl'ova, E. & Szolcsanyi, P. Filbertone: A Review. *J Agric Food Chem* **66**, 11221-11226, doi:10.1021/acs.jafc.8b04332 (2018).

22 Mutsnaini, L. *et al.* Filbertone protects obesity-induced hypothalamic inflammation by reduction of microglia-mediated inflammatory responses. *Biotechnology and Bioprocess Engineering* **26**, 86-92 (2021).

23 Ganz, J. *et al.* A novel specific PERK activator reduces toxicity and extends survival in Huntington's disease models. *Sci Rep* **10**, 6875, doi:10.1038/s41598-020-63899-4 (2020).

24 Lee, D. Y. *et al.* Activation of PERK signaling attenuates Abeta-mediated ER stress. *PLoS One* **5**, e10489, doi:10.1371/journal.pone.0010489 (2010).

25 Chen, Y. *et al.* Carbon monoxide induces the assembly of stress granule through the integrated stress response. *Biochem Biophys Res Commun* **512**, 289-294, doi:10.1016/j.bbrc.2019.03.017 (2019).

26 Kim, H. J. *et al.* Carbon monoxide-induced TFEB nuclear translocation enhances mitophagy/mitochondrial biogenesis in hepatocytes and ameliorates inflammatory liver

injury. *Cell Death Dis* **9**, 1060, doi:10.1038/s41419-018-1112-x (2018).

27 Joe, Y. *et al.* FGF21 induced by carbon monoxide mediates metabolic homeostasis via the PERK/ATF4 pathway. *FASEB J* **32**, 2630-2643, doi:10.1096/fj.201700709RR (2018).

28 Rouschop, K. M. *et al.* The unfolded protein response protects human tumor cells during hypoxia through regulation of the autophagy genes MAP1LC3B and ATG5. *J Clin Invest* **120**, 127-141, doi:10.1172/JCI40027 (2010).

29 Luhr, M. *et al.* The kinase PERK and the transcription factor ATF4 play distinct and essential roles in autophagy resulting from tunicamycin-induced ER stress. *J Biol Chem* **294**, 8197-8217, doi:10.1074/jbc.RA118.002829 (2019).

30 Reddy, P. H. & Oliver, D. M. Amyloid Beta and Phosphorylated Tau-Induced Defective Autophagy and Mitophagy in Alzheimer's Disease. *Cells* **8**, doi:10.3390/cells8050488 (2019).

31 Martini-Stoica, H., Xu, Y., Ballabio, A. & Zheng, H. The Autophagy-Lysosomal Pathway in Neurodegeneration: A TFEB Perspective. *Trends Neurosci* **39**, 221-234, doi:10.1016/j.tins.2016.02.002 (2016).

32 Martina, J. A., Diab, H. I., Brady, O. A. & Puertollano, R. TFEB and TFE3 are novel components of the integrated stress response. *EMBO J* **35**, 479-495, doi:10.15252/embj.201593428 (2016).

33 McGlinchey, R. P. & Lee, J. C. Cysteine cathepsins are essential in lysosomal degradation of alpha-synuclein. *Proc Natl Acad Sci U S A* **112**, 9322-9327, doi:10.1073/pnas.1500937112 (2015).

34 Wu, H., Xie, B., Ke, M. & Deng, Y. High-fat diet causes increased endogenous

neurotoxins and phenotype of Parkinson's disease in mice. *Acta Biochim Biophys Sin (Shanghai)* **51**, 969-971, doi:10.1093/abbs/gmz073 (2019).

35 Elabi, O. F., Cunha, J., Gaceb, A., Fex, M. & Paul, G. High-fat diet-induced diabetes leads to vascular alterations, pericyte reduction, and perivascular depletion of microglia in a 6-OHDA toxin model of Parkinson disease. *J Neuroinflammation* **18**, 175, doi:10.1186/s12974-021-02218-8 (2021).

36 Lizarbe, B., Cherix, A., Duarte, J. M. N., Cardinaux, J. R. & Gruetter, R. High-fat diet consumption alters energy metabolism in the mouse hypothalamus. *Int J Obes (Lond)* **43**, 1295-1304, doi:10.1038/s41366-018-0224-9 (2019).

37 Rivero-Rios, P., Madero-Perez, J., Fernandez, B. & Hilfiker, S. Targeting the Autophagy/Lysosomal Degradation Pathway in Parkinson's Disease. *Curr Neuropharmacol* **14**, 238-249, doi:10.2174/1570159x13666151030103027 (2016).

38 Chartier-Harlin, M. C. *et al.* Alpha-synuclein locus duplication as a cause of familial Parkinson's disease. *Lancet* **364**, 1167-1169, doi:10.1016/S0140-6736(04)17103-1 (2004).

39 Chiba, K., Peterson, L. A., Castagnoli, K. P., Trevor, A. J. & Castagnoli, N., Jr. Studies on the molecular mechanism of bioactivation of the selective nigrostriatal toxin 1-methyl-4-phenyl-1,2,3,6-tetrahydropyridine. *Drug Metab Dispos* **13**, 342-347 (1985).

40 Dauer, W. & Przedborski, S. Parkinson's disease: mechanisms and models. *Neuron* **39**, 889-909, doi:10.1016/s0896-6273(03)00568-3 (2003).

II-IX 국문 요약

알츠하이머병 (AD), 파킨슨병 (PD), 헌팅턴병 (HD)과 같은 신경퇴행성 질환의 발병 메커니즘이나 질환의 개선을 위한 치료적 메커니즘은 아직 완전히 연구되지 않았다. 이전에 *Corylus* 속 헤이즐넛 나무 열매의 향기 성분인 필버톤이 NF-κB를 억제하여 시상하부 염증을 억제할 수 있음을 보고되었다. 본 연구에서는 필버톤이 신경퇴행성 질환을 개선하는 효과를 탐구하고자 하였다. 필버톤은 미토콘드리아 ROS (mtROS) 생성을 통해 PERK를 활성화하여 사람 신경세포주 SH-SY5Y 세포에서 TFEB의 핵 전위를 증가시키는 것을 관찰하였다. TFEB의 핵 전위는 오토파지-라이소좀 경로 (ALP)를 증가시킬 수 있으며, 이 경로의 활성화는 SH-SY5Y 세포에서 α-syn 축적을 감소시켰다. 게다가, 고지방식이 (HFD) 투여가 SNpc에서 도파민 뉴런의 손실을 유발한다는 것을 발견했는데, 이는 필버톤 처리에 의해 개선되었다. 필터톤은 또한 HFD을 투여한 쥐의 중간뇌에서 오토파지-리소좀 관련 유전자와 단백질 발현을 증가시켰다. MPTP 투여로 PD가 유도된 쥐는 운동 기능 장애가 나타난다. 하지만 필버톤의 투여는 운동 기능 장애를 개선한다. 따라서, 필버톤이 신경 퇴행성 질환에 대한 새로운 치료 전략이 될 수 있음을 제시한다.

PART III

Filbertone attenuates MPP^+/MPTP-induced ferroptosis in neurological diseases via Nrf2-GPX4 activation

III-I. ABSTRACT

Parkinson's disease (PD) as a prevalent neurodegenerative disorder is characterized by the loss of dopaminergic neurons in the substantia nigra compacta (SNc), which is considered the primary cause of PD. Ferroptosis is a recently discovered form of cell death that is characterized by iron accumulation, reduction of GPX4, and lipid peroxidation. Several studies have implicated the ferroptotic cell death as a contributing factor of PD. We previously reported that protection of neurodegeneration by filbertone is mediated by enhancing the PERK-ALP pathway. However, the anti-ferroptotic effects of filbertone on PD pathology have not been fully comprehended. Here, we show that filbertone induces the activation of Nrf2 via PERK activation, leading to the upregulation of antioxidant gene transcription, including GPX4 and SLC7A11. In addition, The Nrf2 activation by filbertone mitigate the accumulation of α-synuclein as well as dopaminergic neuron loss in the midbrain region of a mouse model of PD. Our study has shown that filbertone can prevent the reduction of GPX4 induced by specific ferroptosis inducers such as RSL3 or neurotoxins like MPP^+/MPTP, which is achieved through the activation of Nrf2. In conclusion, the findings suggest that filbertone has the potential to act as a ferroptosis inhibitor and could serve as a promising therapeutic approach for PD.

Keywords Ferroptosis; Filbertone; Parkinson's disease; Nrf2

III-II. INTRODUCTION

Ferroptosis is a newly identified type of programmed cell death that is commonly distinguished by the accumulation of iron and lipid peroxidation during the cell death process[1-3]. Ferroptosis-inducing agents possess the capability to affect glutathione peroxidase activity either directly or indirectly, resulting in a decline in antioxidant capacity and accumulation of lipid hydroperoxides within cellular compartments. This process ultimately leads to oxidative cell death, as demonstrated by various studies[1,2,4-7]. Several studies have found that ferroptosis is regulated by numerous genes/proteins, including cyclooxygenase-2 (*PTGS2*)[8], p53[9,10], nuclear factor E2-related factor 2 (Nrf2)[11,12], phosphatidylethanolamine binding protein 1 (PEBP1)[13], and others[3].

Recent studies have demonstrated the role of ferroptosis in various diseases, including neurological diseases[12,14-18], ischemia-reperfusion injury[19], kidney injury[5,20], liver diseases[21,22] and tumors[8,9,11].There is mounting evidence to suggest that ferroptosis plays a role in the pathogenesis of neurodegenerative diseases[10,12,14,16,23-25]. Several studies have indicated that ferrostatin-1, a ferroptosis inhibitor, has a protective effect against Parkinson's disease (PD) models[26,27]. Therefore, the inhibition of ferroptosis may be a promising strategy for preventing PD.

The natural compound filbertone, derived from the hazelnut tree[28], has been shown to potentially provide neuroprotective effects in mice, as previously reported[29]. Numerous studies have reported the protective effects of natural compounds, including quercetin[23], curcumin[30], and others[31], in the context of neurodegenerative diseases. The neuroprotective effects of these compounds are mediated through the reduction of lipid peroxidation mechanisms. However,

the precise underlying mechanism the pathology of PD and its prevention have not yet been fully established.

The nuclear factor erythroid 2 related factor 2 (Nrf2) is transcription factor that has a key role in regulating the redox environment and has been identified as a novel substrate of PERK[30,32,33]. In the context of oxidative stress, Nrf2 undergoes translocation from the cytoplasm to the nucleus where it binds to promoter of target genes known as antioxidant response elements (AREs) to initiate the transcription of ARE-regulated genes[34]. Previous report has indicated that inadequate activation of Nrf2 in humans is associated with chronic neurodegenerative conditions, including PD, Alzheimer's disease (AD), and amyotrophic lateral sclerosis (ALS)[35-40]. In our previous study, we have shown that filbertone activates the PERK-eIf2α-ATF4 pathway, which contributes to amelioration of neurodegeneration induced by MPTP/HFD[29]. Based on our hypothesis, it is postulated that filbertone plays a crucial role in the defense against ferroptosis in neurological disorders. Therefore, our findings highlight the potential preventive effects of filbertone on PD by enhancing Nrf2 activation, leading to increased levels of GPX4 and SLC7A11 and offer a therapeutic potential to prevent the neurodegenerative disorders.

.

III-III. MATERIALS AND METHODS

1. Reagents

Filbertone, Ferrostatin-1, MPP, and 1-methyl-4-phenyl-1,2,3,6-tetrahydropyridine (MPTP) were purchased from Sigma-Aldrich (St Louis, MO, USA). The ferroptosis inducer RSL3 was from selleckchem (Houston, TX, USA).

2. Cell lines

The SH-SY5Y neuroblastoma cells were cultured in Dulbecco's Modified Eagle medium (DMEM) (Gibco, Grand Island, USA), which was supplemented with 10% fetal bovine serum (Gibco, Melbourne, Australia) and 1% penicillin-streptomycin solution (Gibco, Grand Island, NE, USA). The cells were incubated under controlled conditions of 37°C with 5% CO_2 in humidified incubators.

3. Animals

Seven-week-old male C57BL/6 wild-type mice were purchased from Koatech (Pyeongtaek, South Korea). Animals were reared in a specific pathogen-free facility, and maintained under controlled environmental conditions, including a 12h light-dark cycle, at a temperature range of 18–24°C, and a humidity rage of 40–70%. The University of Ulsan animal care and use committee granted approval for the animal studies conducted. The MPTP-induced Parkinson's disease model was employed, and mice were allocated randomly to four experimental groups. The control group and MPTP group were administered either a vehicle or filbertone. The group treated with filbertone + MPTP was administered 0.2% filbertone in vehicle once daily via oral gavage for a period of 15 days. Following oral gavage for 5 days, both the MPTP and

filbertone + MPTP groups were received daily intraperitoneal injection of MPTP (25 mg/kg) for 5 days during course of the experiment.

4. Western blot

Cell pellets and brain tissues were lysed using prepared RIPA buffer (Thermo Scientific, Waltham, MA, USA) containing phosphatase and protease inhibitors (Sigma-Aldrich), and the total protein concentration was determined by BCA protein assay reagents (Pierce Biotechnology, Rockford, IL, USA) using bovine serum albumin (BSA) as the standard. Samples were boiled at 95°C in 2X Laemmli buffer (Bio-Rad, Hercules, CA, USA) for 5 min. Protein were resolved by SDS-PAGE and transferred to polyvinylidene difluoride membrane (Millipore, Burlington, MA, USA). The membrane was blocked with 5% nonfat milk (BD bioscience, San Jose, CA, USA) in phosphate buffered saline-Tween 20 (PBS-T), and then the membrane was incubated with primary antibodies as follows: p-PERK (1:1000, Signalway antibody, Baltimore, MD, USA), PERK (1:1000, Cell Signaling, Danvers, MA, USA), p-Nrf2 (1:2000,), Nrf2 (1:1000, Santa cruz), GPX4 (1:10000, abcam), SLC7A11 (1:2000, invitrogen), PARP (1:2000, Cell Signaling), PTGS2 (1:2000, invitrogen), TH (1:1000, Cell signaling), α-synuclein (1:2000, Cell Signaling), α-tubulin (1:2000, Cell Signaling), and β-actin (1:2500, Thermo Scientific). These were incubated overnight at 4°C. Membranes were washed with 1X PBS-T 3 times 10 min and incubated with HRP-conjugated secondary antibodies. Chemiluminescence signals were read using an Azure Biosystems C300 analyzer (Azure Biosystems, Dublin, CA, USA) using an ECL substrate (Pierce Biotechnology).

5. Measurement of lipid peroxidation

SH-SY5Y cells were incubated with filbertone (20 μM), ferrostatin-1 (1 μM) and RSL3 (1 μM) for 8 h or MPP^+ (500 μM) for 24 h. After treatment, cells were stained with 1.5 μM BODIPY

581/591 C11 (Invitrogen, Carlsbad, CA, USA) at 37°C for 30 min. Prior to flow cytometry analysis, the cells were trypsinized and then subsequently washed three times with 1X PBS. Lipid peroxidation was detected by using a FACSCanto flow cytometry system (BD Bioscience, CA, USA). The fluorescence intensities were analyzed using FlowJo software (Tree Star).

6. Real-time quantitative RT-PCR

Total RNA was isolated from cells and mid-brain using by QIAzol Lysis reagent (QIAGEN, CA, USA), according to the manufacturer's instructions. 2 μg of total RNA was used to synthesize cDNA using oligo [41] primers (BIONICS, Daejeon, Korea) and M-MLV reverse transcriptase (Promega). To analyze real-time quantitative PCR (RT-qPCR), the synthesized cDNA was amplified with SYBR Green qPCR Master Mix on an ABI 7500 Fast Real-Time PCR System (Applied Biosystems, CA, USA). The following qRT-PCR primers were human GAPDH (f-caatgacccttcatcctc, r-agcatcgccccacttgatt), human GPX4 (f-acaagaacggctgcgtggtgaa, r-gccacacacttgtggagctaga), human SLC7A11 (f-ctttgttgccctctcctgcttc, r-cagaggagtgtgcttgtggaca), human PTGS2 (f-gggttgctgggggaagaaa, r-ctctgctctggtcaatggagg).

7. Subcellular fractionation

After harvesting the cells, subcellular fractionation was performed according to the manufacturer's instructions using Nuclear/cytosol fractionation kit (Biovision, CA, USA). Briefly, cell pellets were resuspended with cytosolic extraction buffer A (CEB-A) and CEB-B. After 10 min, the lysates were centrifuged at 4°C for 5 min at 16,000 X *g* in a microcentrifuge to obtain cytosolic protein containing supernatant. The remaining pellets were resuspended in nuclear extraction buffer [42] and vortexed for 15 s. This step was repeated every 10 min, for five times. Samples were centrifuged at 4°C for 10 min at 16,000 X *g* to acquire nuclear extracts.

The purity of cytoplasmic and nuclear fractions was determined by western blotting using anti-α-tubulin and PARP antibodies.

8. WST-8 assay

To analyze cell viability, SH-SY5Y cells were seeded into 96-well plates at a density of 5000 cells per well. Upon reaching 70% confluence, the cells underwent treatment with filbertone (20 μM), ferrostatin-1 (1 μM) and RSL3 (1 μM) for a duration of 8 h, or MPP^+ (500 μM) for 24 h. Following treatment, the cells were incubated with WST-8 (Biomax, Seoul, Korea) for 1 h. To quantify cell viability, the optical density of the samples was measured at 450 nm using a SpectraMax iD3 (Molecular Devices, Sunnyvale, CA, USA).

9. Generation of knockdown cells

To knock down the mRNA expression of Nrf2, the cells were transfected with scramble siRNA (scRNA) obtained from Ambion (Austin, TX, USA) and used as negative control. siRNA against human Nrf2 obtained from Santa Cruz Biotechnology (Santa Cruz, CA, USA). The transfection was carried out using Lipofectamine 2000 from Invitrogen (Carlsbad, CA, USA) according to the manufacturer's protocol.

10. Statistical analysis

Data were analyzed with Prism 7.00 (GraphPad Software, San Diego, CA, USA). All values are expressed as means ± SD. Statistical analyses were performed using one-way ANOVA or two-way ANOVA with Tukey *post hoc* tests.

III-IV. RESULTS

1. Filbertone attenuates MPTP-induced ferroptosis in mouse PD model

To investigate the potential impact of filbertone on MPTP-induced PD, C57BL/6J mice were administered 0.2% filbertone in saline for 2 weeks and injected with MPTP every other day for a total of 4 times (25 mg/kg, beginning at 6 day). In mice treated with MPTP, the midbrain tissue exhibited decrease of tyrosine hydroxylase (TH) protein. However, filbertone treatment significantly increased expression levels of TH (Fig. 1a). Furthermore, MPTP treatment resulted in increased α-syn accumulation in the midbrain region (Fig. 1a). However, filbertone decreased α-syn accumulation in the midbrain. To examine the potential involvement of ferroptosis in the neuronal toxicity induced by MPTP, we measured ferroptosis markers in midbrain tissue samples obtained from mice. The results showed that mRNA levels of PTGS2 were dramatically increased by MPTP treatment, while mRNA levels of PTGS2 were decreased by filbertone treatment (Fig. 1b). Additionally, the administration of MPTP resulted in a reduction of protein levels of SLC7A11 and GPX4, while PTGS2 protein levels were increased. The administration of filbertone abolished MPTP-induced ferroptosis (Fig. 1c). Notably, the phosphorylation of Nrf2, which is responsible for regulating the transcription of SLC7A11 and GPX4, was decreased following MPTP treatment. However, treatment with filbertone alleviates MPTP-induced decrease in Nrf2 phosphorylation (Fig. 1c). These results suggested that filbertone exhibits protective effects against MPTP-induced toxicity in a mouse model of PD by inhibiting ferroptosis, and this mechanism is dependent on the activation of Nrf2.

2. Filbertone inhibits RSL3-induced ferroptosis in SH-SY5Y human neuroblastoma cells

To investigate whether filbertone can protect ferroptosis *in vitro*, SH-SY5Y human neuroblastoma cells were incubated with RSL3, an inducer of ferroptosis. The administration of RSL3 induced cell death (Fig. 2a) and increased lipid peroxidation (Fig. 2b). In comparison to the group treated with RSL3, the group co-treated with filbertone or ferrostatin-1 exhibited a significant reduction in cell death and a decrease in lipid peroxidation (Fig. 2a, b). Furthermore, administration of filbertone or ferrostatin-1 restored the reduction of both GPX4 protein and mRNA levels, which induced by RSL3. (Fig. 2c, d). Moreover, the elevated levels of PTGS2 protein expression induced by RSL3 were mitigated by filbertone or ferrostatin-1 (Fig. 2c). This finding suggests that filbertone provides a protective effect against ferroptosis.

3. Filbertone inhibits MPP^+-induced ferroptosis in SH-SY5Y cells

To investigate the effect of filbertone on MPP^+-induced neuronal toxicity, the present study assessed cell viability and lipid peroxidation measured by WST-8 assay and BODIPY 581/591 staining, respectively. Treatment with MPP^+ resulted in cell death and elevated levels of lipid peroxidation (Fig. 3a, b). However, filbertone mitigates MPP^+-induced cell death and lipid peroxidation (Fig. 3a, b). MPP^+ treatment resulted in a reduction of both GPX4 protein and GPX4 mRNA levels, which were subsequently restored through the administration of filbertone or ferrostatin-1 (Fig. 3c, d). Treatment with filbertone and ferrostatin-1 resulted in a decrease in the levels of PTGS2 protein and mRNA induced by MPP^+ (Fig. 3c, d). Thus, filbertone mitigates MPP^+-induced ferroptosis.

4. Filbertone protects against ferroptosis by increasing SLC7A11-GPX4 axis

Ferroptosis triggers the depletion of antioxidants, including GPX4[20,43], thioredoxin[26], CoQ10[44], and DHODH[45]. GPX4 is a key enzyme of ferroptosis regulator which reduces lipid peroxidation by using GSH. The synthesis of GSH requires the uptake of cystine via the SLC7A11 transporter[46]. Therefore, the levels of SLC7A11 and GPX4 play a crucial role in protecting against ferroptosis. To investigate the effect of filbertone on expression of GPX4 and SLC7A11 in SH-SY5Y cells, cells were treated with filbertone at different time points (0, 1, 2, 4, and 8 h) and at various concentrations (0, 5, 10, and 20 μM). The filbertone treatment showed a gradual increase in the protein and mRNA expression levels of GPX4 and SLC7A11, in a time- and dose-dependent manner (Fig. 4).

5. PERK-Nrf2 activation is required to anti-ferroptosis effect of filbertone

Nrf2 plays a key role as a regulator of ferroptosis[11]. The activation of Nrf2 is shown to increase the expression of various antioxidant genes, such as GPX4, HO-1, and SLC7A11. The activity of Nrf2 is regulated by its phosphorylation and subsequent nuclear translocation, which is facilitated by the activation of PERK. To examine the induction of PERK and Nrf2 activation by filbertone, a western blot analysis was performed. Filbertone increased the phosphorylation of PERK and Nrf2, which is dependent on both the duration and dosage of treatment (Fig.5 a, b). The nuclear translocation of Nrf2 was assessed through western blot analysis. The treatment of filbertone resulted in a reduction of cytosolic Nrf2 protein levels, while simultaneously increasing the levels of nuclear Nrf2 in a time- and dose-dependent manner (Fig. 5c, d). The

data suggest that the upregulation of GPX4 and SLC7A11 by filbertone is mediated through the PERK-Nrf2 pathway. Moreover, to explore whether filbertone-induced anti-ferroptotic effect was depends on Nrf2 activation, we transfected SH-SY5Y cells with scramble RNA (*scRNA*) or siRNA targeting Nrf2 (*siNrf2*). Nrf2 protein levels were significantly reduced in siNrf2-transfected cells. Filbertone treatment increased the protein and mRNA levels of GPX4 and SLC7A11 in scRNA-transfected but not siNrf2-transfected SH-SY5Y cells (Fig. 6a, b). Furthermore, treatment with MPP^+ results in a reduction of GPX4 protein expression and an elevation of PTGS2 protein expression. The administration of filbertone restored GPX4 and PTGS2 levels (Fig. 6c). Moreover, filbertone inhibited the lipid peroxidation induced by MPP^+ (Fig. 6d). However, the effect of filbertone on inhibition of lipid peroxidation and restoration of GPX4 levels were abolished by the Nrf2 knockdown (Fig. 6a-d). Altogether, these results suggest that the anti-ferroptosis effects of filbertone depend on the activation of Nrf2.

III-V. FIGURES

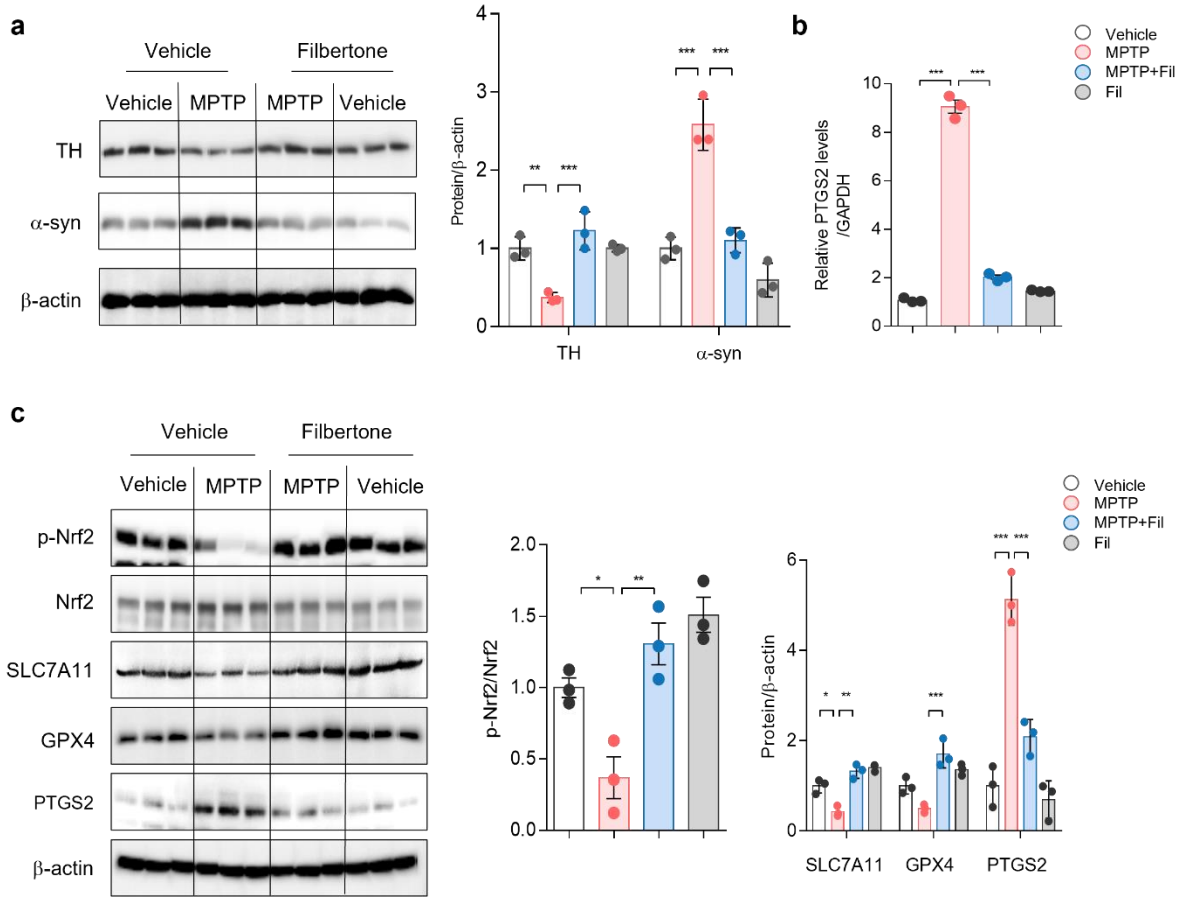

Fig. 1. Filbertone prevents MPTP-induced PD and inhibit ferroptosis in mouse models. To determine filbertone effects in MPTP-induced PD models, mice were administered 0.2% filbertone via oral gavage for 15 d and received daily intraperitoneal injection of MPTP (25 mg/kg, beginning at 6 d). (a) The protein levels of TH and α-synuclein in mouse mid brain. The right panel represents quantification of these protein. (b) Relative mRNA levels of PTGS2 in mouse mid brain. (c) The protein expression of p-Nrf2, SLC7A11, GPX4, and PTGS2 were measured by western blotting. Protein levels were quantifided (*right panel*). Data represent mean ± SD; **p*<0.05, ***p*<*0.005* and ****p*<0.001.

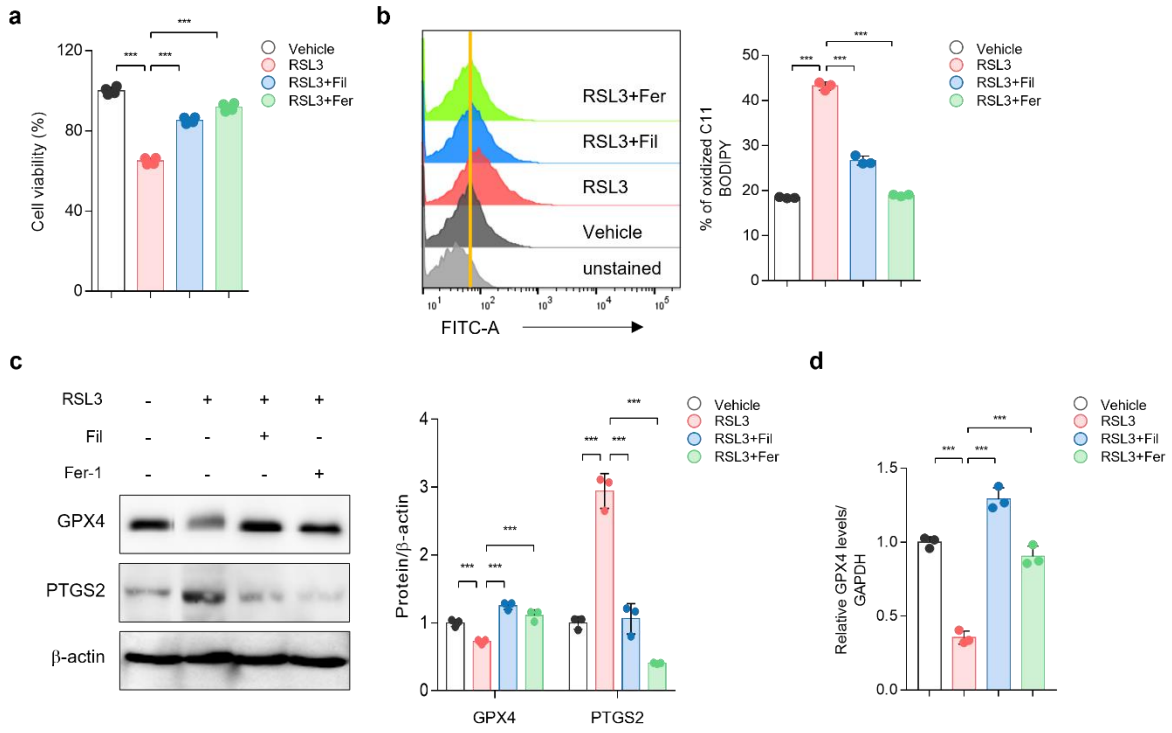

Fig. 2. Filbertone inhibits RSL3-induced ferroptosis in SH-SY5Y human neuroblastoma cells. To determine effects of filbertone on RSL3-induced ferroptosis in SH-SY5Y cells, the cells were incubated with RSL3 (1 μM) for 8 h in the presence of filbertone (20 μM) or ferrostatin (1 μM). (a) Viabilities of SH-SY5Y cells were measured by WST-8 assay. (b) Lipid peroxidation levels were measured by using BODIPY 581/591 and flow cytometry. (c) Protein levels of GPX4 and PTGS2. The right panel represents the quantification levels. (d) GPX4 from SH-SY5Y cells was measured by qRT-PCR. Data represent mean ± SD; ***p<0.001.

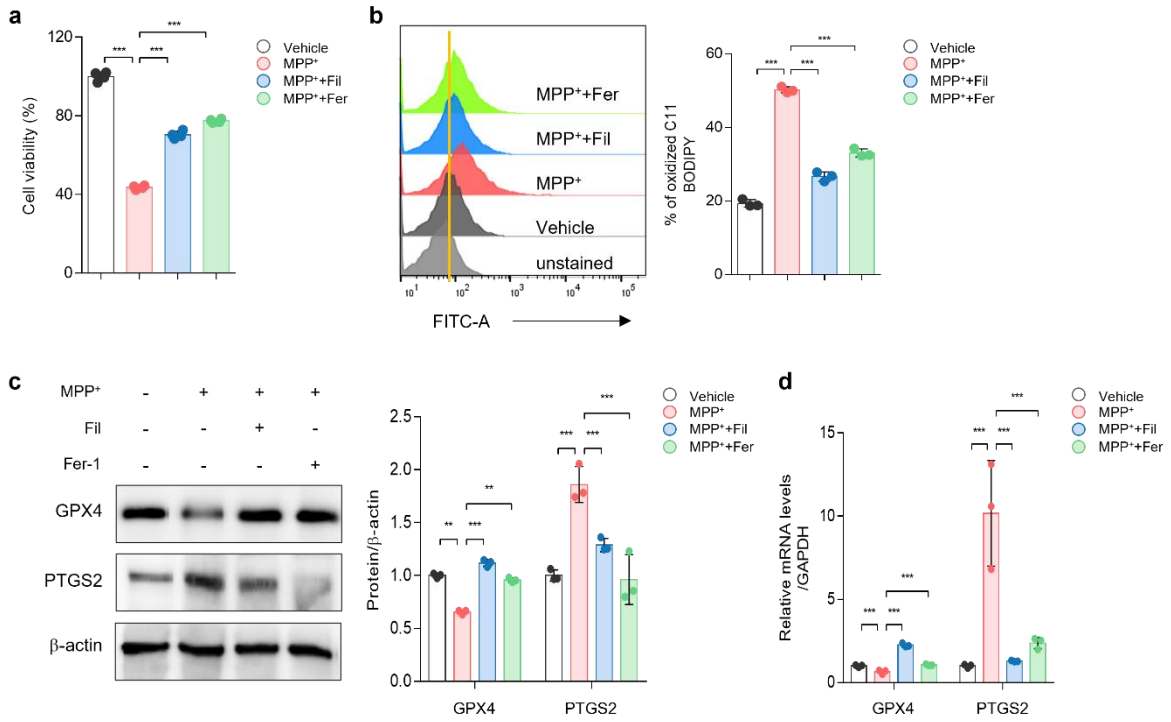

Fig. 3. Filbertone inhibits MPP$^+$-induced ferroptosis in SH-SY5Y cells. To determine effects of filbertone on MPP$^+$-induced ferroptosis in SH-SY5Y cells, the cells were incubated with MPP$^+$ (500 μM) for 24 h in the presence of filbertone (20 μM) or ferrostatin (1 μM). (a) Viabilities of SH-SY5Y cells were measured by WST-8 assay. (b) Lipid peroxidation levels were measured by using BODIPY 581/591 and flow cytometry. (c) Protein levels of GPX4 and PTGS2. The right panel represents the quantification levels. (d) Relative mRNA levels of GPX4 and PTGS2. Data represent mean ± SD; $^{**}p<0.005$ and $^{***}p<0.001$.

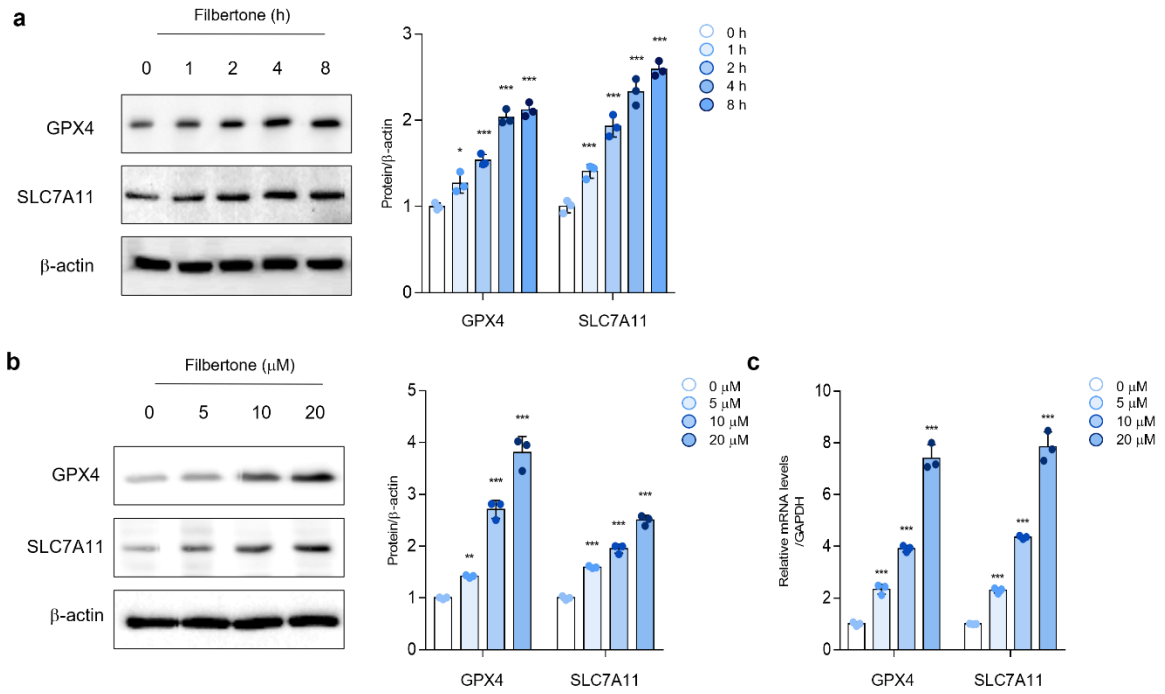

Fig. 4. Filbertone increases GPX4 and SLC7A11 levels. (a) SH-SY5Y cells were treated with filbertone (20 μM) at the indicated time points (0, 1, 2, 4 and 8 h). The protein expression of GPX4 and SLC7A11 were measured by western blotting. The right panel represents the quantification levels of proteins. (b-c) SH-SY5Y cells were treated with filbertone at various concentrations (0, 5, 10, and 20 μM) for 4 h. The Protein and mRNA levels of GPX4 and SLC7A11 were determined by western blotting (b) and RT-PCR (c). Data represent mean ± SD; *p<0.05 and ***p<0.001

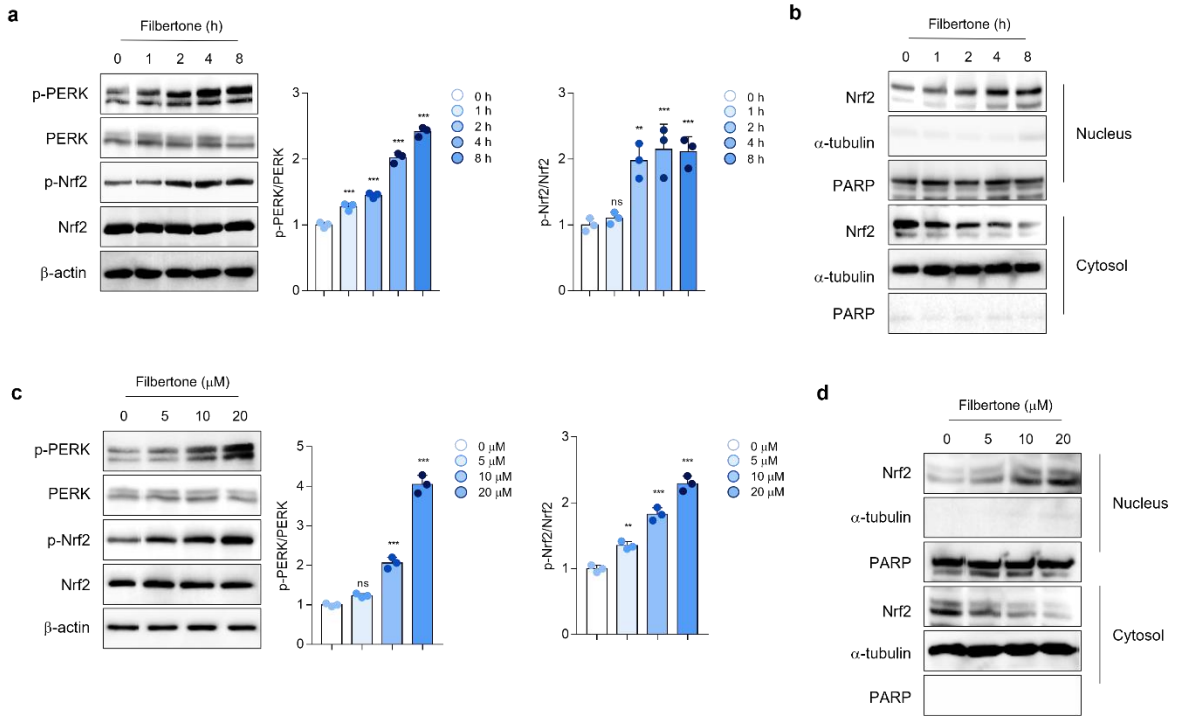

Fig. 5. Filbertone activates PERK-Nrf2 pathway. (a) SH-SY5Y cells were treated with filbertone (20 μM) at the indicated time points (0, 1, 2, 4 and 8 h). PERK and Nrf2 phosphorylation were determined by western blotting. Quantification of p-PERK and p-Nrf2 are shown in the right panel. (b) Cells were treated with filbertone (20 μM) at the indicated time points (0, 1, 2, 4 and 8 h) and subjected to nuclear and cytosolic fractionation. Resulting fractions were then detected with antibody against Nrf2. PARP and α-tubulin were used as nuclear and cytosolic markers, respectively. Quantification of Nrf2 translocation is shown at the right. (c) Cells were treated with filbertone at various concentrations (0, 5, 10 and 20 μM) for 4 h. PERK and Nrf2 phosphorylation were determined by western blotting. Quantification of p-PERK and p-Nrf2 are shown in the right panel. (d) Cells were treated with filbertone at various concentrations (0, 5, 10 and 20 μM) for 4 h and subjected to nuclear and cytosolic fractionation. Resulting fractions were then detected with antibody against Nrf2.

Quantification of Nrrf2 translocation is shown at the right. Data represent mean ± SD; ***p<0.005* and ****p*<0.001, ns : not significant.

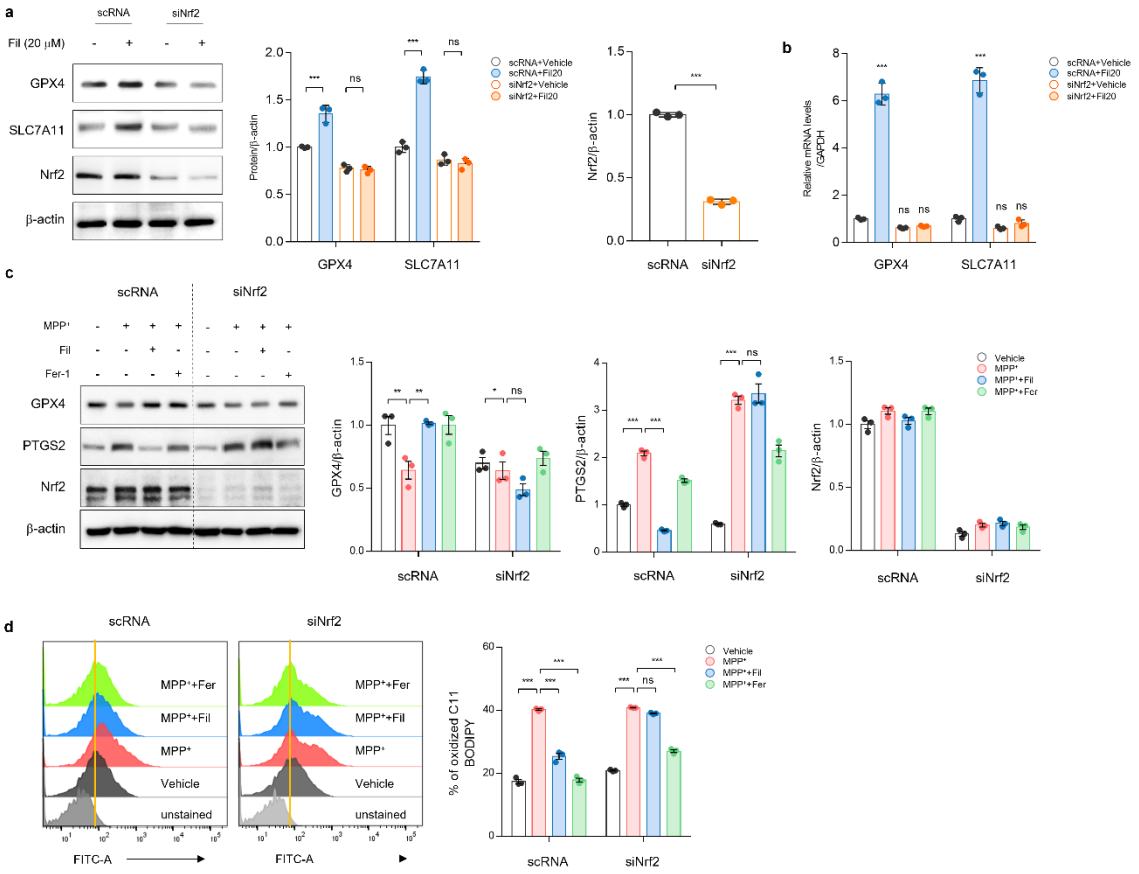

Fig. 6. Ablation of Nrf2 diminishes anti-ferroptosis effect of filbertone. To determined filbertone relies on Nrf2 pathway to inhibit ferroptosis. SH-SY5Y cell were transfected with scrambled RNA (scRNA) and siRNA targeting Nrf2. (a) Protein levels of GPX4, SLC7A11 and Nrf2 in SH-SY5Y cells were treated with filbertone (20 μM) for 4h. The right panel represents the quantification levels of proteins. (b) Relative mRNA levels of GPX4 and SLC7A11 in SH-SY5Y cells. (c) Protein levels of GPX4, PTGS2 and Nrf2 in SH-SY5Y cells were incubated with MPP^+ (500 μM) for 24 h presence of filbertone (20 μM) or ferrostatin (1 mM). (d) Lipid peroxidation levels were measured by using BODIPY 581/591 and flow cytometry. Data represent mean ± SD; ns : not significant, *p<0.05m **p<0.005 and ***p<0.001.

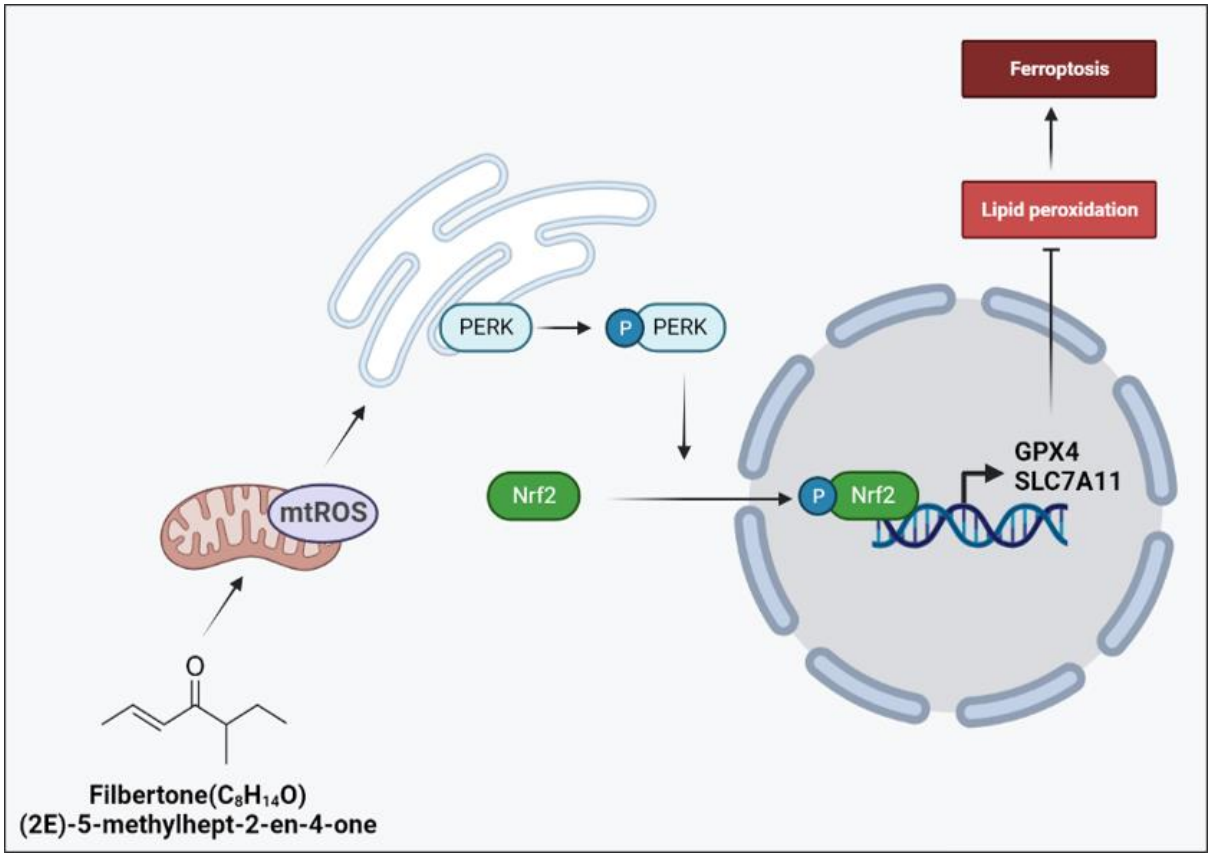

Schematic overview of the mechanisms by which filbertone protects against ferroptosis via Nrf2 activation. Filbertone treatment leads to the activation of PERK by mtROS. Activated PERK leads to the phosphorylation of Nrf2 and subsequently promotes the translocation of Nrf2 into the nucleus, which increases the transcription of GPX4 and SLC7A11. The activation of Nrf2 leads to an increase in GPX4 and SLC7A11, which provides protection against ferroptosis by reducing lipid peroxidation of the cellular membrane. Therefore, filbertone is a potential agent for preventing PD by targeting ferroptosis.

III-VI. DISCUSSIONS

The present study proposes that filbertone may provide as a protection against neuronal toxicity induced by MPP^+/MPTP. Filbertone mitigates cell death and lipid peroxidation caused by RSL3 or MPP^+ through the restoration of GPX4 levels (Fig. 2 and 3). The administration of filbertone increases Nrf2 activation (Fig. 5). Activation of Nrf2 leads to the transcriptional regulation of various ferroptosis-associated genes, including GPX4 and SLC7A11. Therefore, we identify the therapeutic effect of filbertone on PD as a potential ferroptosis inhibitor. In our previous study, it was suggested that filbertone may have a preventative effect on PD by increasing the activation of the PERK-ALP, which can ameliorate amyloidogenesis[29]. However, the understanding of PD pathogenesis is unclear. Several studies have reported that the pathogenesis of PD is associated with neuroinflammation, mitochondrial dysfunction, and the accumulation of α-synuclein[23]. The risks associated with dopaminergic neuron cell death are diverse and include various mechanisms, such as apoptosis[47], necroptosis[34,48,49], pyroptosis[20,40,50], and ferroptosis[12,14-17,43,44]. In Parkinson's disease, ferroptosis appears to occur earlier than apoptosis[10]. Therefore, the inhibition of ferroptosis may potentially alleviate neuronal death in PD.

The transcription factor Nrf2 can bind to the antioxidant response element region of target genes, which includes those involved in antioxidant, anti-inflammatory, and detoxification processes[35,36,39]. Several studies have demonstrated that Nrf2 is a significant target in the context of neurodegenerative diseases, as it is expressed in both glial cells and neurons[35]. The deficiency of Nrf2 increases susceptibility to common neurotoxins, general neurodegeneration, astrogliosis[51], and dopaminergic neuronal dysfunction. This highlights the importance of Nrf2

in protecting against neurological conditions[35,37]. The dysregulated expression of Nrf2 shown to worsen PD[52], whereas the upregulation of Nrf2 delays the progression of PD pathology and the accumulation of α-synuclein[23]. The regulation of Nrf2 involves the phosphorylation of serine or threonine residues[53]. Phosphorylated Nrf2 dissociates from Keap1, leading to its nuclear translocation[35]. The phosphorylation of Nrf2, which is induced by PERK[29,30,32,33] is activated by filbertone treatment[29]. Mechanistically, filbertone prevents RSL3/MPP^+/MPTP-induced GPX4 depletion by activating the PERK-Nrf2 pathway. In the present study, it was observed that the administration of filbertone led to an increase in the phosphorylation of PERK and Nrf2 proteins, along with the nuclear translocation of Nrf2 (Fig. 5). The MPTP-induced PD model resulted in a reduction of Nrf2 phosphorylation and a decrease of TH (Fig. 1). Filbertone shown to prevent the loss of TH neurons in a PD model by increasing Nrf2 activation. Therefore, filbertone exhibits potential as a therapeutic strategy for PD by preventing ferroptotic cell death in dopaminergic neurons.

III-VII. CONCLUSION

In conclusion, the findings of our study demonstrate that filbertone provides potential neuroprotective effects in mice. Our proposal suggests that filbertone inhibits ferroptosis by inducing the expression of GPX4 and SLC7A11 through a Nrf2-dependent mechanism. The administration of filbertone attenuates of α-syn accumulation and the increase of PTGS2 levels induced by MPTP in the midbrain of mice. Furthermore, our study revealed that the administration of MPTP resulted in a decline in the functionality of dopamine neurons, as evidenced by a decrease in TH protein expression. However, treatment with filbertone mitigates loss of TH. Filbertone increases the expression of protein and mRNA levels of GPX4 and SLC7A11 in human neuroblastoma cells. Collectively, our findings suggest that filbertone provides a therapeutic approach for the treatment of neurodegenerative conditions by impeding ferroptosis.

III-VIII. REFERENCES

1 Dixon, S. J. Ferroptosis: bug or feature? *Immunol Rev* **277**, 150-157, doi:10.1111/imr.12533 (2017).

2 Dixon, S. J. *et al.* Ferroptosis: an iron-dependent form of nonapoptotic cell death. *Cell* **149**, 1060-1072, doi:10.1016/j.cell.2012.03.042 (2012).

3 Li, J. *et al.* Ferroptosis: past, present and future. *Cell Death Dis* **11**, 88, doi:10.1038/s41419-020-2298-2 (2020).

4 Dixon, S. J. & Stockwell, B. R. The role of iron and reactive oxygen species in cell death. *Nat Chem Biol* **10**, 9-17, doi:10.1038/nchembio.1416 (2014).

5 Friedmann Angeli, J. P. *et al.* Inactivation of the ferroptosis regulator Gpx4 triggers acute renal failure in mice. *Nat Cell Biol* **16**, 1180-1191, doi:10.1038/ncb3064 (2014).

6 Gaschler, M. M. & Stockwell, B. R. Lipid peroxidation in cell death. *Biochem Biophys Res Commun* **482**, 419-425, doi:10.1016/j.bbrc.2016.10.086 (2017).

7 Imai, H., Matsuoka, M., Kumagai, T., Sakamoto, T. & Koumura, T. Lipid Peroxidation-Dependent Cell Death Regulated by GPx4 and Ferroptosis. *Curr Top Microbiol Immunol* **403**, 143-170, doi:10.1007/82_2016_508 (2017).

8 Yang, W. S. *et al.* Regulation of ferroptotic cancer cell death by GPX4. *Cell* **156**, 317-331, doi:10.1016/j.cell.2013.12.010 (2014).

9 Jiang, L. *et al.* Ferroptosis as a p53-mediated activity during tumour suppression. *Nature* **520**, 57-62, doi:10.1038/nature14344 (2015).

10 Zhang, P. *et al.* Ferroptosis was more initial in cell death caused by iron overload and its underlying mechanism in Parkinson's disease. *Free Radic Biol Med* **152**, 227-234,

doi:10.1016/j.freeradbiomed.2020.03.015 (2020).

11 Chen, D. *et al.* NRF2 Is a Major Target of ARF in p53-Independent Tumor Suppression. *Mol Cell* **68**, 224-232 e224, doi:10.1016/j.molcel.2017.09.009 (2017).

12 Angelova, P. R. *et al.* Alpha synuclein aggregation drives ferroptosis: an interplay of iron, calcium and lipid peroxidation. *Cell Death Differ* **27**, 2781-2796, doi:10.1038/s41418-020-0542-z (2020).

13 Wenzel, S. E. *et al.* PEBP1 Wardens Ferroptosis by Enabling Lipoxygenase Generation of Lipid Death Signals. *Cell* **171**, 628-641 e626, doi:10.1016/j.cell.2017.09.044 (2017).

14 Angelova, P. R., Esteras, N. & Abramov, A. Y. Mitochondria and lipid peroxidation in the mechanism of neurodegeneration: Finding ways for prevention. *Med Res Rev* **41**, 770-784, doi:10.1002/med.21712 (2021).

15 Do Van, B. *et al.* Ferroptosis, a newly characterized form of cell death in Parkinson's disease that is regulated by PKC. *Neurobiol Dis* **94**, 169-178, doi:10.1016/j.nbd.2016.05.011 (2016).

16 Guiney, S. J., Adlard, P. A., Bush, A. I., Finkelstein, D. I. & Ayton, S. Ferroptosis and cell death mechanisms in Parkinson's disease. *Neurochem Int* **104**, 34-48, doi:10.1016/j.neuint.2017.01.004 (2017).

17 Kenny, E. M. *et al.* Ferroptosis Contributes to Neuronal Death and Functional Outcome After Traumatic Brain Injury. *Crit Care Med* **47**, 410-418, doi:10.1097/CCM.0000000000003555 (2019).

18 Ren, J. X., Sun, X., Yan, X. L., Guo, Z. N. & Yang, Y. Ferroptosis in Neurological Diseases. *Front Cell Neurosci* **14**, 218, doi:10.3389/fncel.2020.00218 (2020).

19 Nazzal, M. *et al.* Novel NMP split liver model recapitulates human IRI and

demonstrates ferroptosis modulators as a new therapeutic strategy. *Pediatr Transplant* **26**, e14164, doi:10.1111/petr.14164 (2022).

20 Wang, L. *et al.* GPX4 utilization by selenium is required to alleviate cadmium-induced ferroptosis and pyroptosis in sheep kidney. *Environ Toxicol* **38**, 962-974, doi:10.1002/tox.23740 (2023).

21 Lu, Y. *et al.* Ferroptosis as an emerging therapeutic target in liver diseases. *Front Pharmacol* **14**, 1196287, doi:10.3389/fphar.2023.1196287 (2023).

22 Zhu, L. *et al.* The Emerging Role of Ferroptosis in Various Chronic Liver Diseases: Opportunity or Challenge. *J Inflamm Res* **16**, 381-389, doi:10.2147/JIR.S385977 (2023).

23 Lin, Z. H. *et al.* Quercetin Protects against MPP(+)/MPTP-Induced Dopaminergic Neuron Death in Parkinson's Disease by Inhibiting Ferroptosis. *Oxid Med Cell Longev* **2022**, 7769355, doi:10.1155/2022/7769355 (2022).

24 Shi, L. *et al.* Clioquinol improves motor and non-motor deficits in MPTP-induced monkey model of Parkinson's disease through AKT/mTOR pathway. *Aging (Albany NY)* **12**, 9515-9533, doi:10.18632/aging.103225 (2020).

25 Weiland, A. *et al.* Ferroptosis and Its Role in Diverse Brain Diseases. *Mol Neurobiol* **56**, 4880-4893, doi:10.1007/s12035-018-1403-3 (2019).

26 Bai, L. *et al.* Thioredoxin-1 Rescues MPP(+)/MPTP-Induced Ferroptosis by Increasing Glutathione Peroxidase 4. *Mol Neurobiol* **58**, 3187-3197, doi:10.1007/s12035-021-02320-1 (2021).

27 Wang, Z. L., Yuan, L., Li, W. & Li, J. Y. Ferroptosis in Parkinson's disease: glia-neuron crosstalk. *Trends Mol Med* **28**, 258-269, doi:10.1016/j.molmed.2022.02.003 (2022).

28 Puchl'ova, E. & Szolcsanyi, P. Filbertone: A Review. *J Agric Food Chem* **66**, 11221-11226, doi:10.1021/acs.jafc.8b04332 (2018).

29 Park, J. *et al.* Activation of ROS-PERK-TFEB by filbertone ameliorates neurodegenerative diseases via enhancing the autophagy-lysosomal pathway. *J Nutr Biochem* **118**, 109325, doi:10.1016/j.jnutbio.2023.109325 (2023).

30 Huang, T. *et al.* Curcumin mitigates axonal injury and neuronal cell apoptosis through the PERK/Nrf2 signaling pathway following diffuse axonal injury. *Neuroreport* **29**, 661-677, doi:10.1097/WNR.0000000000001015 (2018).

31 Wu, L. *et al.* Ferroptosis as a New Mechanism in Parkinson's Disease Therapy Using Traditional Chinese Medicine. *Front Pharmacol* **12**, 659584, doi:10.3389/fphar.2021.659584 (2021).

32 Cullinan, S. B. *et al.* Nrf2 is a direct PERK substrate and effector of PERK-dependent cell survival. *Mol Cell Biol* **23**, 7198-7209, doi:10.1128/MCB.23.20.7198-7209.2003 (2003).

33 Zhang, G. *et al.* PERK regulates Nrf2/ARE antioxidant pathway against dibutyl phthalate-induced mitochondrial damage and apoptosis dependent of reactive oxygen species in mouse spermatocyte-derived cells. *Toxicol Lett* **308**, 24-33, doi:10.1016/j.toxlet.2019.03.007 (2019).

34 Iannielli, A. *et al.* Pharmacological Inhibition of Necroptosis Protects from Dopaminergic Neuronal Cell Death in Parkinson's Disease Models. *Cell Rep* **22**, 2066-2079, doi:10.1016/j.celrep.2018.01.089 (2018).

35 Fao, L., Mota, S. I. & Rego, A. C. Shaping the Nrf2-ARE-related pathways in Alzheimer's and Parkinson's diseases. *Ageing Res Rev* **54**, 100942,

doi:10.1016/j.arr.2019.100942 (2019).

36 Gan, L. & Johnson, J. A. Oxidative damage and the Nrf2-ARE pathway in neurodegenerative diseases. *Biochim Biophys Acta* **1842**, 1208-1218, doi:10.1016/j.bbadis.2013.12.011 (2014).

37 Rojo, A. I. *et al.* Nrf2 regulates microglial dynamics and neuroinflammation in experimental Parkinson's disease. *Glia* **58**, 588-598, doi:10.1002/glia.20947 (2010).

38 Sandberg, M., Patil, J., D'Angelo, B., Weber, S. G. & Mallard, C. NRF2-regulation in brain health and disease: implication of cerebral inflammation. *Neuropharmacology* **79**, 298-306, doi:10.1016/j.neuropharm.2013.11.004 (2014).

39 Yamazaki, H., Tanji, K., Wakabayashi, K., Matsuura, S. & Itoh, K. Role of the Keap1/Nrf2 pathway in neurodegenerative diseases. *Pathol Int* **65**, 210-219, doi:10.1111/pin.12261 (2015).

40 Zhong, Y. *et al.* Nrf2 Inhibits the Progression of Parkinson's Disease by Upregulating AABR07032261.5 to Repress Pyroptosis. *J Inflamm Res* **15**, 669-685, doi:10.2147/JIR.S345895 (2022).

41 Quandt, D., Jasinski-Bergner, S., Muller, U., Schulze, B. & Seliger, B. Synergistic effects of IL-4 and TNFalpha on the induction of B7-H1 in renal cell carcinoma cells inhibiting allogeneic T cell proliferation. *J Transl Med* **12**, 151, doi:10.1186/1479-5876-12-151 (2014).

42 Nebrisi, E. E. Neuroprotective Activities of Curcumin in Parkinson's Disease: A Review of the Literature. *Int J Mol Sci* **22**, doi:10.3390/ijms222011248 (2021).

43 Hambright, W. S., Fonseca, R. S., Chen, L., Na, R. & Ran, Q. Ablation of ferroptosis regulator glutathione peroxidase 4 in forebrain neurons promotes cognitive impairment

and neurodegeneration. *Redox Biol* **12**, 8-17, doi:10.1016/j.redox.2017.01.021 (2017).

44 Bersuker, K. *et al.* The CoQ oxidoreductase FSP1 acts parallel to GPX4 to inhibit ferroptosis. *Nature* **575**, 688-692, doi:10.1038/s41586-019-1705-2 (2019).

45 Mao, C. *et al.* DHODH-mediated ferroptosis defence is a targetable vulnerability in cancer. *Nature* **593**, 586-590, doi:10.1038/s41586-021-03539-7 (2021).

46 Du, K. *et al.* Inhibiting xCT/SLC7A11 induces ferroptosis of myofibroblastic hepatic stellate cells but exacerbates chronic liver injury. *Liver Int* **41**, 2214-2227, doi:10.1111/liv.14945 (2021).

47 Chen, Z. *et al.* Tetranectin gene deletion induces Parkinson's disease by enhancing neuronal apoptosis. *Biochem Biophys Res Commun* **468**, 400-407, doi:10.1016/j.bbrc.2015.10.118 (2015).

48 Lin, Q. S. *et al.* RIP1/RIP3/MLKL mediates dopaminergic neuron necroptosis in a mouse model of Parkinson disease. *Lab Invest* **100**, 503-511, doi:10.1038/s41374-019-0319-5 (2020).

49 Onate, M. *et al.* The necroptosis machinery mediates axonal degeneration in a model of Parkinson disease. *Cell Death Differ* **27**, 1169-1185, doi:10.1038/s41418-019-0408-4 (2020).

50 Wang, S., Yuan, Y. H., Chen, N. H. & Wang, H. B. The mechanisms of NLRP3 inflammasome/pyroptosis activation and their role in Parkinson's disease. *Int Immunopharmacol* **67**, 458-464, doi:10.1016/j.intimp.2018.12.019 (2019).

51 Hubbs, A. F. *et al.* Vacuolar leukoencephalopathy with widespread astrogliosis in mice lacking transcription factor Nrf2. *Am J Pathol* **170**, 2068-2076, doi:10.2353/ajpath.2007.060898 (2007).

52 Souza, A. *et al.* Effect of Metabolic Syndrome on Parkinson's Disease: A Systematic Review. *Clinics (Sao Paulo)* **76**, e3379, doi:10.6061/clinics/2021/e3379 (2021).

53 Huang, H. C., Nguyen, T. & Pickett, C. B. Phosphorylation of Nrf2 at Ser-40 by protein kinase C regulates antioxidant response element-mediated transcription. *J Biol Chem* **277**, 42769-42774, doi:10.1074/jbc.M206911200 (2002).

III-IX 국문 요약

파킨슨병(PD)은 뇌 흑질치밀부(SNpc)에서 도파민성 뉴런의 손실을 특징으로 하는 신경퇴행성 질환이다. Ferroptosis는 철 축적, GPX4 감소, 지질 과산화 과정을 포함하는 세포사의 한 종류로 PD 발병에 기여하는 것으로 보고되고 있다. 우리는 이전에 필버톤이 PERK-ALP 경로를 향상함으로써 신경 질환 개선 효과를 나타낸다고 보고했다. 그러나 필버톤이 PD 병리학에 미치는 영향에 대해서는 연구되지 않았다. 따라서 본 연구에서는 필버톤이 ferroptosis로 인해 발생하는 신경퇴행성 질환을 억제할 수 있는지 확인하고자 하였다. 본 연구에서 사람 신경세포주 SH-SY5Y 세포에 필버톤을 투여하였을 때 PERK 활성화를 통해 GPX4 및 SLC7A11 등의 항산화 유전자 전사를 조절하는 Nrf2의 활성화를 증가시키는 것을 관찰하였다. 또한, MPTP를 사용하여 PD를 발생시킨 쥐의 중뇌 영역에서 나타나는 도파민성 뉴런 손실뿐만 아니라 α-synuclein 축적이 필버톤 투여에 의해 감소하는 것을 관찰하였으며, PD 발생 시 감소된 Nrf2의 활성화를 필버톤 투여에 의해 증가시킬 수 있음을 확인할 수 있었다. 또한 필버톤은 Nrf2의 활성화를 통해 RSL3와 같은 ferroptosis 유도제 또는 MPP+/MPTP와 같은 신경독성 물질에 의해 유도된 GPX4의 감소를 막을 수 있다는 것을 관찰하였다. 결론적으로, 본 연구는 필버톤이 ferroptosis 억제제로 작용할 가능성이 있으며, PD 치료 전략으로 사용할 수 있음을 제시한다.